

G8776

**PREPARATION, CHARACTERISATION AND MICROWAVE DIELECTRIC
PROPERTIES OF
 $A_n B_{n-1} O_{3n}$ (n=5, 6, 8) TYPE PEROVSKITE COMPOUNDS**

THESIS SUBMITTED TO
COCHIN UNIVERSITY OF SCIENCE AND TECHNOLOGY
IN FULFILMENT OF REQUIREMENT FOR THE
DEGREE OF DOCTOR OF PHILOSOPHY IN PHYSICS



I. N. JAWAHAR

Under the guidance and supervisions of
Dr. M. T. Sebastian (Supervisor)
Dr. P. Mohanan (Co-Supervisor)



**REGIONAL RESEARCH LABORATORY (CSIR)
THIRUVANANTHAPURAM**

AUGUST 2002



Fax : + + 91- (0) 471 - 491712

Phone : 471- 515294 (O), 471- 446901 (R)

Email : mailadils@yahoo.com, mts1@eth.net

Council of Scientific & Industrial Research

REGIONAL RESEARCH LABORATORY

THIRUVANANTHAPURAM - 695 019, INDIA

Dr. M. T. SEBASTIAN

Scientist

CERTIFICATE

This is to certify that this thesis entitled “**PREPARATION, CHARACTERISATION AND MICROWAVE DIELECTRIC PROPERTIES OF $A_nB_{n-1}O_{3n}$ (n=5, 6, 8) TYPE PEROVSKITE COMPOUNDS**”, is an authentic record of the investigation carried out by Mr. **I. N. JAWAHAR** at Regional Research Laboratory (CSIR), Thiruvananthapuram, India under my supervision and guidance. This thesis or any part thereof has not been submitted for any other degree.



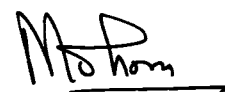
Thiruvananthapuram

Supervisor

Dated: 9/08/02

CERTIFICATE

This is to certify that this thesis entitled “**PREPARATION, CHARACTERISATION AND MICROWAVE DIELECTRIC PROPERTIES OF $A_nB_{n-1}O_{3n}$ ($n = 5, 6, 8$) TYPE PEROVSKITE COMPOUNDS**”, is an authentic record of the investigation carried out by **Mr. I. N. JAWAHAR** at Regional Research Laboratory (CSIR), Thiruvananthapuram, India under my supervision and guidance. This thesis or any part thereof has not been submitted for any other degree.



Dr. P. Mohanan

Co- Supervisor

Professor

Kochi

Department of Electronics

Dated 12/08/02

Cochin University of Science and Technology

CONTENTS

Preface		i
Acknowledgements		v
 Chapter 1		
 INTRODUCTION		
1.1	Dielectric resonators	1
1.1.1	Resonance	3
1.1.2	Types of dielectric resonators	5
1.1.3	Analytical determination of frequencies	6
1.1.4	Mode chart	8
1.2	Materials Requirements	12
1.2.1	High dielectric constant	12
1.2.2	High quality factor (low dielectric loss)	13
1.2.3	The coefficient of temperature variation of the resonant frequency(τ_f)	15
1.3	Polarisation mechanisms in dielectrics	16
1.4	Behaviour of dielectric with respect to frequency	17
1.4.1	Resonant absorption	18
1.4.2	Relaxation absorption	21
1.5	Dielectric constant	22
1.5.1	Determination of ϵ_r	24
1.6	Quality factor (Q factor)	24
1.6.1	Determination of Q factor	26
1.7	Temperature coefficient of resonant frequency	27
1.7.1	Determination of τ_f	28

1.8	Dielectric resonators at microwave frequencies	29
1.9	Dielectric resonator materials	30
1.10	Applications of dielectric resonators	30
1.10.1	Dielectric resonator oscillators (DRO)	31
1.10.2	Dielectric resonator filters	32
1.10.3	Whispering Gallery Mode (WGM) DRs	33
1.10.4	Dielectric resonator antennas (DRAs)	33
	References	34

Chapter 2

PREPARATION AND CHARACTERISATION

2.1	Ceramic preparation	40
2.1.1	Powder forming	41
2.1.1.1	Weighing of raw materials	41
2.1.1.2	Mixing	42
2.1.1.2.1	Ball milling	43
2.1.1.3	Calcination	45
2.1.1.4	Grinding	46
2.1.1.5	Shaping or forming	47
2.1.2	Sintering	49
2.1.2.1	Sintering aids	51
2.1.3	Specific preparation methods	51
2.2	Microwave characterisation of dielectric resonators	53
2.2.1	Introduction	53
2.2.2	Material characterisation at microwave frequencies	55
2.2.2.1	Measurement of ϵ_r	57
2.2.2.2	Measurement of quality factor (Q)	65
2.2.2.3	Measurement of τ_f	68

2.3	Other characterisation of DR ceramics	69
2.3.1	Powder X-ray Diffraction (XRD)	69
2.3.2	Scanning Electron Microscopy (SEM)	70
2.3.3	Spectroscopic methods	70
	References	71

Chapter 3

THE $A_5B_4O_{15}$ (A=Ba, Sr, Mg, Ca, Zn; B=Nb, Ta) MICROWAVE DIELECTRIC CERAMICS

3.1	Introduction	76
3.2	The $A_5B_4O_{15}$ (A=Ba, Sr, Mg, Ca, Zn; B=Nb, Ta) ceramics	78
3.2.1	Preparation and characterisation	78
3.2.2	Results and discussion	81
3.2.2.1	Density and X-ray diffraction	81
3.2.2.2	Microwave dielectric properties	88
3.3	Far Infrared and submillimeter studies of $A_5B_4O_{15}$ (A=Ba, Sr, Mg, Ca, Zn; B=Nb, Ta) ceramics	91
3.3.1	Introduction	91
3.3.2	Experimental	94
3.3.3	Results and Discussion	95
3.3.3.1	Infrared and submillimeter spectra	95
3.3.3.2	Phonon spectra and crystal structure	100
3.3.4	Conclusion	105
3.4	$Ba_{5-x}Sr_xTa_4O_{15}$, $Ba_5Nb_xTa_{4-x}O_{15}$ and $Sr_5Nb_xTa_{4-x}O_{15}$ solid solution phases	107
3.4.1	Introduction	107
3.4.2	Experimental	108
3.4.3	Results and discussion	109
3.4.3.1	<i>Density</i>	109

3.4.3.2	X-ray diffraction analysis	111
3.4.3.3	Microwave dielectric properties	119
3.4.3.3.1	Ba _{5-x} Sr _x Ta ₄ O ₁₅	119
3.4.3.3.2	Ba ₅ Nb _x Ta _{4-x} O ₁₅	121
3.4.3.3.3	Sr ₅ Nb _x Ta _{4-x} O ₁₅	122
3.4.4	Conclusion	125
3.5	The microwave dielectric properties of (1-x)ZnNb₂O₆- xZn₃Nb₂O₈ mixtures	126
3.5.1	Introduction	126
3.5.2	Experimental	127
3.5.3	Results and discussion	128
3.5.3.1	Density	128
3.5.3.2	X-ray diffraction analysis	131
3.5.3.3	Microwave dielectric properties	133
3.5.4	Conclusion	138
3.6	The microwave dielectric properties of xZnO-(5-x)MgO-2Nb₂O₅	138
3.6.1	Introduction	138
3.6.2	Experimental	139
3.6.3	Results and discussion	140
3.6.3.1	Density and XRD	140
3.6.3.2	Microwave dielectric properties	144
3.7	Conclusion	146
	References	148

Chapter 4

THE MICROWAVE DIELECTRIC PROPERTIES OF MO-La₂O₃-TiO₂ (M=Ca, Sr, Ba) CERAMICS

4.1	Introduction	151
4.2	Preparation and characterisation	153
4.3	Results and discussion	155
4.3.1	X-ray diffraction and SEM analysis	156
4.3.2	Microwave dielectric properties	161
4.4	Conclusion	166
	References	167

Chapter 5

A NOVEL METHOD OF TEMPERATURE COMPENSATION BY STACKING POSITIVE AND NEGATIVE τ_f RESONATORS

5.1	Introduction	169
5.2	Experimental	172
5.3	Results and Discussion	174
5.3.1	Ba ₅ Nb ₄ O ₁₅ : 5ZnO-2Nb ₂ O ₅ stacked resonators	174
5.3.2	Ba ₅ Nb ₄ O ₁₅ : Sr(Y _{1/2} Nb _{1/2})O ₃ stacked resonators	180
5.4	Conclusion	183
	References	185

Chapter 6

SUMMARY AND CONCLUSION	187
-------------------------------	-----

PREFACE

Dielectric Resonators (DR) are ceramic pieces that can act as frequency determining components at microwave frequencies. DRs should have high dielectric constant (ϵ_r) in the range 20 to 100 for better miniaturization, high Q factor ($Q > 2000$) for better frequency selectivity and nearly zero temperature coefficient of resonant frequency (τ_f) for frequency stability with temperature. In addition to the above characteristics, their low cost of production and excellent integrability to microwave integrated circuits (MICs) make them indispensable components in microwave oscillators, filters, duplexers used in cellular phones and in dielectric resonator antennas. Dielectric resonators increasingly replace the conventional resonators such as metallic cavities or micro strip circuits. Though several temperature-stable DRs are available at present, investigation is still going on to find new materials having better dielectric resonator properties. In this work we investigate the microwave dielectric properties of (1) $A_5B_4O_{15}$ ($A = \text{Ba, Sr, Mg, Ca, Zn}$; $B = \text{Nb, Ta}$) ceramics, their solid solutions and mixtures (2) $MO\text{-}La_2O_3\text{-}TiO_2$ ($M = \text{Ba, Sr, Ca}$) ceramics which mainly consists of $A_nB_{n-1}O_{3n}$ ($n = 5, 6, \text{ or } 8$) type cation deficient hexagonal perovskites and (3) a novel method of achieving temperature compensation by stacking positive and negative τ_f resonators. Dielectric resonator properties were studied in terms of phases, crystal structure, crystal symmetry, polarisability of ions, lattice parameters and characterization techniques such as XRD and SEM are employed.

Chapter 1 is a general introduction about material, scientific and technological aspects of DRs. Three important parameters, ϵ_r , Q and τ_f , used for the DR

characterization are described. The relationship of the above parameters with the fundamental material characteristics is discussed. Different modes are excited when a DR is excited with suitable microwave spectrum of frequencies. A description of analytical determination of frequencies and construction of mode charts used for sample design and mode identification are also discussed.

Chapter 2 presents the methods used for the preparation of ceramics and the various techniques used for the microwave characterization of dielectric properties. The ceramic samples were prepared through the solid-state ceramic route. The dielectric constant of the ceramics at microwave frequencies are measured using the end shorted dielectric post resonator. The quality factors are determined by a transmission mode cavity. The temperature coefficient of resonant frequency (τ_f) is measured by heating the end shorted dielectric post resonator set up in the temperature range 20 to 75°C and by noting the variation of the resonant frequency with temperature. The crystal structure of the samples is analysed using powder X-ray diffraction pattern and surface morphology and grain size is observed using Scanning Electron Microscopy.

Chapter 3 describes the investigation of microwave dielectric properties of $A_5B_4O_{15}$ (A = Ba, Sr, Mg, Ca, Zn; B = Nb, Ta) ceramics. The ceramics show dielectric constant in the range 11 to 51. The hexagonal perovskites show higher dielectric constants than the orthorhombic phases $Mg_5Nb_4O_{15}$ and $Mg_5Ta_4O_{15}$. The FIR and submillimeter techniques are used to study the above compounds. The basic theory of the techniques is discussed. An indirect estimation of the lower limit of dielectric loss and upper limit of dielectric constant at microwave frequencies can be obtained by the extrapolation of real part and imaginary part of the dielectric function down to

microwaves from data obtained through far infra-red spectroscopy. The solid solution phase of the type $Ba_{5-x}Sr_xTa_4O_{15}$, $Sr_5Nb_xTa_{4-x}O_{15}$, $Ba_5Nb_xTa_{4-x}O_{15}$ are prepared and microwave dielectric properties are characterized. The $Sr_5Nb_xTa_{4-x}O_{15}$ phases show abnormal dielectric properties where a decrease in dielectric constant is observed for the intermediate compounds when compared to the end members. This is attributed to the possible structural changes and is evident from analysis of X-ray diffraction data. The $Ba_5Nb_xTa_{4-x}O_{15}$ show linear behaviour for solid solution and intermediate dielectric properties of the end members are obtained. In section of the chapter $xZn_3Nb_2O_8-(1-x)ZnNb_2O_6$ mixture phases are discussed. The results are interpreted based on the method of mixtures. The mixture phases show good sinterability and higher quality factors than the end members. The substitution of Zn at Mg site in $Mg_5Nb_4O_{15}$ also gave mixture phases and the compositions $xZnO-(5-x)MgO-2Nb_2O_5$ showed high quality factors ($Q \times f$ up to 89000 GHz) with ϵ_r in the range 11 to 22. The mixture phases showed intermediate dielectric properties of the end compounds.

Chapter 4 describes the microwave dielectric properties of $MO-La_2O_3-TiO_2$ ($M = Ba, Sr, Ca$) ceramics. All the ceramics, except $CaLa_4Ti_5O_{17}$ and $CaLa_8Ti_9O_{31}$, which are orthorhombic structured, belong to the cation deficient hexagonal perovskites belonging to the $A_nB_{n-1}O_{3n}$ ($n=5, 6$) type compounds. The ceramics show high dielectric constant in the range 41 to 54 with high quality factors and small temperature coefficients of resonant frequencies. The applicability of Claussius - Mossotti equation to these ceramics is discussed. These ceramics are suitable for low frequency applications requiring narrow bandwidth and low insertion loss. The orthorhombic phases show comparatively higher dielectric constants than the hexagonal phases.

Chapter 5 describes a novel method of achieving temperature compensation by stacking positive and negative τ_f resonators. The stack acts as a single resonator. The τ_f of the resultant stack depends on the volume fraction of the positive τ_f and negative τ_f DR materials. The τ_f can be tuned to zero or to a desired value by adjusting the volume fraction of the positive and negative τ_f materials. The dielectric constant and quality factor also change depending on the volume fraction of the two different DR materials. The experiment is performed with varying volume fraction of $\text{Ba}_5\text{Nb}_4\text{O}_{15}$ as the positive τ_f DR and $\text{Sr}(\text{Y}_{1/2}\text{Nb}_{1/2})\text{O}_3$ and $5\text{ZnO}-2\text{Nb}_2\text{O}_5$ as the negative τ_f DR materials. The DR material in the bottom of the stack has greater influence on the τ_f of the resultant stacked resonator.

Chapter 6, gives a summery and conclusion of the present investigation and also discusses the scope for further work in this field.

Chapter 1

INTRODUCTION

1. 1 DIELECTRIC RESONATORS

Dielectric resonators (DRs) are frequency determining components in filters and oscillators used in modern communication systems. Until recently quartz resonators were used to generate, stabilize and filter frequencies in the communication devices. The piezoelectric quartz crystal resonators can be used only up to a few hundred MHz. The recent advances in the communication system increased the number of transmitters and receivers in a particular geographical area, which led to crowding of channels. The only way to prevent interference due to crowding of the channels is to go towards higher frequency range (microwave range). One can use quartz resonators at high frequencies by a frequency multiplication process but leads to high noise and are expensive. Metallic cavity resonators were tried but were very large in size and not integrable in a microwave integrated circuit. Microstrip resonators were also tried but they have low Q with large temperature variation of the resonant frequency. In 1939 Richtmeyer theoretically predicted [1] that a suitably shaped dielectric material could behave as an electromagnetic resonator. In 1960 Okaya [2] found that a

piece of rutile acted as a resonator and later in 1962 Okaya and Barash [3] for the first time analyzed the different modes of a dielectric resonator. In 1968 Cohen [4] for the first time experimentally determined the microwave dielectric properties of a rutile resonator with dielectric constant $\epsilon_r=104$, quality factor $Q=10.000$ and coefficient of temperature variation of the resonant frequency $\tau_f=+400$ ppm/ $^{\circ}$ C. The τ_f of rutile resonator is too high for practical applications. A real breakthrough for dielectric resonators occurred in early 1970's with the development of the first temperature stable, low loss barium tetra-titanate (BaTi_4O_9) resonator [5]. Since then extensive work has been carried out on microwave ceramic dielectric resonators.

The recent progress in microwave telecommunication and satellite broadcasting has resulted an increasing demand for Dielectric Resonators (DRs). Technological improvements in DRs have contributed to considerable advancements in wireless communications [8-22]. Ceramic dielectric resonators have advantage of being more miniaturized as compared to traditional microwave cavities, while having a significantly higher quality factor than transmission lines and microstrips. DRs are advantageous in terms of compactness, light weight, stability and relatively low cost of production as compared to the conventional bulky metallic cavity resonators. In addition temperature variation of the resonant frequency of dielectric resonators can be engineered to a desired value to meet circuit designers requirements. Table 1.1 gives comparison of the properties of metallic cavities, microstrips and dielectric resonators. Functioning as

important components in communication circuits, DRs can create, filter [31-39] and select frequencies in oscillators [24-30], amplifiers and tuners.

Table 1.1: Comparison of the properties of metallic cavity, microstrip and dielectric resonator

Component	Size	Q factor	τ_r	Integability in a MIC
Metallic Cavity (Cu, Brass, invar etc)	Large	High	Low	Nonintegrable
Microstrip resonators	Very small	Very low	Very High	Integrable
DR	Small	Very high	Very Low	Integrable

DRs are important components in duplexers, multiplexers, combiners, radar detectors, collision avoidance systems, automatic door opening systems, telemetry, cellular radio, cordless phones or personnel communication systems, global positioning systems, TVRO, satellite and military communication systems.

1.1.1 Resonance

A dielectric resonator should have maximum confinement of energy within the resonator when used at a particular resonant frequency. The resonance occurs by total multiple internal reflections of microwaves at the boundary or dielectric-air interface (see Fig. 1. 1). If the transverse dimensions of the dielectric

are comparable to the wave length of the microwave, then certain field distributions

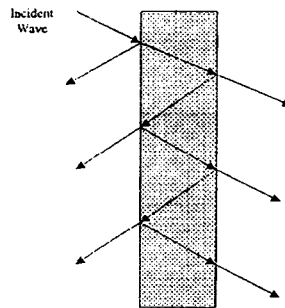


Fig.1. 1 Schematic sketch showing total multiple internal reflections at the air-dielectric interface

or modes will satisfy Maxwell's equations and boundary conditions. It was found that through multiple total internal reflections, a piece of dielectric with high dielectric constant can confine microwave energy at a few discrete frequencies, provided that the energy is fed in the appropriate direction. The reflection coefficient approaches unity when the dielectric constant approaches infinity. In the microwave frequency range free space wavelength (λ_0) is in centimeters and hence the wavelength (λ_g) inside the dielectric will be in millimeters only when the value of the dielectric constant ϵ is in the range 20-100. Hence the dimensions of the dielectric sample must be of the same order (in millimeters) for the resonance to occur. Still larger values of the dielectric constant gives better confinement of energy, reduced radiation loss and further miniaturization but will result in higher dielectric losses because of the inherent material properties. A high dielectric constant material can confine most of the standing electromagnetic wave within its volume due to reflections at the air dielectric interface. The

frequency of the standing wave depends on the dimensions and dielectric constant of the dielectric. The electromagnetic fields outside the dielectric sample decay rapidly. One can prevent radiation losses by placing the DR in a small metallic enclosure. Since only a small radiation field sees the metallic surface, the resulting conduction loss will be too small and can be neglected.

1. 1. 2 Types of Dielectric Resonators

The disk shaped dielectric material is the simplest form of a dielectric resonator. The usual geometries of DRs are discs, rings and parallelepipeds. By inserting a metal or ferrite screws into the central hole of a ring resonator, the resonant frequency of modes can be tuned. Similar techniques are used to suppress the modes adjacent to the desired mode, to avoid interference and to reduce the dielectric loss. The mode spectrum and resonant frequencies of DRs greatly depend on the aspect ratio (diameter D /length L). The dimensions of the specimen are important to achieve wide separation of modes. The proper aspect ratios are 1.0 to 1.3 and 1.9 to 2.3. In practice the specimen diameters in the range 7 to 25 mm have been found most suitable.

There are two main types of resonators, coaxial and dielectric resonators, employed in the frequency range 500MHz to 30 GHz using the available materials today ($10 < \epsilon_r < 120$). The coaxial resonators which are tubular

in appearance are used for frequencies up to 3 GHz. The coaxial resonators are also called $\lambda/4$ resonators. Their length is determined by

$$l = \frac{\lambda_0}{4\epsilon_r} \text{ where } \lambda_0 \text{ is the vacuum wave length at the resonant frequency}$$

They have four times more size reduction than the dielectric resonators. The tubular coaxial resonators are given a thin metallic coating and the resonance is by the total multiple internal reflections at the dielectric-metal interface. The quality factor of coaxial resonators is limited to values less than 1500 by the finite conductivity of the metallic surface of the tubular resonator. These types of resonators are commonly used in cellular telephone systems at about 800MHz where miniaturization is very important. At higher frequencies cylindrical dielectric resonators (DRs) are used. For a cylindrical resonator the required diameter is proportionally reduced as follows

$$D = \lambda_0 \frac{1}{\sqrt{\epsilon}}$$

1. 1. 3 Analytical Determination of Frequencies

Practical circuits employing DRs are of different types. DRs placed between two parallel conducting plates, DRs enclosed by metal shields, DR enclosed in substrate-box system, open dielectric resonators are some of the common structures. When the DR enclosed structure is fed with microwaves different modes gets excited. The $TE_{01\delta}$ mode is the most commonly used mode

for practical applications. It is of great importance if the resonant frequency of the DR enclosed structure can be analytically determined. An exact analysis usually lead to complex solutions, which is very difficult to implément. Hence using some simple models we can compute the resonant frequencies with a small percentage of error.

One of the first model to suggest was the magnetic wall model [74-76]. Here the cylindrical surface containing the circumference of the resonator is replaced with a fictitious open circuit boundary (magnetic wall). The tangential magnetic field component and normal field component vanish at the DR-air boundary. Some of the field leaks out of the DR and if not taken into account results in discrepancies with the measured results. The method often leads to an error of less than 10 %. The variational method developed by Konishi et al. [77] has an error of less than 1 %. The method is computationally complex. Itoh Rudokas [78] Model is less complex and gives accuracies very near to the variational method. Guillon and Garault [79] proposed a method where all the surfaces are simultaneously considered as imperfect magnetic walls. The method has an accuracy of better than 1 %. Some rigorous analytical formulation is also found which determine the complex resonant frequencies of isolated cylindrical dielectric resonators. Glisson et al. [80] have applied a surface integral formulation and the method of moments. Tsuji et al. [81] have presented an alternative method, in which the resonator fields are expanded into truncated series of solutions of the Helmholtz equation in spherical polar coordinates, and the boundary condition on the resonator surface is treated in the least square

sense. Both these methods are reported to give highly accurate values of resonant frequencies and Q factors, substantiated by experiment. Mongia et al. [82] have reported an effective dielectric model that is a simple analytical technique to determine the resonant frequencies of isolated dielectric resonators. The method yields results as accurate as those reported using rigorous methods. Tobar et al. [83] has developed an improved method, which allows the determination of mode frequencies to high accuracy in cylindrical anisotropic dielectric resonators. Yousefi et al. [84] have applied the GIBC (generalised Impedance boundary condition) formulation for the determination of resonant frequencies and field distribution of a substrate mounted dielectric resonator. Apart from that one can find several other different methods for finding the resonant frequencies reported during the last two decades.

1.1.4 Mode Chart

If one can analytically determine frequencies corresponding to various modes mode charts can be constructed. A mode chart helps to find out how different modes behaves with resonator parameters. It helps to find out sample dimensions of dielectric resonator filter circuits corresponding to aspect ratio where maximum mode separation with adjacent modes are obtained.

As an example a typical mode chart is constructed (Fig.1. 2). The mode chart is constructed for the end shorted dielectric rod configuration based on the

theory developed by Pospieszalski [85]. The dielectric resonator in the shape of a cylinder with diameter D and length L placed between two conducting plates constitute the resonant structure. For very high ϵ_r and $D/L > 0$, the solution for the characteristic equation corresponding to the HE_{111} , HE_{211} modes in the broad

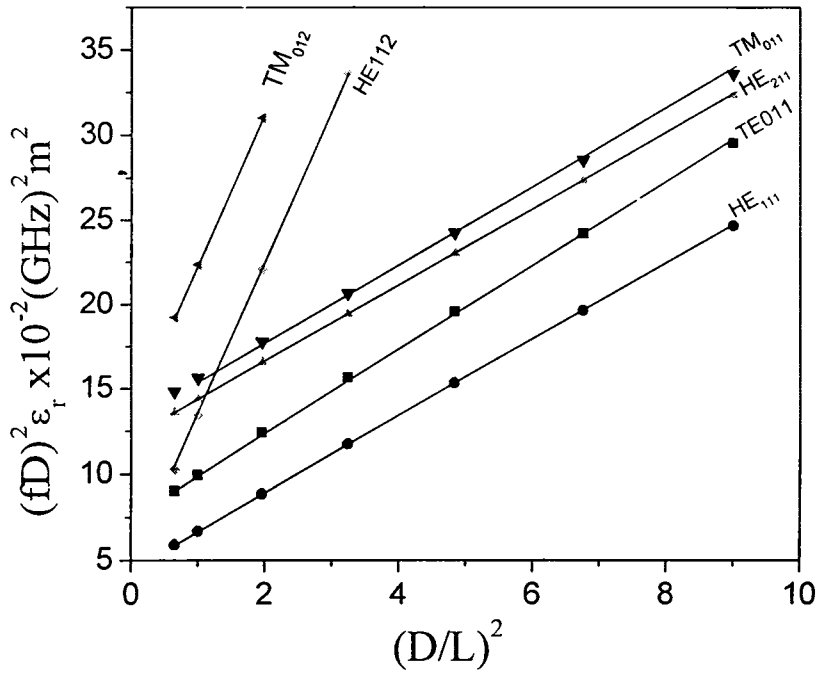


Fig. 1. 2 The mode chart constructed for a material with $\epsilon_r = 22$

range of ϵ_r and D/L are almost straight lines from which simple approximate formulas can be derived.

For HE_{111} modes if $\epsilon_r > 500$ and $1 \leq (D/L)^2 \leq 15$

$$F_0^2 = (2.21)^2 + \left(\frac{\pi D l}{2L}\right)^2 \quad (1.1)$$

where $F_0 = \left(\frac{\pi D}{\lambda_0}\right)^2 \epsilon_r$, with accuracy better than 0.7%. D is the diameter of the

dielectric rod, L its length and l is the no of field variations along the axis.

Similarly for HE_{2,1l} mode

$$F_0^2 = (3.65)^2 + \left(\frac{\pi D l}{2L}\right)^2 \quad (1.2)$$

Accuracy of expression (2) is better than 0.7% if $\epsilon_r \geq 500$ and $2 \leq (D/L)^2 \leq 15$.

For circularly symmetric modes the characteristic equation has very simple forms.

For the TM_{0ml},

$$\frac{J_1(u)}{uJ_0(u)} = -\frac{1}{\epsilon_r} \frac{K_1(w)}{wK_0(w)} \quad (1.3)$$

For the TE_{0ml}

$$\frac{J_1(u)}{uJ_0(u)} = -\frac{K_1(w)}{wK_0(w)} \quad (1.4)$$

If ϵ_r is large enough the solution of (3) for $w > 0$ can be approximated by the solution of

$$J_1(u) = 0 \quad (1.5)$$

Therefore for TM_{0ml}

$$F_0^2 = \rho_{1m}^2 + \left(\frac{\pi D l}{2L}\right)^2 \quad (1.6)$$

where ρ_{1m} is the m^{th} greater than zero solution of (5). For $\epsilon_r > 20$; $(D/L)^2 \geq 1$, the accuracy is better than 2%. The accuracy is better than 0.5% if $\epsilon_r > 100$ and $(D/L)^2 \geq 1$.

For the TE_{0ml} modes the approximate solution is

$$F_0^2 = \rho_{1m}^2 \left(1 - \frac{1}{\sqrt{\rho_{1m}^2 + \left(\frac{\pi D l}{2L}\right)^2}}\right)^2 + \left(\frac{\pi D l}{2L}\right)^2 \quad (1.7)$$

Accuracy is better than 0.5% if $\epsilon \geq 500$, $3 \leq (D/L)^2 \leq 15$.

Computer program is developed such that the resonant frequency can be obtained as a function of dielectric constant, length and diameter of the sample. As an example mode chart is constructed for a material with dielectric constant =22 by plotting different values of $(fD)^2 \epsilon_r$ for different values of $(D/L)^2$ for different modes (See Fig. 1. 2). It is evident from the graph that $(D/L)^2$ around 4 is good for maximum mode separation. For low value of D/L various modes tends to interfere to destroy the quality of resonance.

1.2. MATERIALS REQUIREMENTS

The important characteristics required for a dielectric resonator material for practical applications are

1.2.1. High dielectric constant.

High dielectric constant (ϵ_r) in the range 20-100 or more are needed for applications. High dielectric constant facilitates miniaturization of the devices and the miniaturization is proportional to $1/(\epsilon)^{1/2}$. According to classical dispersion theory [6,7] the crystal is approximated as a system of damped oscillators having an appropriate frequency and dipole moment. The real and imaginary parts of the complex dielectric constant (ϵ', ϵ'') as functions of ω where $\omega=2\pi\nu$) are given by

$$\epsilon'(\omega) = \epsilon_{\infty} + \sum_j \frac{4\pi\rho_j(\omega_j^2 - \omega^2)\omega_j^2}{(\omega_j - \omega^2)^2 + (\gamma_j\omega)^2} \quad (1.8)$$

where $4\pi\rho_j$ is the oscillator strength, ω_j is the resonant angular frequency of frequency of the j th oscillator, ϵ_{∞} is the dielectric constant caused by electronic polarization at higher frequencies and γ_j is the damping constant which is given

by the width of the peak. The summation is over the j resonances in the spectrum.

Each resonance is characterized by its dispersion parameters.

For $\omega_j \gg \omega$,

$$\varepsilon'(\omega) = \varepsilon_\infty + \sum_j 4\pi\rho_j \quad (1.9)$$

From the above equation it is clear that the dielectric constant is independent of frequency in the microwave frequency region.

1. 2. 2 High quality factor (low dielectric loss).

Any type of defects such as grain boundaries, stacking faults, chemical or structural disorder, point defects, planar defects, line defects, inclusions, secondary phases, twinning, porosity etc contribute losses. For an ideal crystal quality factor is approximately equal to the reciprocal of the dielectric loss ($\tan \delta$). In the microwave region the loss is mainly due to the interaction of the applied field with phonons [8]. The microwave energy is transferred to transverse optical phonons. These optical phonons can then generate thermal phonons. This leads to damping of the optical lattice vibrations and therefore causes dielectric loss. Hence there is a linear increase of loss with frequency and is a characteristic phonon effect. From the classical dispersion theory,

$$\varepsilon''(\omega) = \sum_j \frac{4\pi\rho_j(\gamma_j\omega)\omega_j^2}{(\omega_j^2 - \omega^2)^2 + (\gamma_j\omega)^2} \quad (1.10)$$

For $\omega_j \gg \omega$

$$\varepsilon''(\omega) = \sum_j \frac{4\pi\rho_j(\gamma_j\omega)}{\omega_j^2} \quad (1.11)$$

The above equation shows that loss is frequency dependent. Several phonon processes contribute to intrinsic losses in a dielectric depending on the ac field frequency, temperature range and the symmetry of the crystal under consideration. In general the losses are lower for Centro symmetric crystals than the non-Centro symmetric crystals.

In the case of a resonator the unloaded quality factor can be expressed as

$$1/Q_u = 1/Q_d + 1/Q_r + 1/Q_c \quad (1.12)$$

where $1/Q_d$, $1/Q_r$ and $1/Q_c$ are the dielectric loss, radiation loss and conduction loss respectively. Normally a quality factor greater than 2000 is required for practical applications

1. 2. 3 The coefficient of temperature variation of the resonant frequency (τ_f).

The coefficient of temperature variation of the resonant frequency (τ_f) determines the frequency stability. τ_f is defined as

$$\tau_f = (1/f)(\Delta f/\Delta T) \quad (1. 13)$$

where f is the resonant frequency at room temperature, Δf is the variation of resonant frequency from room temperature for a change in temperature ΔT . The τ_f depends on the temperature variation of ϵ_r and coefficient of linear thermal expansion according to the expression

$$\tau_f = -\alpha_L - \epsilon_r/2 \quad (1. 14)$$

The value of τ_f should be near to zero for practical applications. However often the device engineer requires a low positive or negative τ_f to compensate for the temperature variation of the resonant frequency due to the circuit.

The extensive research in last three decades has provided several suitable DR materials like (Mg,Ca)TiO₃ [42-47], complex perovskites [48-52], BaTi₄O₉-Ba₂Ti₉O₂₀ [53-59], (Zr,Sn)TiO₄ [60-62], BaO-Ln₂O₃-TiO₂ [63-72] system

1. 3 POLARISATION MECHANISMS IN DIELECTRICS

Under the influence of an electric field on a dielectric material four types polarisation mechanisms can occur, i.e. interfacial, dipolar, ionic and electronic. Piling up of mobile charge carriers at physical barrier such as grain boundary causes for interfacial polarisation or space charge polarisation. At low frequencies the mechanism gives rise to high dielectric constant and in some cases may extend up to 10^3 Hz.

In zero field the permanent dipoles will be randomly oriented and the system has no net polarisation, but an electric field will tend to align the dipoles and the materials will acquire a net moment. This is called orientational polarisation. In other words, the perturbation of thermal motion of the ionic or molecular dipoles, producing a net dipolar orientation in the direction of the applied field. Two mechanisms can be operative in this case. [16]. (a) In linear dielectrics (non-ferroelectrics) dipolar polarisation results from the motion of the charged ions between the interstitial positions in ionic structures parallel to the applied field direction. The mechanism is active in the 10^3 - 10^6 Hz range. (b) Molecules having permanent dipole moment may be rotated about an equilibrium position against an elastic restoring position. Its frequency of relaxation is very high of the order of $\sim 10^{11}$ Hz. The dipolar polarisation contributes to the dielectric constant in the sub-infrared range of frequencies.

The displacement of positive and negative ions with respect to each other gives rise to ionic polarisation. The mechanism contributes to the dielectric constant at infrared frequency range ($\sim 10^{12}$ - 10^{13} Hz).

When an electric field is applied the valence electron cloud shifts with respect to the nucleus the atom acquires a dipole moment. This occurs at high frequencies of about 10^{15} GHz. The refractive index (η) and electronic polarisability (α_e) are related by the relation as α_e are related by the equation

$$\alpha_e = \left[\frac{4\pi V_m}{3} \left(\frac{\eta^2 - 1}{\eta^2 + 2} \right) \right]^{-1} \quad (1.15)$$

where V_m is the molar volume of the material and η the refractive index is equal to $\epsilon_r^{1/2}$ which is valid for all materials well at optical frequencies, but there is disagreement when dipolar polarisation is present. At microwave frequencies the mechanisms due to ionic and electronic polarisation contribute to the dielectric properties.

1. 4 BEHAVIOUR OF DIELECTRIC WITH RESPECT TO FREQUENCY

From Maxwell's equations, it can be shown that the refractive index (η) of a material is equal to $\epsilon_r^{1/2}$. But experiments show much difference between two

values for most of the materials. The measured ϵ_r usually found to decrease with frequency. It follows fairly sharp drops at certain frequencies. Associated with each of these drops there is a region of energy dissipation or dielectric loss. This indicates the switching of one of these polarisation mechanisms because polarisation can no longer keep in step with the applied field. There are two different types of mechanisms, which can give rise to this kind of behaviour. They are resonance absorption and dipole relaxation.

1. 4. 1 Resonant absorption

A dipole will have a natural frequency of oscillation. The dipole follows the variation of an applied field of frequency ω , only if $\omega < \omega_0$. If x is the relative separation of charges on a dipole, then mathematically

$$m \frac{d^2 x}{dt^2} + \gamma \frac{dx}{dt} + \omega_0^2 x = -eE \exp(-i\omega t) \quad (1. 16)$$

The steady state solution of the above equation is

$$x = -\frac{eE}{m\{(\omega_0^2 - \omega^2) - i\gamma\omega\}} \exp(-i\omega t) \quad (1. 17)$$

The displacement x is proportional to polarisability α_D .

Polarisability can be written as

$$\alpha_D = e \frac{x}{E} \quad (1.18)$$

Then the susceptibility is

$$\chi = \frac{Ne}{\epsilon_0} \left(\frac{x}{E} \right) \quad (1.19)$$

Hence

$$\chi = \frac{Ne^2}{m\epsilon_0} \left\{ \frac{\omega_o^2 - \omega^2}{(\omega_o^2 - \omega^2)^2 + \gamma^2 \omega^2} - \frac{i\gamma\omega}{(\omega_o^2 - \omega^2)^2 + \gamma^2 \omega^2} \right\} \quad (1.20)$$

The dielectric constant is related to susceptibility as

$$\epsilon_r - 1 = \chi \quad \text{or} \quad \epsilon_r = 1 + \chi \quad (1.21)$$

The complex dielectric constant $\epsilon^* = \epsilon_r - i\epsilon_r''$ (1.22)

Hence we can write

$$\varepsilon_r = 1 + \frac{Ne^2}{m\varepsilon_0} \left\{ \frac{\omega_0^2 - \omega^2}{(\omega_0^2 - \omega^2)^2 + \gamma^2 \omega^2} \right\} \quad (1.23)$$

$$\varepsilon_r'' = \frac{Ne^2}{m\varepsilon_0} \left\{ \frac{\gamma\omega}{(\omega_0^2 - \omega^2)^2 + \gamma^2 \omega^2} \right\} \quad (1.24)$$

The above equations are known as dielectric dispersion formula. The peaking of ε'' shows that the loss is maximum at $\omega = \omega_0$.

The following dispersion relations can be obtained from the classical theory

$$\varepsilon_r = \varepsilon_\infty + \sum_i \frac{4\pi\rho_i\omega_i^2(\omega_i^2 - \omega^2)}{(\omega_i^2 - \omega^2)^2 + \gamma_i^2\omega_i^2} \quad (1.25)$$

$$\varepsilon_r'' = \sum_i \frac{4\pi\rho_i\omega_i\gamma_i\omega}{(\omega_i^2 - \omega^2)^2 + \gamma_i^2\omega_i^2} \quad (1.26)$$

where $4\pi\rho_i$ is the strength of oscillation of the i^{th} dipole, ω_i its natural frequency of oscillation and ω is the frequency of the external field.

1.4.2 Relaxation Absorption

The phenomenon of dielectric relaxation arises only within polar molecules. If a permanent dipole is oriented in an electric field and is then displaced, it will vibrate about the field direction and eventually by interaction with its surroundings it will relax back to the original position. The Debye expressions for the relaxation mechanism are [15]

$$\epsilon = \epsilon_{\infty} + \frac{\epsilon_s - \epsilon_{\infty}}{1 + \omega^2 \tau^2} \quad (1.27)$$

and

$$\epsilon'' = \frac{(\epsilon_s - \epsilon_{\infty})\omega\tau}{1 + \omega^2 \tau^2} \quad (1.28)$$

where ϵ_s is the low frequency(static) dielectric constant and ϵ_{∞} is the dielectric constant at very high frequency and τ is the relaxation time. These two phenomena gives rise to a frequency dependant dielectric constant in materials.

1.5 DIELECTRIC CONSTANT

Consider unit volume of a material containing N atoms. When a dielectric is subjected to an external electric field E_{ext} dipole moments are induced inside the material. Let P be the dielectric polarisation, which is equal to the total dipole moment induced in the material by the electric field. The total polarisation

$$P = N\alpha E_{local} \quad (1.29)$$

It can be shown that the local field acting on the dipoles

$$E_{local} = E_{Ext} + 4\pi \frac{P}{3} \quad (1.30)$$

where E_{local} is the local electric field, E_{ext} is the external electric field, P -polarisation

The dipole moment of a single atom p is proportional to the field. $p = \alpha E_{local}$ where α is the electrical polarisability of the atom. The total polarisation of an insulator containing N atoms is

$$\sum_{i=1}^n n_i \alpha_i E_{local} \quad (1.31)$$

where n_i is the number of i atoms having polarisabilities α_i and acted on by local field E_{local} . Hence from equations (22) and (23), by rearranging terms we can obtain the Clausius - Massotti equation

$$\frac{\epsilon_r - 1}{\epsilon_r + 2} = \frac{4\pi}{3} \sum_i n_i \alpha_i \quad (1.32)$$

From the expression polarisabilities are additive. The additive relation is valid for electronic, ionic and dipolar polarisation. Hence expression can be written in the total polarisability form. If N is the number of atoms or ions per unit volume

$$\frac{\epsilon_r - 1}{\epsilon_r + 2} = \frac{4\pi}{3} N\alpha \quad (1.33)$$

The above formula gives Clausius-Massotti relation.

In other words

$$\epsilon_r = \frac{3 + 8\pi N\alpha}{3 - 4\pi N\alpha} \quad (1.34)$$

But $N = 1/V_m$

Hence

$$\epsilon_r = \frac{3 + \frac{8\pi\alpha}{V_m}}{3 - \frac{4\pi N\alpha}{V_m}} \quad (1.35)$$

which simplifies to

$$\epsilon_r = \frac{3V_m + 8\pi\alpha}{3V_m - 8\pi\alpha} \quad (1.36)$$

The above expression gives the dielectric constant in relation with molar volume in \AA^3 and α gives the total dielectric polarisability of individual ions using Shannon's dielectric polarisability [77].

1.5.1 Determination of ϵ_r

From the classical dispersion equation, at frequencies very much less than the oscillation frequency of dipole, i. e, when $\omega \ll \omega_i$, it can be shown that ϵ_r is independent of frequencies in the microwave range. Hence we can write

$$\epsilon' = \epsilon_\infty + \sum 4\pi\rho_i \quad (1.37)$$

where ϵ_∞ is the dielectric constant caused by electronic polarisability at very high frequencies and $4\pi\rho_i$ is the strength of oscillation. It can be understood that ϵ_r is a constant in the microwave region since it is independent of frequency. Using Far-Infrared spectroscopy the reflectance as well as transmittance can be recorded. From the reflection band, ϵ_r is calculated using Krammer- Kronig Analysis. The method gives an indirect estimation of the dielectric constant. In the microwave frequency region ϵ_r is measured from the resonance spectra using the resonance method. The methods used will be discussed in the next chapter.

1.6 QUALITY FACTOR (Q FACTOR)

The figure of merit for assessing the performance or quality of a resonator

is Q factor. It is a measure of energy loss or dissipation per cycle as compared to the energy stored in the fields inside the resonator. Q factor is defined by

$$Q = \frac{\text{Maximum energy stored per cycle}}{\text{Average energy-Dissipated per cycle}} \quad (1.38)$$

$$Q = \frac{2\pi W_0}{PT} = \frac{\omega_0 W_0}{P} \quad (1.39)$$

where W_0 is the stored energy, P is power dissipation, ω_0 is resonant radian

frequency and period $T = \frac{2\pi}{\omega_0}$

To a very good approximation, it can be shown that

$$Q = \frac{\omega_0}{\Delta\omega} = \frac{f_0}{\Delta f} \quad (1.40)$$

When a resonant circuit or cavity is used as a load in a microwave circuit, several different Q factors can be defined. First Q accounts for internal losses. It is the unloaded Q factor Q_0 . Next external Q factor Q_e , accounts for external losses. When the resonator is used in actual circuit there arises the loaded Q factor, Q_L which is the overall Q factor and includes both internal and external losses.

The dielectric Q factor Q_d for homogeneous dielectric material is given by

$$Q_d = \frac{1}{\tan \delta} \quad (1.41)$$

For a dielectric loaded cavity where cavity containing an aperture

$$\frac{1}{Q_0} = \frac{1}{Q_c} + \frac{1}{Q_d} + \frac{1}{Q_r} \quad (1.42)$$

where Q_c is the conduction Q factor, Q_d is the dielectric Q factor and Q_r the radiation Q factor. When the resonator is connected to load

$$\frac{1}{Q_L} = \frac{1}{Q_e} + \frac{1}{Q_o} \quad (1.43)$$

where Q_L is the loaded Q factor, Q_e the external Q factor and Q_o the unloaded Q factor.

The Q factor can be determined by the resonance method, which will be described in the next chapter.

1.6.1 Determination of Q factor

It follows from classical dispersion relation [7] where $\omega < \omega_i$

$$\varepsilon''(\omega) = \sum_i \frac{4\pi\rho_i\gamma_i\omega}{\omega_i^2} \quad (1.44)$$

The above equation shows that $\varepsilon''(\omega)$ is directly proportional to applied frequency. That means loss factor increases with frequency. At microwave frequencies, for an ideal DR material $Q \approx \frac{1}{\tan \delta}$. Hence a decrease in Q factor with respect to frequency in the microwave range.

ε' and ε'' can be determined by FTIR reflectance spectra using Krammer-Kronig analysis. However far infrared reflectivity spectra has limited sensitivity to the weak modes in the submillimeter (SMM) region ($10-100\text{cm}^{-1}$). Hence a generalised factorised four parameter oscillator model of complex permittivity is used.

$$\varepsilon^*(\omega) = \varepsilon_{\infty} \prod_j \frac{\omega_{LOj}^2 - \omega^2 + i\omega\gamma_{LOj}}{\omega_{TOj}^2 - \omega^2 + i\omega\gamma_{TOj}} \quad (1.45)$$

Here reflectivity spectra are fitted together with the transmission spectra. The reason for simultaneous fitting is that in many cases the parameters of a good reflectivity spectra do not fit satisfactorily with transmission spectra.

1.7 TEMPERATURE COEFFICIENT OF RESONANT FREQUENCY

The stability of the resonant frequency of a resonator with temperature is an important parameter for practical applications. The temperature coefficient of

resonant frequency is defined as

$$\tau_f = \frac{1}{f} \frac{\Delta f}{\Delta T} \quad (1.46)$$

The unit of τ_f is in parts per million per Kelvin. It can be shown that in the case of cavity resonators, the temperature coefficient of resonant frequency $\tau_f = -\alpha_T$.

In the case of a dielectric resonator we can write $\lambda = \lambda_0 \epsilon_r^{-1/2} = 2L$. WE can show that $\tau_f = -(\tau_\epsilon / 2 + \alpha_T)$. In order to get $\tau_f = 0$, $\tau_\epsilon = -2\alpha_T$.

1.7.1 Determination of τ_f

The τ_f can be determined by finding τ_ϵ at low frequencies from the change in capacitance with temperature and also by finding out linear expansivity α_T . In the cases of dielectric resonators we can determine τ_f directly by noting the change in resonant frequency with temperature. The method we have used is described in the next chapter.

1.8 DIELECTRIC RESONATORS AT MICROWAVE FREQUENCIES

For practical applications DRs are developed in different shapes. The most popular one is disk shaped DRs. When a spectrum of microwave frequencies is applied several modes get excited. DRs supports not only the transverse electric (TE) and transverse magnetic (TM) modes but also a family of hybrid (HEM) modes. Among the various modes the $TE_{01\delta}$ is the most commonly used mode. The subscripts denote the azimuthal, radial and axial modes respectively. Due to the finite dielectric constant a part of the field exists outside the DR. Hence the subscript δ is used, which is not a whole number.

In $TE_{01\delta}$ mode, the magnetic field lines are confined in the meridian plane. The electric field lines are concentric circles around z-axis. An exact solution to Maxwell's equation to such simple shapes such as cylindrical DR is not simple. Hence numerical techniques are employed to get exact solutions.

In the case of DRs the presence of evanescent fields helps for coupling or tuning with adjacent DRs. Different types of coupling are employed in DR circuits. DR coupled to a micro strip line is most commonly used configuration. Coupling between adjacent DRs is made easy because of the presence of evanescent field. The resonant frequency of a DR can be controlled by changing its length, diameter or both. Once DR is put into use tuning will be required to get the desired frequency. DRs can be tuned using mechanical structures, varactors or other electronic devices.

1. 9 DIELECTRIC RESONATOR MATERIALS

There are a number of research works for developing new ceramics and also for improving the dielectric properties. $(\text{Mg}, \text{Ca})\text{TiO}_3$ [42-47] has been attempted as DR material. Complex perovskite [48-52] materials showed excellent microwave dielectric properties. $\text{Ba}(\text{Mg}_{1/3}\text{Ta}_{2/3})\text{O}_3$ showed high dielectric constant of 25 with high Q factor as high as $Q \times f = 350000$ and near to zero τ_f . $\text{Ba}(\text{Zn}_{1/3}\text{Ta}_{2/3})\text{O}_3$ showed high dielectric constant 29 with high Q x f as high as 150000 and near to zero τ_f , BaTi_4O_9 , $\text{Ba}_2\text{Ti}_9\text{O}_{20}$ [53-59] $(\text{Zr}, \text{Sn})\text{TiO}_4$ [60-62] ceramics also gained commercial acceptance. Complex perovskite type materials showed excellent microwave dielectric properties. All these ceramics possess $\epsilon_r < 45$ and for applications near 1 GHz their size will be large. Hence tungsten Bronze type $\text{BaO-RE}_2\text{O}_3\text{-TiO}_2$ [63-72] mixed oxide with high dielectric constant > 80 is used in this range. Still the search for new materials is going on to get ceramics with improved properties.

1. 10 APPLICATIONS OF DIELECTRIC RESONATORS

Coupling to the dielectric resonator is easy because of field existing outside the DR. The strength of coupling is usually determined by the geometrical placing of the resonator.

1.10.1 Dielectric Resonator Oscillators (DRO)

The performance of modern radar and communication systems is determined by the spectral purity of the local oscillators in the transmitters and receivers. Hence high Q ceramics having low value of residual noise are required. A DR can confine most of the electromagnetic energy within itself and is suitable for oscillator applications. Single crystal sapphire is known to have lowest microwave loss. In certain applications such as frequency modulated continuous wave radar sources, narrow band mode communication systems and phase locked loop systems need electronic tuning with bandwidth 0.1 to 1%. The schematic diagram of an oscillator using DR is shown in Fig. 1. 3.

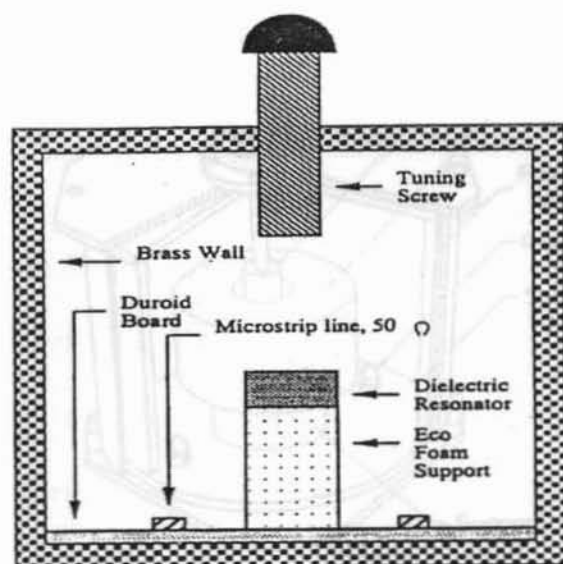


Fig. 1. 3 Schematic diagram of an oscillator using DR

1. 11. 2 Dielectric Resonator Filters

The high-unloaded Q factor of dielectric resonators makes it possible to produce filters with very narrow bandwidth and very low insertion loss. A variety of filter configurations are developed. The major disadvantage of DR band pass filters is that the necessary encapsulation in a metal case to minimize radiation loss makes them bulky, especially for medium and low frequencies. Therefore several miniaturisation techniques such as multimode reuse of space, supplementary energy resonators, low stored energy filter using transversal filter and mirror image techniques are developed. The schematic diagram of a filter using DR is shown in Fig. 1. 4

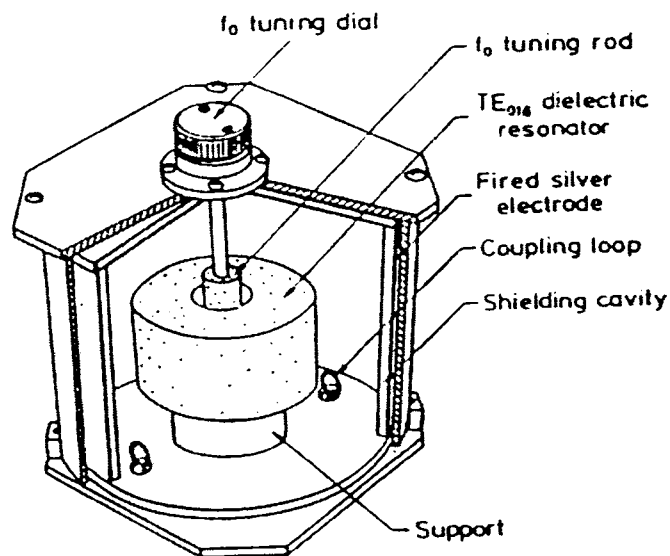


Fig. 1. 4 Schematic diagram of a filter using DR

1. 11. 3 Whispering Gallery Mode (WGM) DRs

The use of conventional DR modes is significantly limited at millimeter wavelengths because the resonator dimensions are too small to be easily realized. WGM DRs overcome this drawback because they have oversized dimensions for millimeter wavelengths. They suppress spurious modes that leak out the resonator and can be absorbed without perturbing the desired ones. This mode is described as a comprising wave running against the concave side of the cylindrical boundaries of the resonator. The waves move essentially in the plane of the circular cross section.

1. 11. 4 Dielectric Resonator Antennas (DRAs)

DRAs are found to be advantageous in terms of small size, mechanical simplicity, high radiation efficiency, relatively large bandwidth, simple coupling schemes to nearly all commonly used transmission lines, and can obtain different radiation characteristics using different modes. The radiation Q factor of a DRA depends on its excitation modes as well as the dielectric constant of the ceramic material. DRs of relatively low ϵ_r are mostly used in DR applications. On the other hand, high ϵ_r DRs result in low profile DRAs with low resonant frequency is obtained.

REFERENCES

- [1] R. D. Richtmeyer, *J. Appl. Phys.*, **10** (1939) 391
- [2] A. Okaya, *Proc. IRE.*, **48**(1960) 192
- [3] A. Okaya and L. F. Barash, *Proc. IRE*, **50** (1962) 2081
- [4] S. B. Cohen, *IEEE Trans. Microwave Theory Tech.*, **MTT-16** (1968) 218
- [5] D. J. Masse, R.A. Purcel, D. W. Ready, E. A. Maguire and C. D. Hartwig,
Proc. IEEE **59** (1971) 1628
- [6] W. G. Spitzer, R. C. Miller, D. A. Kleinman and L. E. Howarth, *Phys. Rev.*,
126 (1962) 1720
- [7] R. Kudesia, Structure property relationship in zirconium tin titanate
microwave dielectrics, Ph.D. thesis, Alfred University, New York (1992)
- [8] W. Wersing, *Electronic Ceramics*, Ed B.C.H. Steele (1991) Elsevier Pub
Co. Inc.
- [9] Y. Kobayashi and M. Katoh, *IEEE Microwave Theory Tech.*, **MTT-33**
(1985) 586
- [10] D. Kajfez and P. Guillon, *Dielectric Resonators*, (1986), Artech House,
Massachusetts.
- [11] W. Wersing, *Electronic Ceramics*, Ed. By B.C.H. Steele, Elsevier Pub. Co.
Inc., (1991) 67
- [12] W. Wersing, *Current Opinion in Solid State and Materials Science*, **1** (1996)
715
- [13] L. A. Trinogga. G. Kaizhou and I. C. Hunter, *Practical microstrip circuit*

- design, Ellis Horwood (1991)
- [14] A. J. Moulson and J. M. Herbert, *Electroceramics*, Chapman and Hall (1990)
- [15] H. M. Rosenberg, *The solid state*, Oxford University Press, (1988) New York
- [16] L. L. Hench and J. K. West, *Principles of Electronic ceramics*, John Wiley and Sons, (1990) Singapore
- [17] Y. Ishikawa, H. Tamura, T. Nishikawa and K. Wakino, *Ferroelectrics*, **135** (1992) 371
- [18] J. Takahashi, K. Kageyama and K. Kodaira, *Jpn. J. Appl. Phys.*, **32** (1993) 4327
- [19] T. Negas, Y. Yeager, S. Bell, N. Coats and I. Minis, *Am. Ceram. Soc. Bull.*, **72** (1993) 80
- [20] J. K. Plourdie and C. L. Ren, *IEEE Trans. Microwave Theory Tech.*, **MTT-29** (1981) 54
- [21] R. Freer, *Silicates Industriels*, **9-10** (1993) 191
- [22] S. Nomura, *Ferroelectrics*, **49** (1983) 61
- [23] K. Wakino, T. Nishikawa, Y. Ishikawa and H. Tamura, *Br. Ceram. Trans. J.*, **89** (1990) 39
- [24] K. Wakino and H. Tamura, *Ceram. Trans.*, **15** (1990) 305
- [25] Y. Konishi, *Proc. IEEE* **79** (1991) 726
- [26] M. Mizan, *Proc. IEEE Freq. Control Symp.*, (1992) 409
- [27] A. P. S. Khanna, *Proc. 41st Annual Freq. Control. Symp.*, (1987) 478
- [28] H. Abe, Y. Takayama, A. Higashisaka and H. Takamizawa, *IEEE Trans. On*

Microwave Theory. Tech., **MTT-26** (1978) 156

- [29] C. Tsironis, *IEEE Trans. Microwave Theory Tech.*, **MTT-33** (1985) 310
- [30] D. G. Blair, M. E. Costa, A. N. Luiten, A. G. Mann and M. E. Tobar *Proc. EFTF '93*
- [31] M. E. Tobar, A. J. Gibbs, S. Edwards and J. H. Searles, *IEEE Trans. On Ultrasonics, Ferroelectrics and Frequency Control*, **41** (1994) 391
- [32] A. M. Pavio and M. A. Smith, *IEEE Trans. Microwave Theory Tech.*, **MTT-33** (1985) 1346
- [33] A. P. S. Khanna, *Microwaves and RF*, (1992) 120
- [34] W. H. Harrison, *IEEE Trans. Microwave Theory Tech.*, **MTT-16** (1968) 210
- [35] S.B. Cohn, *IEEE Trans. Microwave Theory Tech.*, **MTT-16** (1968) 218
- [36] T. D. Iveland, *IEEE Trans. Microwave Theory Tech.*, **MTT-19** (1971) 643
- [37] A. Podcameni and L .F. M. Conrado, *IEEE Trans. Microwave Theory Tech.*, **MTT-33** (1985) 1329
- [38] V. Madrangeas, M. Aubourg, P. Guillon, S. Vigneron and B. Theron, *IEEE Trans. Microwave Theory Tech.*, **MTT-40** (1992) 120
- [39] J. P. Cousti, S. Verdeyme, M. Aubourg and P. Guillon, *IEEE Trans. Microwave Theory Tech.*, **MTT-40** (1992) 925
- [40] K. Wakino, T. Nishikawa and Y. Nishikawa, *IEEE Trans. Microwave Theory Tech.*, **MTT- 42** (1994) 1295
- [41] M. A. Gerdine, *IEEE Trans. Microwave Theory Tech.*, **MTT-17** (1969)

- [42] H. Tamura, J. Hattori, T. Nishikawa and K. Wakino, *Jpn. J. Appl. Phys.*,
28 (1989) 2528
- [43] A. E. Paladino, *J. Am. Ceram. Soc.*, 54 (1971) 168
- [44] V. M. Ferreira and J. L. Baptista, *Mater. Res. Bull.*, 29 (1994) 1077
- [45] R. C. Kell, A. C. Greenham, and G.C. E. Olds, *J. Am. Ceram. Soc.*,
56 (1973) 352
- [46] G. R. Shelton, A. S. Creamer, and E. N. Bunting, *J. Am. Ceram. Soc.*,
31 (1948) 205
- [47] H. Takahashi, Y. Baba, K. Esaki, Y. Okamoto, K. Shibata, K. Kuroki, and S.
Nakano, *Jpn. J. Appl. Phys.*, 30 (9B)(1991) 2339
- [48] V. M. Ferreira, F. Azhough, J. L. Baptista and R. Freer, *Ferroelectrics*,
133 (1992) 127
- [49] M. Takata and K. Kageyama, *J. Am. Ceram. Soc.*, 72 (1989) 1955
- [50] H. Kagata and J. Kato, *Jpn. J. Appl. Phys.*, 33 (1994) 5463
- [51] M. Onoda, J. Kuwatta, K. Kaneta, K. Toyama and S. Nomura, *Jpn. J. Appl.
Phys.*, 21 (1982) 1707
- [52] S. Nomura, K. Toyama, and K. Kaneta, *Jpn. J. Appl. Phys.*, 21 (1982) L 624
- [53] Y. Kawashima, M. Nishida, I. Ueda and H. Ouchi, *J. Am. Ceram. Soc.*,
66 (1983) 421
- [54] H. M. O'Bryan Jr., J. Thomson Jr. and J. K. Plourde, *J. Am. Ceram. Soc.*,
57 (1974) 450
- [55] J. K. Plourde, D. F. Linn, H. M. O'Bryan Jr. and J. Thomson Jr., *J. Am.
Ceram. Soc.*, 58 (1975) 418

- [56] D. Hennings and P. Schnabel, *Philips J. Res.*, **38** (1983) 295
- [57] S. Nomura, K. Toyama and K. Kaneta, *Jpn. J. Appl. Phys.*, **22** (1983) 1125
- [58] C. Chatterjee, A. N. Virkar and A. Paul., *J. Mater. Sci. Lett.*, **9** (1990)
1049
- [59] S. Hirano, T. Hayashi, K. Kikuta and J. Otsuka, *Ceram. Trans.*, **12** (1990)
733
- [60] S. G. Mhaisalkar, D. W. Ready and S. A. Akbar, *J. Am. Ceram. Soc.*, **74**
(1991) 1894
- [61] G. Wolfram and H. E. Gobel, *Mater. Res. Bull.*, **16** (1981) 1455
- [62] K. Wakino, M. Minai and H. Tamura, *J. Am. Ceram. Soc.*, **67** (1984) 278
- [63] R. Kudesia, Ph. D. Thesis, Alfred University (1992)
- [64] S. Marzullo and E. N. Bunting, *J. Am. Ceram. Soc.*, **41** (1958) 40
- [65] S. Nishigaki, H. Kato, S. Yano and R. Kamimura, *Am. Ceram. Soc. Bull.*,
66 (1987) 1405
- [66] J. P. Mercurio, M. Manier and B. Frit, *Mater. Lett.*, **8** (1989).
- [67] J. Kato, H. Kagata and K. Nishimoto, *Jpn. J. Appl. Phys.*, **30** (1991) 2343
- [68] J. Kato, H. Kagata and K. Nishimoto, *Jpn. J. Appl. Phys.*, **31** (1992) 3136
- [69] P. Laffez, G. Desgardin and B. Raveau, *J. Mater. Sci.*, **27**(1992) 5229
- [70] H. Ohsato, S. Nishigaki, and T. Okuda, *Jpn. J. Appl. Phys.*, **31**(1992) 3136
- [71] K. Ezaki, Y. Baba, H. Takahashi, K. Shibata and S. Nakano, *Jpn. J. Appl.
Phys.*, **32** (1993) 4319
- [72] J. Takahashi, K. Kageyama and K. Kodaira, *Jpn. J. Appl. Phys.*, **32** (1993)
4327

- [73] H. Kagata, J. Kato, K. Ishimoto and T. Inoue *Jpn. J. Appl. Phys.*, **32** (1993) 4332
- [74] Fiedziuszko, A. Jelenski, *IEEE Trans. Microwave Theory Tech.*, **MTT-19** (1971) 778
- [75] S. B. Cohn, *IEEE Trans. Microwave Theory Tech.*, **MTT-16** (1968) 218
- [76] Y. Yee, *IEEE Trans. Microwave, Theory Tech.*, **MTT-13** (1965) 256
- [77] Y. Konishi, N. Hoshino, Y. Utsumi, *IEEE Trans. Microwave Theory Tech.*, **MTT-24** (1976) 112
- [78] T. Itoh, R. S. Rudokas, *IEEE Trans. Microwave Theory Tech.*, **MTT-25** (1977) 52
- [79] P. Guillon, Yves Garault, *IEEE Trans. Microwave Theory Tech.*, **MTT-25** (1977) 916
- [80] A. W. Glisson, D. Kajfez, J. James, *IEEE Trans Microwave Theory Tech.*, **MTT-3** (1983) 1023
- [81] M. Tsuji, H. Shigesawa and K. Takiyama, *IEEE Trans. Microwave Theory Tech.*, **MTT- 32** (1984) 628
- [82] R. K. Mongia, B. Bhat, *Electron. Lett.*, **21** (1985) 479
- [83] M. E. Tobar and A. G. Mann, *IEEE Trans. Microwave Theory Tech.*, **MTT-39** (1991) 2077
- [84] M. Yousefi, S. K. Choudhuri and S. S. Naeimi, *IEEE Trans Antenna. Prop.*, **42** (1994) 38
- [85] M. W. Pospieszalski, *IEEE Trans. Microwave Theory Tech.*, **MTT - 25** (1977) 228

Chapter 2

PREPARATION AND CHARACTERISATION

This chapter briefly describes the different preparation and characterisation methods used for ceramic microwave dielectric resonators.

2.1 CERAMIC PREPARATION

Almost all ceramics are compounds of the electropositive and electronegative elements of the periodic table. Mostly the bonding is ionic, but in a few cases covalent or metallic bonding occurs [1-4]. High heat resistance, electrically insulating or semiconducting with varying magnetic and dielectric properties, strong resistance to deformation and low toughness are the common features of these materials. Ceramics have inorganic structures. Almost all ceramics have definite crystal structure though there are cases like glass, which is amorphous in nature. Ceramics are polycrystalline materials, which contain fine crystalline grains, grain boundaries, impurities segregated in the grain boundaries as well as the grains, pores in the grains, grain boundaries and imperfections. The size of the grain depends on the size of the particles in the raw materials, the

impurities and sintering conditions. The strength of a ceramic is lowered by unusual grain growth and unusual large average grain size.

The ceramic preparation process involves different steps like powder forming, calcination, shaping and sintering. Standard preparation techniques are discussed below.

2. 1. 1 Powder forming

The making of the ceramic begins from the powder. The various methods of powder forming are shown in Table 2.1. The solid-state reaction method, which is employed in the present work, involves the following steps.

2. 1. 1. 1 Weighing of raw materials

The first step in the solid-state reaction method is to weigh the different powders which act as reactants according to the stoichiometry. The presence of impurities in the raw materials can affect reactivity as well as dielectric properties of the fired ceramics. The raw material purity of greater than 99 % is essential for obtaining phase pure compounds. Electronic Balance is used to obtain accuracy up to four decimal places.

Table 2. 1
Powder forming methods (After Ichinose et al. [2])

SOLID	Chemical Reaction	Solid state reaction
		Thermal Decomposition of solid
		Oxidation/Reduction
	Crushing	Mechanical crushing
		Chemical pulverising
LIQUID	Desolvent	Spray Dying
		Freeze Drying
		Emulsion
		Sol-Gel
	Precipitation	Coprecipitation
		Alkoxide
		Electrolysis
	Evaporation Condensation	
	GAS	Gas Phase Reduction
Gas phase oxidation		
Gas phase synthesis		

2.1.1.2 Mixing

Lack of homogeneity can affect the dielectric properties. Hence the raw materials constituting the batch must be intimately mixed. The mixing and milling eliminates agglomerates and reduces particle size. If agglomerates are present

they densify more rapidly resulting in pores. During the mixing process agglomerates are broken and defects are introduced into the grains that enhance diffusion mechanism. Therefore the mixture of powders is ground well and thoroughly mixed using distilled water or acetone. Ball mills are used for the mixing purpose. Zirconia balls are used in the present investigation.

2.1.1.2.1 Ball Milling

A process in which small particles are produced by reducing the size of larger ones by mechanical force is usually referred to as comminution. Comminution involves operation such as crushing, grinding and milling. The most efficient way to achieve size reduction of particles is by ball milling. Ball mills are categorised into various types depending on the method used to impart motion to the balls. Let us define two interrelated terms that are used in the process of ball milling. The first is the energy utilization of the milling method that is defined as the ratio of the new surface area created to the mechanical energy supplied. Second, we define, the rate of grinding as the amount of new surface area created per unit mass of the particle per unit time. A comminution method that has a high-energy utilization will also have a high rate of grinding so that the achievement of a given particle size will take a shorter time.

In the milling process, the particles experience mechanical stresses at their contact points due to compression, impact or shear with the milling medium or

with other particles. The mechanical stress leads to elastic and inelastic deformation. If the stresses exceed ultimate strength of the particle, it will fracture the particles. The mechanical energy supplied to the particle is used not only to create new surfaces but also to produce other physical changes in the particle.

Tumbling ball mills usually refer to simply as ball mills consisted of a slowly rotating horizontal jar that is partially filled with grinding media and particle to be ground. In a tumbling ball-mill the rate of grinding depends on a number of factors including mill parameters (diameter, speed, amount of milling media), properties of the milling media (size, hardness, shape) and the properties of the particles to be ground. Generally ball mills that run at low speed contain large balls, because most of the mechanical energy supplied to the particle is in the form of potential energy. Those run at higher speeds contain small balls because in this case most of the energy supplied to the particles is in the form of kinetic energy. The size of grinding medium is also an important consideration. The rate of grinding increases inversely as the radius of the balls. However balls must not be too small because they must impart sufficient mechanical energy to the particle to cause fracture. The rate of grinding depends upon the radii of the mill bottle and density of the milling media and initial particle size of the powder [32].

$$\text{Rate of grinding} \approx \frac{AR^{1/2} \rho d}{r} \quad (2.1)$$

where A = numerical constant that is specific to the mill being used, R = radius of the mill, ρ = density of the balls, d = particle size of the powder and r = radius of the balls. According to the above equation, the rate decreases with decreasing particle size, but after a finite time a practical grinding limit is reached.

For wet milling, a useful guide is for the balls and slurry together should occupy 50 % of the mill volume with the solid content of the slurry equal to 20-40%. For dry milling, for a quantity of balls filling about 50 % of the mill volume, the permissible charge content is 25 %. Wet milling has the advantage of higher energy utilisation (by 10-20 %) over dry milling. A further advantage is the ability to produce fracture of finer particles.

Chemical methods such as co-precipitation of mixed oxides, organic precursors and sol-gel process make the mixing effective on an atomic scale and yield optimum homogeneity [5]. But these methods are more expensive than mechanical mixing and the product consists of small crystals bound to agglomerates so that special conditions of calcination and deflocculation have to be adopted in order to get dense compacts.

2.1.1.3 Calcination

The next step involved in the preparation of ceramics is the calcination. Calcination is the intermediate heat treatment at a lower temperature prior to sintering. Hence it can be thought as a part of mixing. In some cases, when

powders of the compounds are available, the calcination step can be avoided and the powder can be directly compacted into a shape and sintered without prior heat treatment. The calcination conditions such as temperature, duration of heating and atmosphere are important factors controlling shrinkage during sintering. Though the final phases of interest may not be completely formed the calcination yields a consistent product.

2.1.1.4 Grinding

Grinding can be accomplished by any suitable means. It prepares the reacted material for ceramic forming. The grinding also helps to homogenise the compositional variations that may still exist or that may arise during calcination. Generally, grinding to somewhere around 1 to 10 μm is advisable. If the grind is coarser the ceramic can have larger intergranular voids and lower fired density. If grinding is too fine, the colloidal properties may interfere with subsequent forming operations. Generally for grinding purpose ball mill or mortar with pestle is used. In large scale operation a grinding medium is chosen that suffers very little wear. To produce dense ceramics various organic additives are added to the ground powder. These include binder(s) for strength, plasticisers that produce deformative granules and lubricants that mitigate frictional effects [24].

2.1.1.5 Shaping or forming

Forming or shaping is the process of making the powder in the desired form or shape. The various methods of shaping for various types of products are listed in Table 2.2.

Table 2. 2
Various shaping methods used in ceramic preparation
for various uses

i) dry pressing	small simple shapes
(ii) isostatic pressing	larger; more intricate shapes
(iii) calendaring	thin plates
(iv) extrusion	elongated shapes of constant cross section
(v) jiggering	large simple shapes
(vi) injection moulding	complex shapes
(vii) slip casting	mainly hollow shapes
(viii) band casting	thin plates and sheets
(ix) Silk screening	thin layers and substrates

Since the calcined product undergoes a limited amount of sintering, it is again thoroughly ground. The fine powder is then compacted into cylindrical specimen by dry-pressing. Compaction is done slowly to facilitate the escape of the entrapped air.

Powder pressing or die pressing is the most common method used for the production of the ceramic components [25]. The object of a pressing process is to form a net shaped homogeneously dense powder compact that is normally free of defects. A typical pressing operation has three basic steps

- (i) filling the die with powder
- (ii) compacting the powder to a specific size and
- (iii) ejecting the compact from the die.

Die filling/uniformity influences compaction density, which ultimately determines the size, shape, microstructure and properties of the final sintered product [26]. To optimise die filling and packing uniformity, free flowing grounded powders are generally used. During powder pressing, the compaction pressure promotes consolidation by granule rearrangement and granule deformation. The number of nearest neighbours, green density and compact strength all increase with increasing pressure while the volume and size of the porosity in the compact decrease [27-29]. Pressures of 50-150 MPa is common in ceramic forming.

Friction between the powder and die wall decreases the pressure available for compaction with increasing distance from the pressing punch. Since compact density is directly related to forming pressure, a forming pressure gradient becomes a density gradient in the compact [30]. Friction is influenced by the die material and its surface finish, nature of the powder and the organic additives used. Die wall friction effects can be minimised by simple shaped low aspect ratio parts. Internal and topical lubricants can aid processing. Expansion of a

compact upon ejection from the die also influences the ejection process. This expansion depends on the powder, the organic pressing additives, the pressing rate etc.

Binders have strong influence on the properties of granules, such as bulk density, flow rate, and compaction behaviour [29]. A good binder for ceramic applications should provide high green strength at a low level of usage. Green strength is controlled by the polymer-polymer and polymer ceramic powder interactions. Among binders for dry pressed ceramics, poly vinyl alcohol (PVA) and poly ethylene glycol (PEG) are the most popular. In comparison studies PVA binders generally provide high green strength. The PVA burn out on heating to about 600°C.

2. 1. 2 Sintering

Sintering is the densification process by firing by which the green compact achieves mechanical strength. As in calcination, the temperature, duration of firing, and atmosphere play an important role in the development of ceramic microstructure during sintering. The sintering converts the compacted powder into a denser structure.

The various sintering processes are:

- (1) Standard pressure sintering
- (2) Hot pressing
- (3) Hot isostatic pressing (HIP)
- (4) Atmospheric pressure sintering
- (5) Ultra high pressure sintering
- (6) Reaction sintering
- (7) Post-reaction sintering
- (8) Recrystallisation sintering
- (9) Chemical vapour deposition

The standard pressure sintering is usually called sintering. This method is inexpensive. Generally when ceramic powders are pressed and then heated, there is a certain temperature at which they begin to diffuse and shrinkage occurs resulting in densification. Usually the sintering temperature is a little below the melting point. Sintering processes can be divided into three large categories: (1) Solid phase sintering, (2) liquid phase sintering and (3) gas phases sintering. In solid state sintering mechanism, the bulk material transport can be by (i) volume diffusion (ii) grain boundary diffusion (iii) surface diffusion or (iv) evaporation condensation

During sintering the surface energy is reduced by transferring matter from the interior of grain to adjacent pores. Grain boundaries acts as vacancy sinks. Grain growth is also takes place parallel to densification, the main driving force of which is the reduction in the area of grain boundaries. If the material contains a

large fraction of lower-melting vitreous phases, then densification is accelerated by liquid phases sintering. During sintering if rapid growth of discontinuous grains occurs, porosity is trapped and results in incomplete densification.

2.1.2.1 Sintering aids

Impurities and additives can significantly affect the sintering process. Additives play an important role in sintering either by allowing densification to occur in shorter times or by inhibiting discontinuous grain growth and allowing pore elimination to proceed to completion. However use of additives is mostly empirical and experimental verification of their role is impossible due to the limited region over which they act.

2.1.3 Specific preparation methods

The preparation method employed for the ceramics presented in the fourth coming chapter, chapter 3, 4 and 5 is discussed below.

All the ceramics used in the present study have been prepared by the conventional solid state ceramic route. Starting materials are high purity (99.9 %) carbonates or oxides. The component carbonates or oxides were weighed as per the stoichiometry. The component powders were mixed by means of a ball mill

using distilled water as the wetting medium. Zirconia balls are used for the milling. The mixture is dried in an oven, and ground again. The mixed powder is calcined in alumina or platinum crucible at appropriately higher temperatures. During calcination the carbonates decompose and solid state reaction takes place. The calcined powder is thoroughly ground for about an hour into fine powder. 5-wt% PVA solution is added to the fine powder, dried and ground. This fine powder is uniaxially pressed into cylindrical compacts using tungsten carbide dies under 150 to 250 MPa pressure depending on the materials. Slow initial heating up to 800°C (400°C/h) is given to expel the PVA. During sintering a heating rate of 10°C/minute upto the sintering temperature is given. The sintering temperature and sintering duration are optimised after making several trial runs at different temperatures and duration and by density measurements and microstructure studies. The duration of sintering is normally 4 h and in some cases where densification is found poor, duration up to 8 h is given. The sintered compacts are polished and used for density measurements by Archimedes method, SEM and Microwave dielectric property measurements. The sintered compacts are powdered and used for XRD measurements.

2.2 MICROWAVE CHARACTERISATION OF DIELECTRIC RESONATORS

2.2.1 Introduction

There are various types of resonators, composed of conductor, dielectric or ferrite, of finite dimensions, which are capable of resonance when the wavelength of the electromagnetic field is related to the dimension. Generally every microwave resonator is fully characterised by three quantities: resonant frequency (f_0), quality factor (Q_0) and characteristic impedance (Z_0). These quantities represent intrinsic characteristics of the resonator irrespective of the external network to which the resonator is connected. In addition, stability of resonance with respect to temperature, power handling capacity etc. are also important from the application point of view. The resonator frequency is defined as the frequency at which the time average of the stored energy (E_{av}) in the electric field

$$E_{av} = \frac{\epsilon}{4} \int E \cdot E^* dV \quad (2.2)$$

and the time average of the stored energy (H_{av}) in the magnetic field(H)

$$H_{av} = \frac{\mu}{4} \int H.H^* dV \quad (2.3)$$

of the resonator are equal. This condition is fulfilled for an infinite number of discrete frequencies corresponding to separate modes of oscillation in the given microwave resonator. At resonant frequency, the reflection coefficient will become purely real and hence maximum power is transmitted by the resonator.

Typical resonance curves obtained in the reflection and transmission modes and the corresponding Smith chart (impedance chart) of resonator are shown in Fig. 2. 1.

In Fig 2. 1 (a) the resonator shows maximum transmission at the resonant frequency f_0 . Fig 2. 1 (c) shows the variation of the impedance of the resonator with frequency with the diameter of the larger circle as the real axis. The portion above this shows positive reactance and the portion below shows negative reactance. The resonance is displayed as a closed loop (small circle in Fig. 2. 1(c)). At the resonant frequency, since the impedance is purely real, the circle meets the real axis.

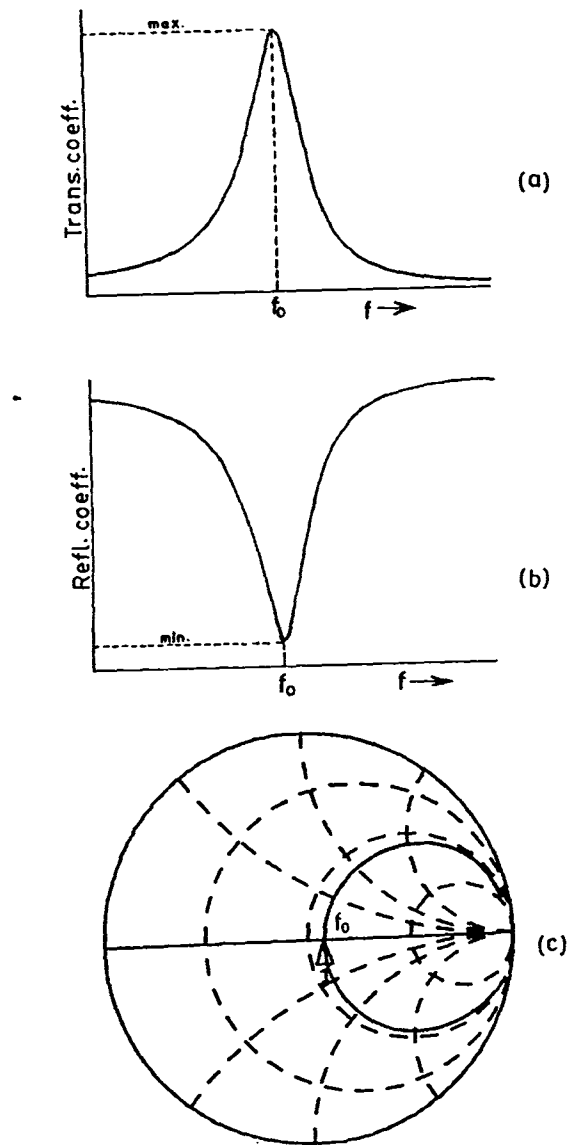


Fig. 2. 1 Typical resonance curves in (a) transmission and (b) reflection configurations of a DR. (c) Impedance chart (Smith chart) corresponding to the resonance

2. 2. 2 Material Characterization at Microwave Frequencies

Generally the methods for the measurement of dielectric and magnetic properties of materials at microwave frequencies can be subdivided into perturbation methods, optical methods, transmission line methods, reflection methods and exact resonance methods [6-9]. The choice of method or combination of methods will depend on the value of ϵ_r and loss factor, the amount of material available, the accuracy required, and whether the technique is required for research or routine measurements.

The perturbation methods are highly suitable for materials of small size since the material should not alter the field configuration considerably. These techniques are suitable for dielectric constants less than 10, although this range can be extended by an exact solution of the resonator containing the specimen. Hence this technique is not commonly used for DR characterisation.

Optical methods are applicable for below wavelength of one centimetre. Since this method requires large amount of material it is not suitable for DRs.

Transmission line techniques have been used widely. They have the serious disadvantage of the very small waveguide size used below 4 mm, which gives rise to practical difficulties. More over imperfections in the sample dimensions produce errors in the measurement.

In reflection methods, waves reflected from the dielectric are studied. When the dielectric constant becomes large, there occurs considerable error in the measurement of complex voltage reflection coefficient.

Exact resonance method is the most accurate method as compared to the above-mentioned methods for the measurement of DRs. In this method, the exact resonant frequency of the resonator is measured using different techniques [11,12]. From the resonant characteristics, all other parameters like ϵ_r , Q etc are determined. Special techniques of exact resonance methods are used in the present study, which are described in detail in the following sections.

2.2.2.1 Measurement of ϵ_r

Dielectric resonator possesses high $\epsilon_r > 20$ and Q factors above 2000 ($\tan\delta < 5 \times 10^{-4}$). Hence Hakki and Coleman [6] developed an exact resonance method known as 'rod resonator method', which is now widely used for measurements.

In this method a circular disc of material to be measured is inserted between two mathematically infinite conducting plates, as shown in Fig 2.2. The apparatus used by them is shown in Fig. 2. 3. If the dielectric material is isotropic then the characteristic equation for this resonant structure operating in the TE_{0n1} mode is written as

$$\alpha \frac{J_0(\alpha)}{J_1(\alpha)} = -\beta \frac{K_0(\beta)}{K_1(\beta)} \quad (2.4)$$

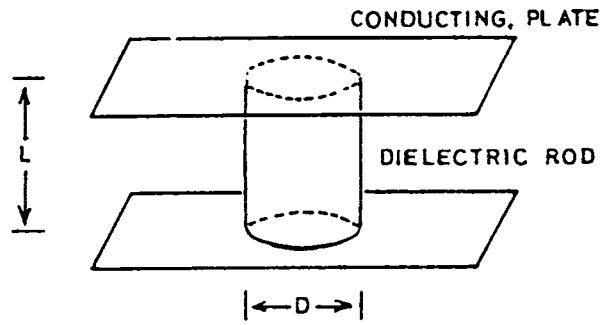


Fig. 2. 2 A dielectric rod kept end shorted between two mathematically infinite conducting plates (After Hakki and Coleman [6])

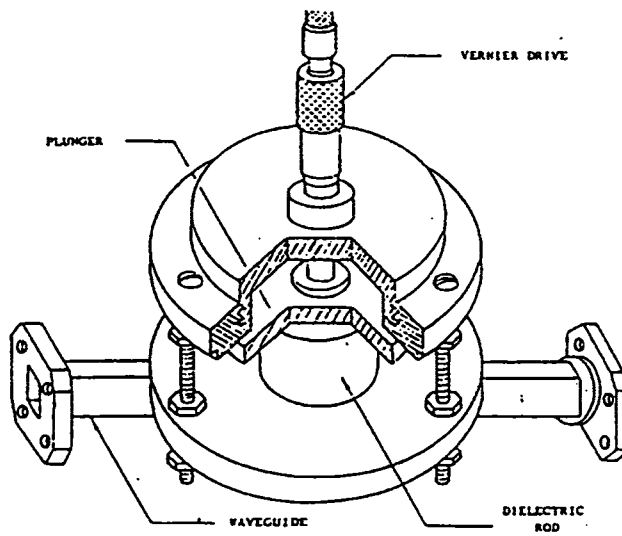


Fig. 2. 3 The dielectric rod cavity arrangement of Hakki and Coleman used for ϵ_r measurement of DRs

where $J_0(\alpha)$ and $J_1(\alpha)$ are Bessel functions of the first kind of orders zero and one respectively. The $K_0(\beta)$ and $K_1(\beta)$ are the modified Bessel functions of the second kind of order zero and one respectively. The parameter α and β depend on the geometry, the resonant wavelength inside and outside the DR respectively and dielectric properties. Thus

$$\alpha = \frac{\pi D}{\lambda_0} \left[\epsilon_r - \left(\frac{l \lambda_0}{2L} \right)^2 \right]^{1/2} \quad (2.5)$$

$$\beta = \frac{\pi D}{\lambda_0} \left[\left(\frac{l \lambda_0}{2L} \right)^2 - 1 \right]^{1/2} \quad (2.6)$$

where

l = the longitudinal variations of the field along the axis

L = Length of the DR

D = Diameter of the DR

λ_0 = free space resonant wave length

The characteristic equation is a transcendental equation and hence a graphical solution is necessary [6]. Corresponding to each value of β there are infinite number of (α_n) that solves the characteristic equation. Hakki and Coleman obtained a mode chart showing the variation of first six α values as a function of β and are shown in Fig. 2. 4.

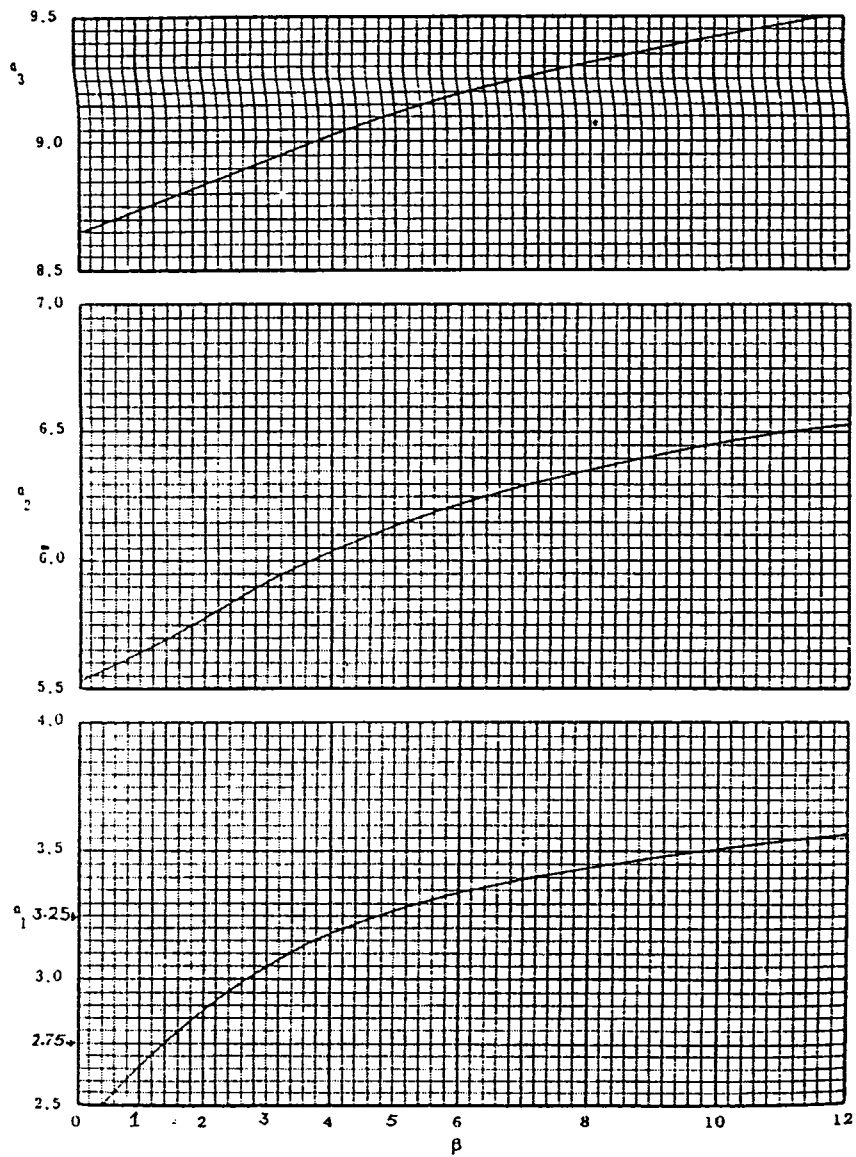


Fig. 2.4 Mode charts of Hakki and Coleman giving α_1 , α_2 and α_3 as functions of β .

Hakki and Coleman used an iris coupling from a wave guide to couple microwave to the DR (see Fig 2. 3). Later Courtney [7] modified the method using two horizontally oriented E field probes for coupling microwaves to the DRs, as shown in Fig. 2.5.

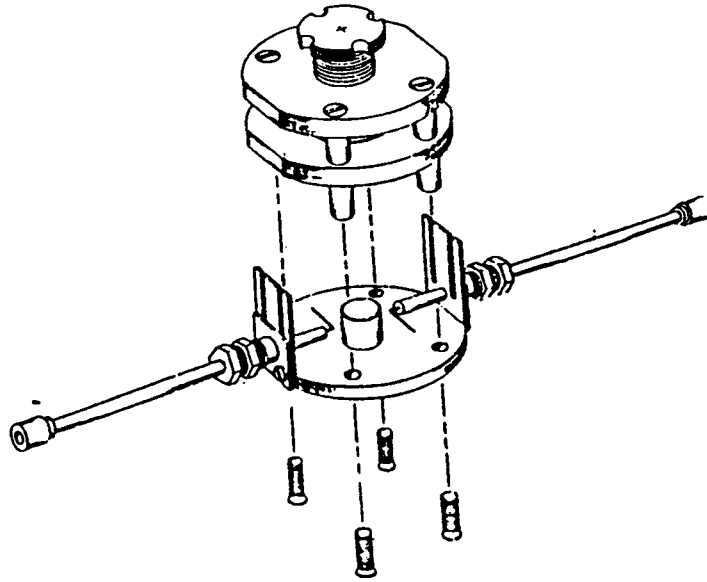


Fig. 2. 5 Exploded view of the dielectric post resonator used by Courtney [Ref. 7] showing the DR and E field probes.

This helped to span a wide range of frequencies, since there is no cut-off frequency for coaxial lines. Courtney [7] and Cohn and Kelly [9] showed that since TE_{011} modes are used for the calculation of ϵ_r , the effect of air gap between the dielectric and the conducting plate is negligible. In the end shorted condition the E field becomes zero close to the metal wall and electric energy vanishes in the air gap.

In the present work, A vector Network Analyser, HP 8510 C is used for taking measurements at microwave frequencies. The schematic view of the DR under end shorted condition and the coupling probes is shown in Fig. 2. 6.

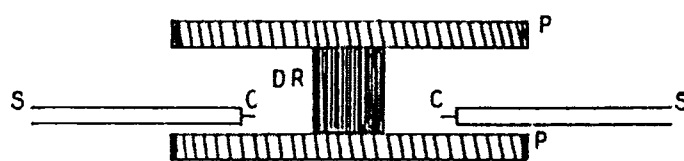


Fig. 2. 6 Schematic view of the DR between two metallic plates and the coupling probes

The photograph of the actual set up is shown in Fig. 2.7 (a). In the actual measurements a cylindrical specimen placed between the conducting plates and two probes from the sides.

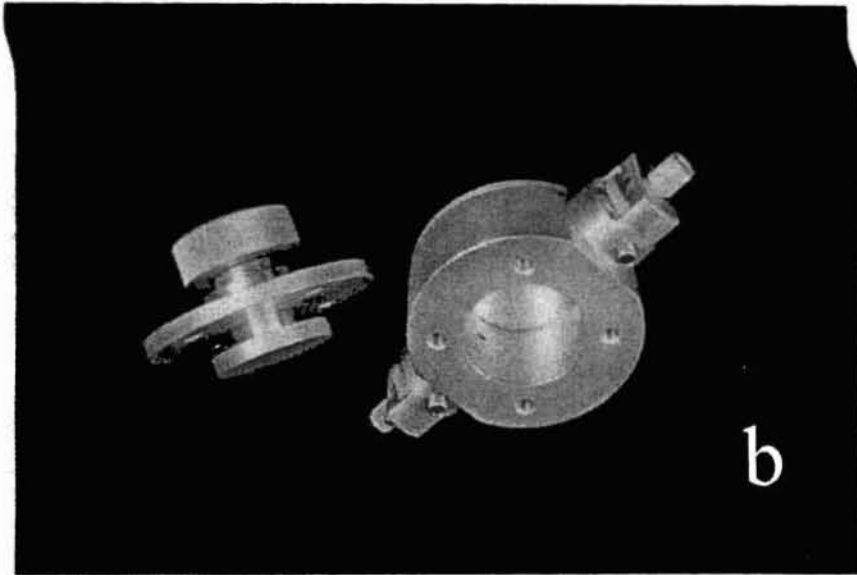
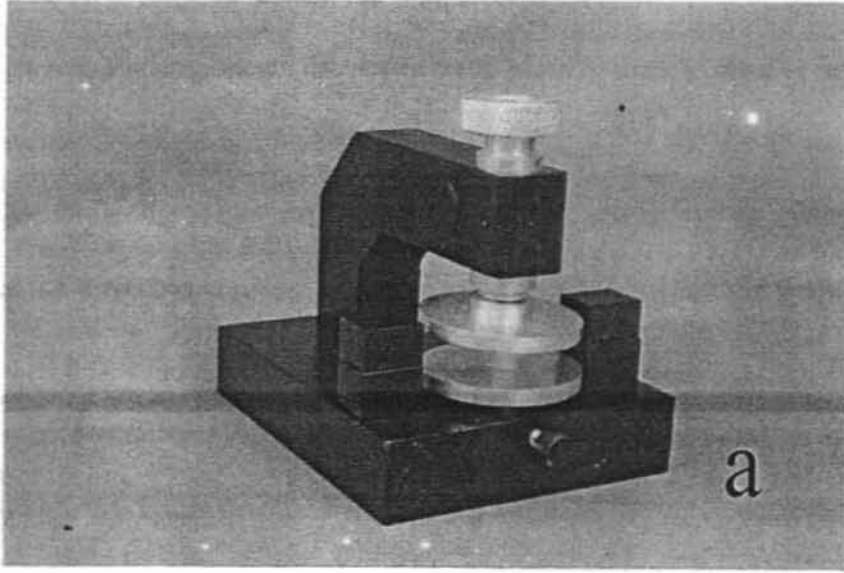


Fig. 2. 7 The Photographs show (a) the set up used for DR measurements at the end shorted condition (b) the cavity set up used for Q factor measurements

The specimen is placed approximately symmetrical with the two probes.
The resonant modes are visualised by giving a wide frequency range by adjusting

the Network Analyser. To select the TE_{011} resonance from the several modes having non zero E_z components the upper metal plate is slightly tilted to introduce an air gap. As the plate is tilted all the TM modes move rapidly to the higher frequencies while the TE_{011} mode remains almost stationary. In most of the situations, the dielectric constant is known approximately so that the frequency of the TE_{011} resonance can be predicted. After identifying the TE_{011} resonant frequency or central frequency (f_0) the span around f_0 is reduced as much as possible to get maximum resolution. The 3 dB width of the curve decreases and a stage of saturation is reached when the width will remain the least possible. The coupling loops are fixed at this position and the centre frequency can be noted corresponding to the maxima as f_0 . By knowing the diameter 'D' and length 'L' of the sample β is calculated using equation 2. 6. From the mode chart the value of α_1 corresponding to β_1 value is noted. The dielectric constant ϵ_r is calculated using the following equation.

$$\epsilon_r = 1 + \left(\frac{\lambda_0}{\pi D}\right)^2 (\alpha_1^2 + \beta_1^2) \quad (2. 7)$$

Maximum size of the DR sample for measurement is limited by the diameter of the shorting plates and minimum size is determined by the diameter of the coupling probes. The dielectric constant can be calculated automatically using HP 9000, 300 series instrumentation computer, using a computer program. The accuracy of the method depends on the accuracy in measuring the dimensions of the DR samples and the resonant frequency. The TE_{011} resonance of a standard sample with $\epsilon_r=76$ is shown in Fig. 2.8.

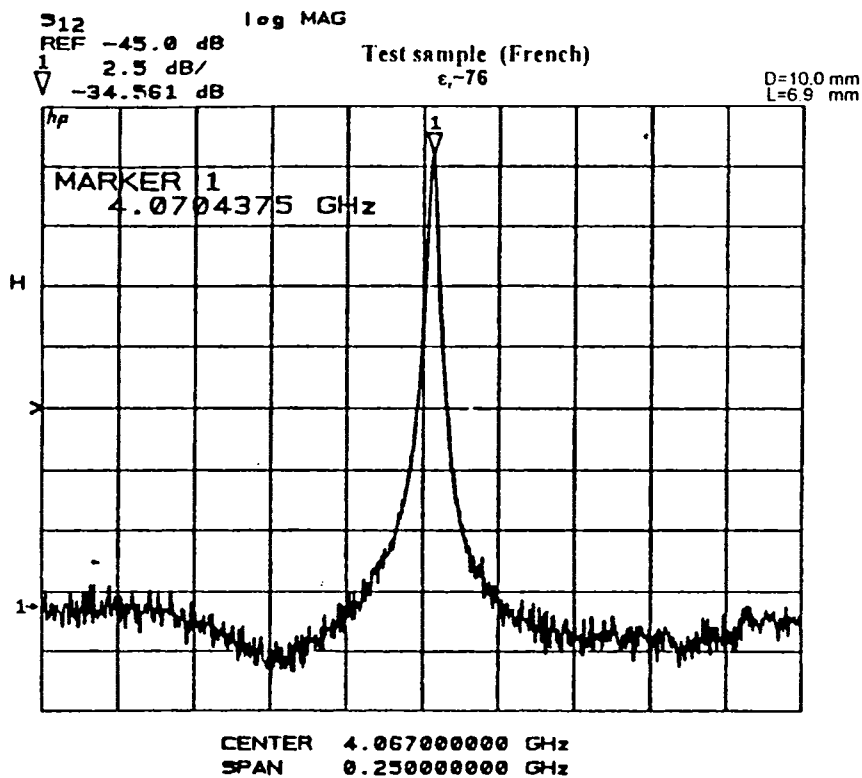


Fig 2. 8 TE_{011} resonance of standard sample with $\epsilon_r \sim 76$

2. 2. 2 Measurement of quality factor (Q)

Many researchers (6,8,10-20) proposed different techniques to calculate $\tan\delta$ or quality factor (Q) of the resonator material. In all these techniques the quality factor is increased by reducing loss due to radiation and metallic conductivity. For a DR, the quality factor measured for the TE_{011} mode using the parallel plate rod resonator is very low since there occurs losses due to conducting

plates, radiation etc. under end shorted condition. (21-22). This can be mathematically written as

$$\frac{1}{Q_L} = \frac{1}{Q_D} + \frac{1}{Q_c} + \frac{1}{Q_r} + \frac{1}{Q_{EXT}} \quad (2.8)$$

where $\frac{1}{Q_L}$ is the total loss of the system, $\frac{1}{Q_D}$ is dielectric loss, $\frac{1}{Q_c}$ loss due to

conductivity of the metallic plates, $\frac{1}{Q_r}$ is the loss due to radiation and $\frac{1}{Q_{EXT}}$ is

the loss due to external coupling. First three terms on the right hand side of the equation 2.8 comprise what is usually called the unloaded loss factor of the resonant cavity. That is

$$\frac{1}{Q_u} = \frac{1}{Q_D} + \frac{1}{Q_c} + \frac{1}{Q_r} \quad (2.9)$$

In the present study the Q factor of the DRs is measured using a transmission mode cavity proposed by Krupka et al. [23]. The DR is placed inside a cylindrical cavity. The cavity is made of copper and the inner surfaces are silver coated. It has a diameter of 40 mm and height of 18 mm when closed with the metallic lid. The sample can be mounted centrally on a cylindrical quartz support. Microwave is fed using loop coupling. The loops are slightly penetrated into the cavity with minimum radiation loss. The figure of the cavity is shown (Fig. 2. 9).

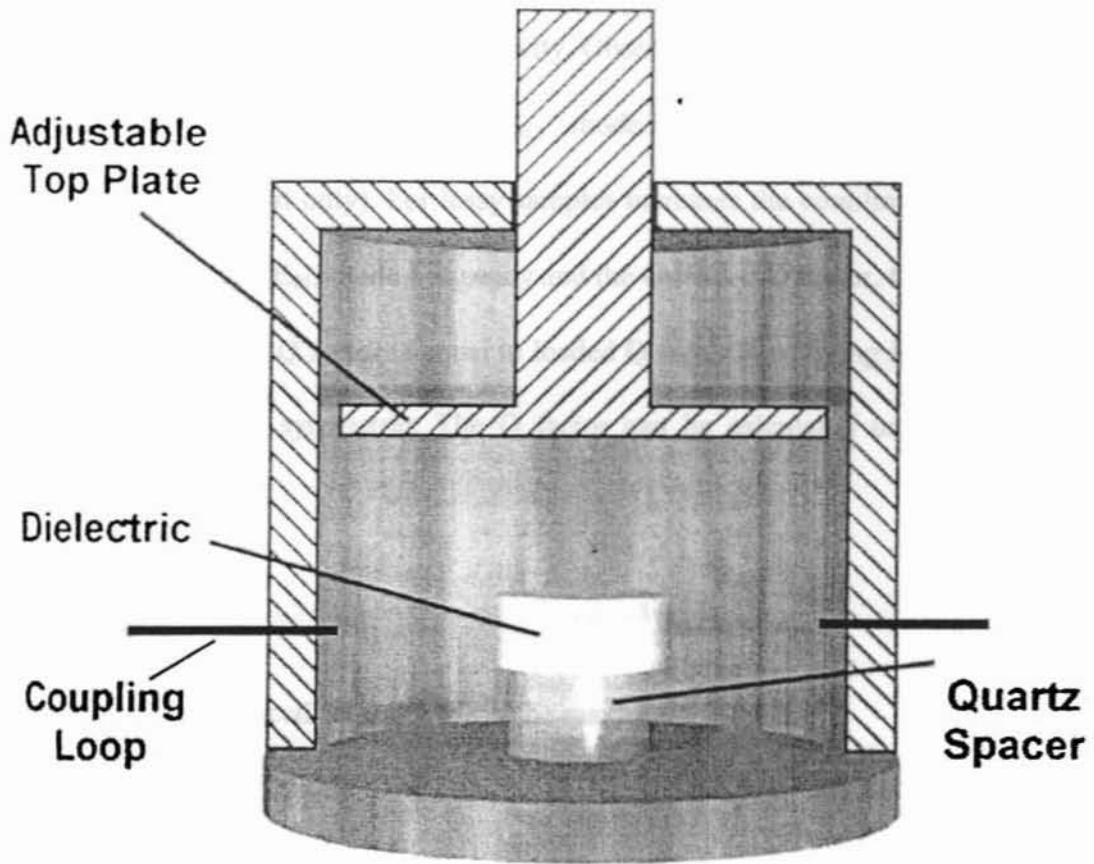


Fig 2. 9 The cavity set up for the measurement of Q factor

The photograph showing the cavity set up is shown in Fig 2. 7.b. In principle the cavity has infinite number of modes, when excited with microwave spectrum of frequencies. The TE_{016} mode is used for the measurements, which is typically the first or second mode for high permittivity samples. Samples with 12.5 to 20 mm diameter is the optimum for the measurements. Usually D/L ratio of 2-2.5 is maintained to get maximum mode separation to avoid interference from other modes.

In order to measure the Q factor the sample is mounted centrally at the cavity on the quartz support and close the cavity. Observe S_{21} versus frequency in the frequency range below 12.18 GHz. ($TE_{01\delta}$ mode resonant frequency of the cavity with quartz support only). For lossy samples increases the coupling to get the resonance. Measure $TE_{01\delta}$ mode frequency and the unloaded Q factor. One can assume that the unloaded Q factor is equal to loaded Q factor if coupling is weak. The coupling is assured symmetric. The Q factor can be calculated using the expression

$$Q = \frac{f}{\Delta f} \quad (2.7)$$

The sample should be placed centrally to get the maximum Q factor.

2.2.2.3 Measurement of τ_f

For an ideal resonator the temperature coefficient of resonant frequency (τ_f) should be near to zero. Since resonators are used in communication systems temperature stability is an important factor and should be near to zero.

In order to measure τ_f , DR is kept end shorted between two copper plates. This is then kept on a hot plate and insulated with thermocol. The E-field probe is kept near the DR in such a way to get resonance. The TE_{011} mode is identified as described in section 2.2.2.1. The set up is then slowly heated ($\sim 2^\circ\text{C}/\text{minute}$) in the range 25 to 80°C . The probe of the thermocouple is kept just outside the metal

plate so that it does not disturb the resonant frequency. Shift of the resonant frequency as a result of heating in the reflection mode is noted using Network Analyser and HP 8350 B Sweep Oscillator . The variation of resonant frequency is plotted as function of temperature. The τ_f is calculated from the slope of the curve using equation

$$\tau_f = \frac{1}{f} \frac{\Delta f}{\Delta T} \quad (2.8)$$

2.3 OTHER CHARACTERISATION OF DR CERAMICS

2.3.1 Powder X-ray Diffraction (XRD)

The sintered samples are powdered and used for XRD to study the phase purity, crystal system etc using Cu K_α radiation using a Philips X-ray diffractometer. The reflections are recorded. Using JCPDS, the reflections are indexed wherever possible. A scan speed of 5°/minute is given for recording data.

2.3.2 Scanning Electron Microscopy (SEM)

The sintered specimens are polished and thermally etched by heating the pellet near to the sintering temperature for about 30 minutes. The surfaces are coated with gold and examined using a scanning Electron Microscope (JEOL, JFM-35C, Japan). The secondary electron images are recorded.

2.3.3 Spectroscopic Methods

The Far infrared spectroscopic method is used for the indirect estimation of intrinsic dielectric loss and dielectric constant of certain samples. The IR reflectivity and Transmission spectra were obtained at room temperature using Fourier transform spectrometer (Bruker IFS 113 v) in the frequency range of 30 – 2000 and 15-100 cm^{-1} respectively. The resolution of the reflectivity spectra was 2 cm^{-1} , although accurate determination of the interferences in the transmission spectra required a resolution of 0.5 cm^{-1} . The experimental set up for TDTTS (Time Domain Terahertz Transmission Spectroscopy) uses a biased large antenna (low temperature grown GaAs) as a terahertz emitter and an electro-optic sampling detection technique [31].

REFERENCES

- [1] D. Kingery, H. K. Bowen and D. R. Uhlmann, Introduction to Ceramics, John Wiley & Sons, New York (1976)
- [2] N. Ichinose, K. Komeya, N. Ogino, T. Tsuya and Y. Yokomizo, Introduction to Fine Ceramics, Ed. By N. Ichinose (English Translation), John Wiley & Sons Ltd., (1987)
- [3] A. J. Moulson and J. M. Herbert, Electroceramics, Chapman and Hall (1990)
- [4] L. L. Hench and J. K. West, Principles of Electroceramics, John Wiley & Sons, Singapore (1990)
- [5] C. J. Brinker and G. W. Schere, Sol-Gel Science- The Physics and Chemistry of Academic Press, New York (1990).
- [6] B. W. Hakki and P. D Coleman, IRE Trans on Microwave Theory Tech., **MTT-8**, (1960) 402
- [7] W. E. Courtney, IEEE Trans on Microwave Theory Tech., **MTT-18** (1970) 476
- [8] O. V. Karpova, Sov. Phys., **1** (1959) 220
- [9] S. B. Cohn and K. C. Kelly, IEEE Trans on Microwave Theory Tech., **MTT-14** (1966) 406
- [10] E. Snitzer, J. of the Opt. Soc. Am., **51** (1961) 491
- [11] D. Hennings and P. Schnabel, Philips J. Res., **38** (1983) 295
- [12] Y. Kobayashi and S. Tanaka, IEEE Trans on Microwave Theory Tech., **MTT-28** (1980) 1077
- [13] Y. Kobayashi and M. Kato, IEEE Trans on Microwave Theory Tech., **MTT-33**

- (1985) 586
- [14] A. Podcameni, L. F. M. Conrado and M.M. Musso, *Electron. Lett.*, **17** (1981) 56
- [15] A. P. S. Khanna and Y. Garault, *IEEE Trans on Microwave Theory Tech.*, **MTT- 31** (1983) 261
- [16] A. P. S Khanna, *Microwaves & RF* (1984) 81
- [17] D. Kajfez and E. J. Hwan, *IEEE Trans on Microwave Theory Tech.*, **MTT-32** (1984) 666
- [18] D. Kajfez and M. Crnadak, *Proc. of the IEEE South Eastern Conference* (1985) 83
- [19] E. N. Ivanov, D. G. Blair and V. I. Kalinichev, *IEEE Trans on Microwave Theory Tech.*, **MTT- 41**(1993) 632
- [20] M. E. Tobar, E. N. Ivanov, R. A. Woode, and J. H. Searls, *Proc. IEEE Freq. Control. Symp.*, (1994) 433
- [21] V. Giordano, W. Daniau, G. Martin, F. Lardet-Vieudrin, M. Olivier, O. di Monaco and M. Chaubet, *Proc. 9th Euro. Freq. Time Forum*, (1995)
- [22] *A Designer's Guide to Microwave Dielectric Ceramics*, Trans Tech Inc. Adamstown (1993)
- [23] J. Krupka, K. Derzakowsky, B. Riddle and J. B. Jarvis, *Meas. Sci. Tech.*, **9** (1998) 1751
- [24] R. B. Cass, K. G. Ewsuk, W.B. Blumenthal, *Ceram. Ind.*, **147** (1997)
- [25] K. G. Ewsuk, *Characterisation of Ceramics*, Butterworth - Heinemann, Greenwich (1993) 77

- [26] A. Broese van Groenou and R. C. D. Lisenburg, *J. Am. Ceram. Soc.*, **66** (1983) 156
- [27] R. M. German, *Particle Packing Characteristics*, Metal powder Industries Federation, Princeton, NJ. (1989)
- [28] E. Artz, *Acta Metall.*, **30** (1982) 1883
- [29] X. K. Wu, D. W. Whitman, W. L. Koufell, W. C. Flinch, and D. I. Cumbers, *Ceramic Eng. Sci. Proc.*, **18** (1997) 422
- [30] S. Jill Glass, and Kewin G. Ewsuk, *MRS Bulletin*, (1997) 24
- [31] S. Kamba, J. Petzelt, E. Buixaderas, D. Haubrich, P. Vanek, P. Kuzel, I. N. Jawahar, M. T. Sebastian and P. Mohanan, *J. Appl. Phys.*, **89** (2001) 3900
- [32] M. N. Rahaman, *Ceramic Processing and Sintering*, Marcel Dekker Inc. (1995)

Appendix I

```
10 ! HAKKI & COLEMAN METHOD
20 ! RE-STORE "HAKKI"
30 PRINTER IS CRT
40 PRINT "This is to calculate Dielectric constant by Hakki &
Coleman method"
50 PRINT "Please setup the Network Analyzer in LOGMAG S21"
52 PRINT "Connect the two probes in between the samples"
53 PRINT "Determine the 01 mode"
54 DIM Alpha(21)
56 FOR I = 1 TO 21
57 READ Alpha(I)
58 NEXT I
59 !
60 DATA
2.65,2.7,2.75,2.8,2.85,2.9,2.9,2.95,3,3,3.05,3.05,3.1,3.15,3.15
7 3.2,3.2,3.2,3.25,3.25,3.25
61 PRINTER 9
62 Nn=0
64 Nn=Nn+1
65 IF Nn > 1 THEN GOTO 68
66 ! PRINTER IS 9
67 ! PRINT "FREQ S21 BAND WIDTH Q FACTOR SAMPLE"
68 ! PRINTER IS CRT
69 DIM Sam$(50)
70 INPUT "Please Press RETURN to continue", M
71 ASSIGN @Nwa TO 716
72 INPUT "Enter the Sample Name", Sam$
73 INPUT "Please enter the diameter and length in mm", D,L
74 DIM Data(200,1)
75 DIM Formatted_data(400,1)
76 DIM Inputs(80)
77 REAL Freq, Real, Imag, Mag, Phase
78 LOCAL 716
79 ASSIGN @Nwa_data1 TO 716; FORMAT ON
80 ASSIGN @Nwa_data2 TO 716; FORMAT OFF
81 ASSIGN @Nwa_systbus TO 717
82 !
83 !
84 !
85 OUTPUT @Nwa; "MARK1; MARKMAXI;"
86 WAIT .1
87 OUTPUT @Nwa; "OUTPMARK;"
88 ENTER @Nwa_data1; Mag, Phase
89 WAIT .1
90 OUTPUT @Nwa;"OUTPACTI;"
91 ENTER @Nwa_data1; Freq
92 WAIT .1
93 Mar1=Mag
94 Fr=Freq/10^9
95 !
86 PRINT Fr
97 !INPUT A
98 !OUTPUT @Nwa; "STAR 2 GHz; STOP 10 GHz;"
99 !OUTPUT @Nwa;"CONT;"
100 LOCAL 716
```

```

101 C = 30
102 L=L*10^(-1)
103 D = D*10^(-1)
104 Beta=PI*D*Fr/C*((C/(2*Fr*L))^2-1)^.5
106 Kk = INT((Beta-1)/.2+1)
107 IF FRACT((Beta-1)/.2+1)>.5 THEN Kk=Kk+1
108 Er = 1+((C/(PI*D*Fr))^2*(Alpha(Kk)^2+Beta^2))
109 Alpha=PI*D*Fr/C*(Er-(C/2*Fr*L)^2)^.5
110 IF Alpha (Kk)-Alpha<.1 THEN GOTO 113
111 PRINT "Alpha Is Not Matching"
112 GOTO 115
113 PRINT "Name", TABXY(1,15), "Fr", TABXY(1,15), "Er"
114 PRINT Sam$, TABXY(1,15), Fr, TABXY(1,15), INT(Er*100)/100
115 GOTO 64
116 I
118 I
119 END

```

Chapter 3

$A_5B_4O_{15}$ (A = Ba, Sr, Mg, Ca, Zn; B = Nb, Ta) MICROWAVE DIELECTRIC CERAMICS

3.1 INTRODUCTION

In the previous chapters we have seen that dielectric materials with dielectric constant greater than 20 and high quality factors ($Q \times f > 2,000$) are needed for microwave applications. Cation deficient hexagonal perovskites are attractive in this regard. $Ba_5Nb_4O_{15}$ type materials are characterized with high dielectric constant and quality factor. Galasso and Katz [1] reported the existence of $Ba_5Ta_4O_{15}$, $Ba_5Nb_4O_{15}$ and $Sr_5Ta_4O_{15}$ ceramics. This type of materials is called cation deficient perovskites in the sense that, if written in the perovskite form (ABO_3), $A_5B_4O_{15}$ reduces to $AB_{0.8}O_3$. Hence there is a vacancy of 0.2 B cation per one A cation, i.e., overall one B cation vacancy per 5 A cations. The structures of $Ba_5Ta_4O_{15}$, $Ba_5Nb_4O_{15}$ and $Sr_5Ta_4O_{15}$ are well studied [1-5]. These compounds have hexagonal structure and crystallize in the $P\bar{3}m1$ space group with one formula unit per cell ($Z = 1$). The compounds have five layer closest packing of oxygen and barium ions [1-5]. The tantalum or niobium ions are located in the

octahedral holes between layers with one layer of octahedral holes are missing tantalum ions to accommodate the charge neutrality (Fig. 3. 1).

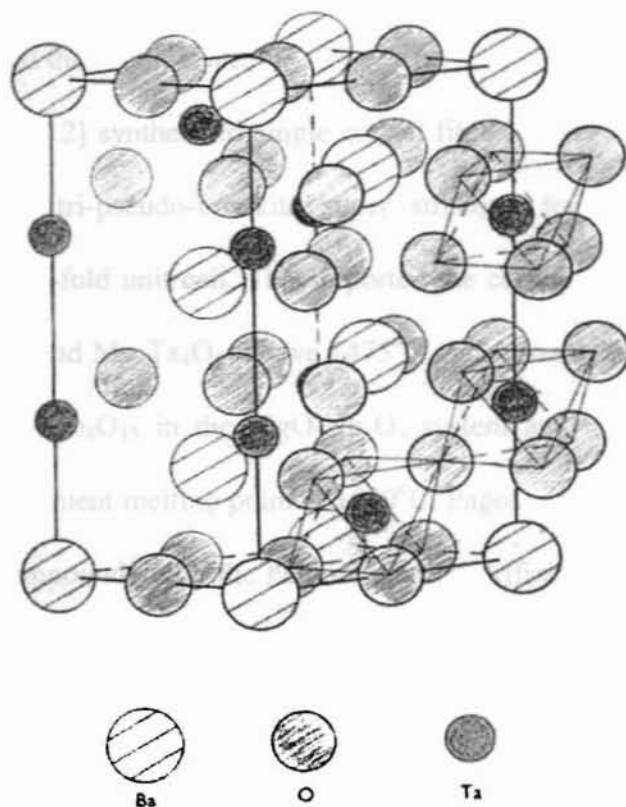


Fig. 3. 1 The structure of Ba₅Ta₄O₁₅

In addition to that Ba₅Nb₄O₁₅ is a hexagonal polytype that is the (5H) member of a series of polytypes characterized by Hutchison and co-workers [3, 4] containing 4, 5, 6, 8, 10 and 12 layered (4H, 5H, 6H, 8H, 10H, & 12H) species. Whiston and Smith [6] have reported the existence of Sr₅Nb₄O₁₅ iso-structural with the tantalum analogue. Though Weiden et al. [7] reported monoclinic structure ($C_{2h}^1 - P2/m$ with $Z=2$) for the compound; its structure was later confirmed to be hexagonal based on Raman, IR and single crystal X-ray diffraction [8-11] studies. The c-parameter is doubled due to an anti-tilting of

TiO₆ octahedra (~15°) around the *c* axis [11]. The structure of all four above mentioned compounds consists of five AO₃ close-packed layers with B ions located in corner-sharing octahedral holes between the layers. No B atom lies between the third and the fourth layer.

Brook et al. [12] synthesised single crystal fibres of Mg₅Nb₄O₁₅. Kasper et al. [13] reported tri-pseudo-brookite super structure for Mg₅Nb₄O₁₅ and Mg₅Ta₄O₁₅ with three-fold unit cell. They reported the compound Mg₅Nb₄O₁₅ is stable above 1400°C and Mg₅Ta₄O₁₅ above 1475°C. Abbatista et al. [14] reported the existence of Mg₅Nb₄O₁₅ in the MgO-Nb₂O₅ system and is stable between 1200°C and its incongruent melting point at 1580°C. Pagola et al. [15] studied the structure of both compounds with the help of neutron diffraction and found that the compounds are iso-structural with pseudo-brookite Fe₂TiO₅, and the presence of any superstructure could not be noticed. The compounds crystallize with the orthorhombic structure within the space group D_{2h}^{17} - *Cmcm* with *Z* = 4. The structure consists of double chains of (Mg, B)O₆ units, sharing edges of the *bc* plane, interconnected through common oxygen along the *a* axis to give a three-dimensional array [15]. The microwave dielectric properties of one of the compounds (Ba₅Nb₄O₁₅) in the A₅B₄O₁₅ are reported earlier [16, 17, 18]. In the present report we make a detailed study of the preparation, characterisation and microwave dielectric properties of title compounds A₅B₄O₁₅ (A=Ba, Sr, Mg, Ca, Zn; B=Nb, Ta). Solid solution phases between the members of the A₅B₄O₁₅ have also been prepared to tailor the microwave dielectric properties.

3.2 $A_5B_4O_{15}$ (A=Ba, Sr, Mg, Ca, Zn; B=Nb, Ta)

CERAMICS

3.2.1 Preparation and characterization

The ceramics were prepared through the conventional solid-state ceramic route. The high purity carbonates or oxides i.e., $BaCO_3$ (>99.5 % Aldrich Chemicals), $SrCO_3$ (99.9 % Aldrich), $CaCO_3$ (>99.5 % Aldrich Chemicals), MgO (99+%, CDH India), ZnO (99.99%, Aldrich Chemicals), Nb_2O_5 (99.9%, NFC, Hyderabad, India) and Ta_2O_5 (99.9%, NFC, Hyderabad, India) were used. The MgO is calcined at $1000^\circ C$ for 3 hours to remove hydroxides or carbonates [21]. $Mg_5Nb_4O_{15}$ and $Mg_5Ta_4O_{15}$ were prepared using both calcined MgO and uncalcined MgO . The oxide or carbonate powders were weighed as per the molar ratios to get a gross amount of about 20 g, mixed thoroughly in agate mortar using distilled water or acetone as the wetting medium for a duration of 1 hour, dried and again mixed for 1 hour. The reaction mixtures of the niobates were calcined at $1050-1275^\circ C$ and tantalates at $1200-1400^\circ C$ for a duration ranging from 4 to 8 hours. The calcined mixture is ground well for 1 hour, 3 wt% PVA is added, dried and again ground. The fine powder is uni-axially pressed at a pressure of 150 MPa using a tungsten carbide die of 11 mm diameter. The dimensions of the ceramic compacts are controlled such that the sintered body has aspect ratio (D/L) of 1 to 1.3 or 2 to 2.3 to obtain maximum mode separation during measurements. Stearic acid dissolved in isopropyl alcohol is used as lubricant while pressing. This can reduce the friction between powder and die wall. The samples are heated

3.2.2 Results and Discussion

3.2.2.1 Density and X-ray diffraction

Table 3. 1 gives the calcination temperature, sintering temperature, density and percentage density of all the ceramics. The ceramics could be sintered into dense bodies. Most of the compounds have sintered densities more than 93% of their theoretical densities. The phase pure $Mg_5Nb_4O_{15}$ and $Mg_5Ta_4O_{15}$ are obtained by calcining at $1300^\circ C$ for 8h and at $1400^\circ C$ for 8 hours respectively using calcined MgO. The $Ba_5Ta_4O_{15}$, $Ba_5Nb_4O_{15}$, $Sr_5Nb_4O_{15}$ and $Sr_5Ta_4O_{15}$ are hexagonal structured in accordance with the earlier reports. When uncalcined MgO was used the sintered product contained $MgNb_2O_6$ and $MgTa_2O_6$ as the secondary phases. Single phase $Mg_5Ta_4O_{15}$ could not densify more than 91% without additives. 1 wt % of CeO_2 , Nd_2O_3 , Sm_2O_3 , MnO_2 and Bi_2O_3 are tried as sintering aids to $Mg_5Nb_4O_{15}$ and $Mg_5Ta_4O_{15}$, both prepared from MgO heat treated to $1000^\circ C$ for 3 hours.

Table 3. 1

The list of Calcination temperatures, sintering temperatures, densities and percentage densities of the $A_5B_4O_{15}$ ceramics

Material	Calcination Temp (°C)	Calcination time (h)	Sint. Temp (°C)	Sint. time (h)	Density (g/cm ³)	Theoretical density (g/cm ³)	% density
Mg ₅ Ta ₄ O ₁₅	1400	8	1550	4	6.47	--	--
Mg ₅ Ta ₄ O ₁₅ *	1400	8	1560	4	5.56	6.11	91
Sr ₅ Ta ₄ O ₁₅	1400	8	1610	4	7.00	7.32	96
Ba ₅ Ta ₄ O ₁₅	1325	4	1550	4	7.63	8.02	95
Mg ₅ Nb ₄ O ₁₅	1300	8	1475	4	4.20	--	--
Mg ₅ Nb ₄ O ₁₅ *	1300	8	1450	4	3.90	4.15	94
Ba ₅ Nb ₄ O ₁₅	1250	4	1380	2	6.07	6.30	96
Ba ₄ SrNb ₄ O ₁₅	1250	4	1400	4	5.64	6.10	92
Ba ₃ Sr ₂ Nb ₄ O ₁₅	1250	4	1400	4	5.44	5.86	93
Ba ₂ Sr ₃ Nb ₄ O ₁₅	1250	4	1400	4	5.41	5.67	95
BaSr ₄ Nb ₄ O ₁₅	1250	4	1400	4	5.46	5.74	95
Sr ₅ Nb ₄ O ₁₅	1250	4	1400	4	5.20	5.57	93
5ZnO-2Nb ₂ O ₅	1050	4	1220	2	5.61	--	--
5CaO-2Ta ₂ O ₅	1400	4	1550	4	6.25	--	--
5CaO-2Nb ₂ O ₅	1300	4	1500	4	4.20	--	--

* Prepared from MgO powder heat treated at 1000°C for 3 hours.

-- % Density could not be evaluated due to multiphase.

Table 3. 2
The densities, ϵ_r and Q x f with 1 wt% of
dopant to $Mg_5Nb_4O_{15}$ and $Mg_5Ta_4O_{15}$

Ceramics	Dopant	% density	ϵ_r	Q x f (GHz)
$Mg_5Nb_4O_{15}$ *	Pure	94	11.0	37400
	CeO ₂	93	11.8	24700
	Nd ₂ O ₃	92	11.6	27000
	Sm ₂ O ₃	92	11.6	21600
	MnO ₂	91	11.4	25700
	Bi ₂ O ₃	92	11.5	14000
$Mg_5Ta_4O_{15}$ *	Pure	91	11.0	18100
	CeO ₂	90	11.2	18600
	Nd ₂ O ₃	92	14.0	14000
	Sm ₂ O ₃	89	12.0	14500
	MnO ₂	93	14.7	6500
	Bi ₂ O ₃	96	15.2	10100

*MgO is heat treated at 1000°C for 3 hours

Table 3. 2 shows the densities of the compounds with 1 wt% of the sintering aids. The addition of sintering aids did not increase the sintered density in the case of $Mg_5Nb_4O_{15}$. But 1 wt % Bi₂O₃ added as sintering aid has improved the density to 96% in the case of $Mg_5Ta_4O_{15}$. All the ceramics gave single phase except the compounds of calcium and zinc. Attempts to prepare $Zn_5Nb_4O_{15}$ were not successful, but resulted in multiphase. The multiphase ceramics was a mixture

of ZnNb_2O_6 and $\text{Zn}_3\text{Nb}_2\text{O}_8$. The calcium based ceramics $\text{Ca}_5\text{Nb}_4\text{O}_{15}$ and $\text{Ca}_5\text{Ta}_4\text{O}_{15}$ also did not form. The different phases present in the resultant ceramics could not be identified. Fig. 3. 2(a) shows the XRD patterns of $\text{Mg}_5\text{Nb}_4\text{O}_{15}$, $\text{Mg}_5\text{Ta}_4\text{O}_{15}$, $5\text{CaO}\cdot 2\text{Nb}_2\text{O}_5$, $5\text{CaO}\cdot 2\text{Ta}_2\text{O}_5$ and $5\text{ZnO}\cdot 2\text{Nb}_2\text{O}_5$ ($\text{ZnNb}_2\text{O}_6 + \text{Zn}_3\text{Nb}_2\text{O}_8$). Fig. 3. 2(b) shows the XRD patterns of $\text{Ba}_5\text{Ta}_4\text{O}_{15}$, $\text{Sr}_5\text{Nb}_4\text{O}_{15}$, $\text{Ba}_5\text{Nb}_4\text{O}_{15}$ and $\text{Sr}_5\text{Ta}_4\text{O}_{15}$.

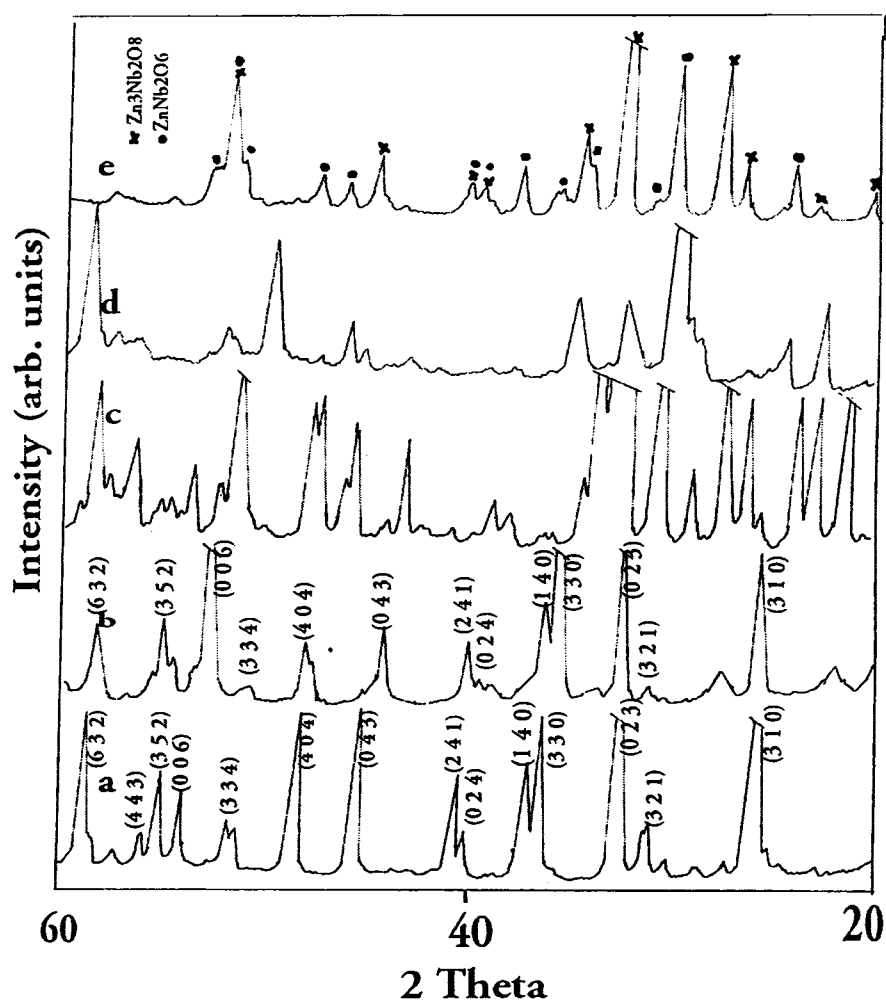


Fig. 3. 2 (a) The XRD patterns of (a) $\text{Mg}_5\text{Nb}_4\text{O}_{15}$ (b) $\text{Mg}_5\text{Ta}_4\text{O}_{15}$ (c) $5\text{CaO}\cdot 2\text{Nb}_2\text{O}_5$ (d) $5\text{CaO}\cdot 2\text{Ta}_2\text{O}_5$ (e) $5\text{ZnO}\cdot 2\text{Nb}_2\text{O}_5$

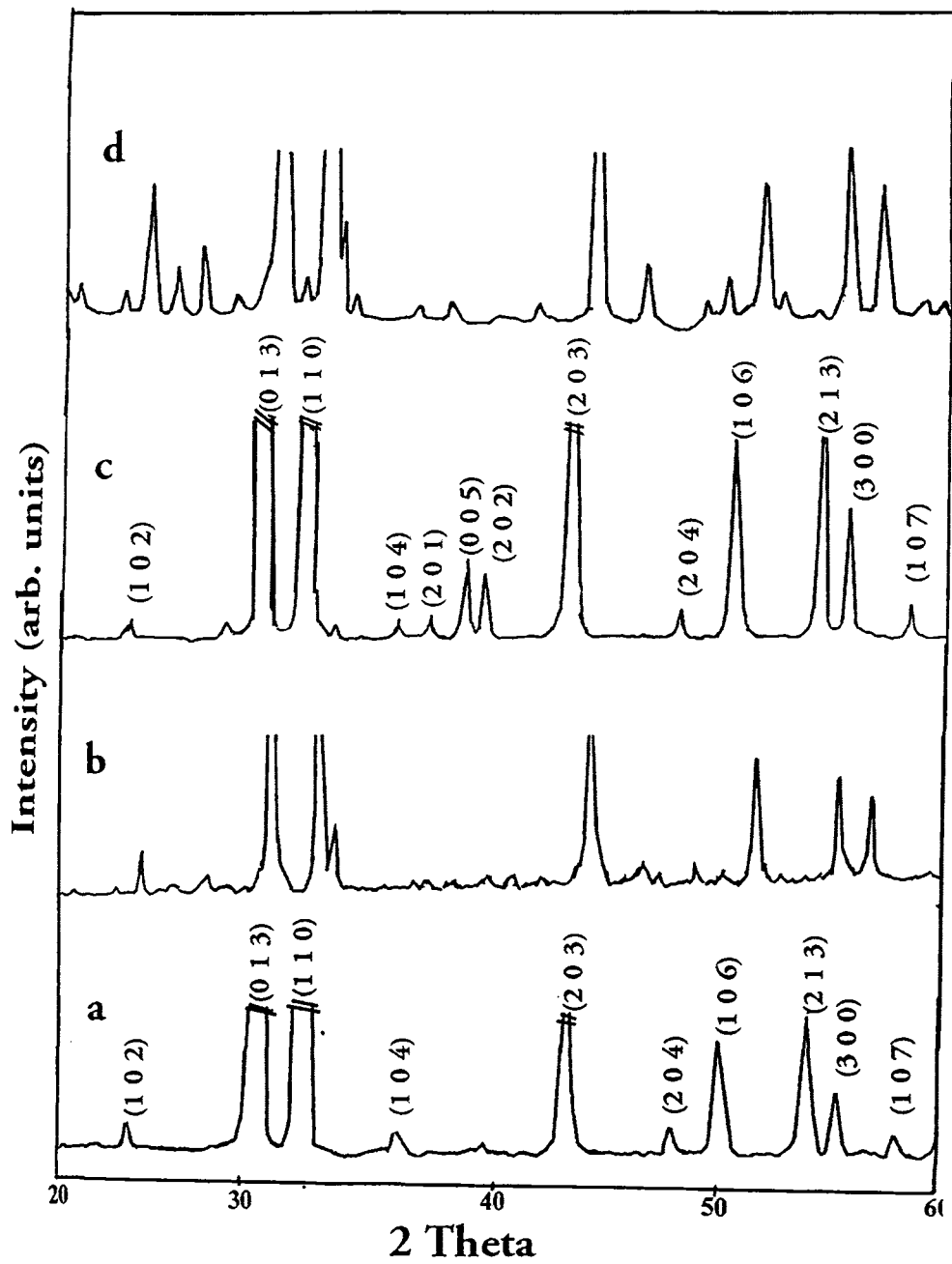
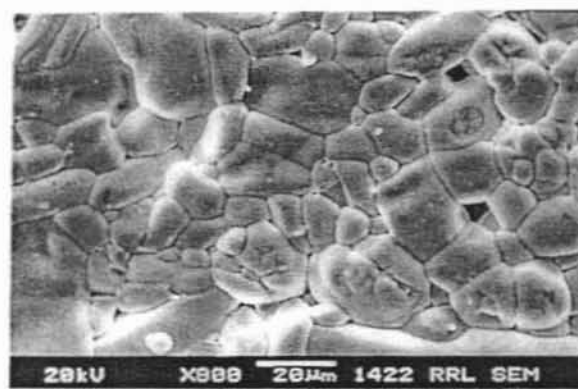
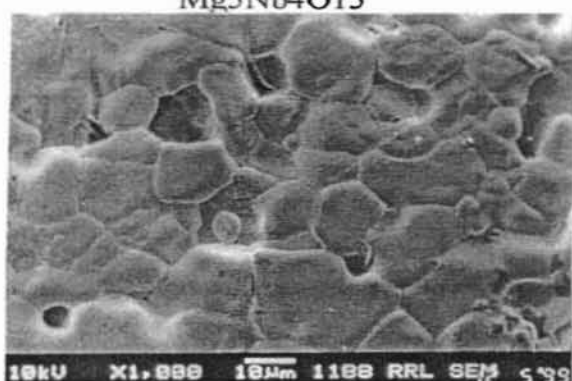


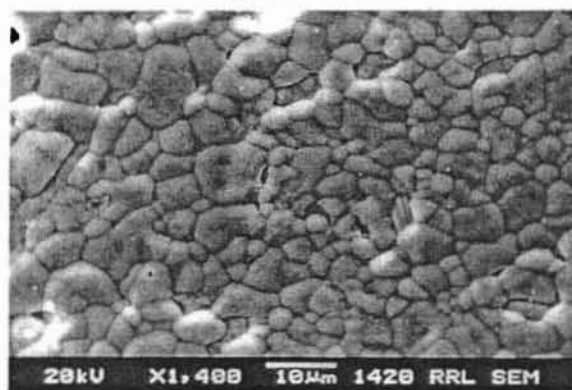
Fig. 3.2(b) XRD patterns of (a) $\text{Ba}_5\text{Ta}_4\text{O}_{15}$ (b) $\text{Sr}_5\text{Nb}_4\text{O}_{15}$
(c) $\text{Ba}_5\text{Nb}_4\text{O}_{15}$ (d) $\text{Sr}_5\text{Ta}_4\text{O}_{15}$



$Mg_5Nb_4O_{15}$



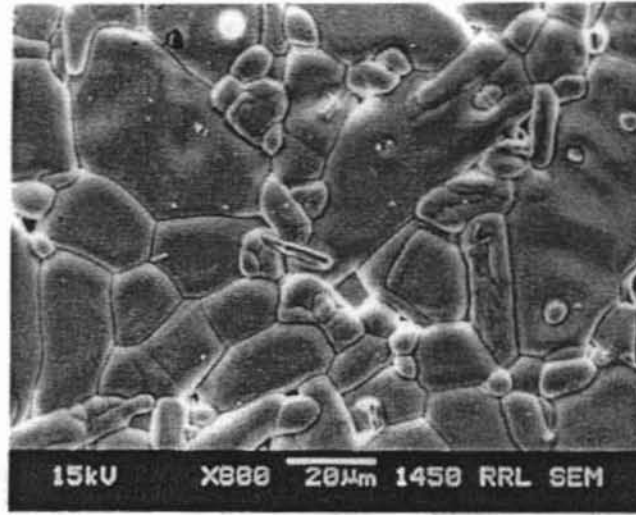
$Mg_5Ta_4O_{15}$



$5CaO-2Nb_2O_5$

Fig. 3.3 The SEM pictures of $Mg_5Nb_4O_{15}$,
 $Mg_5Ta_4O_{15}$ and $5CaO-2Nb_2O_5$

Fig. 3. 3 shows the SEM pictures of $Mg_5Nb_4O_{15}$, $Mg_5Ta_4O_{15}$ and $5CaO-2Nb_2O_5$. The presence of porosity of $Mg_5Nb_4O_{15}$ and $Mg_5Ta_4O_{15}$ is evident from the SEM. The grains are relatively large in size of about $20\ \mu m$. Fig. 3. 4 shows the SEM picture of $5ZnO-2Nb_2O_5$.



$5ZnO-2Nb_2O_5$

Fig. 3. 4 The SEM picture of $5ZnO-2Nb_2O_5$ ($ZnNb_2O_6+Zn_3Nb_2O_8$)

The grains are very large up to $40\ \mu m$ in size. The $5ZnO-2Nb_2O_5$ ceramics is dense. A possible liquid phase sintering might have taken place, which is the cause for bigger grains and lower porosity. The presence of two types of grains is evident in Fig. 3. 4.

3. 2. 2. 2 Microwave dielectric properties

The ceramics showed good resonance at microwave frequencies. The microwave dielectric properties of the ceramics were summarised in Table 3. 3.

Table 3. 3
The list of dielectric constants, Quality factors, frequencies, and temperature coefficient of resonant frequencies of $A_5B_4O_{15}$ ceramics

Material	ϵ_r	Q	f GHz	Q x f GHz	τ_f ppm/ $^{\circ}$ C	Structure
$Mg_5Ta_4O_{15}$	17	2000	7.19	14400	-15	Orthorhombic
$Mg_5Ta_4O_{15}^{\bullet}$	11	2000	9.06	18100	-54	Orthorhombic
$Mg_5Nb_4O_{15}$	14	2000	7.28	14600	-58	Orthorhombic
$Mg_5Nb_4O_{15}^{\bullet}$	11	4500	8.30	37400	-54	Orthorhombic
$Sr_5Ta_4O_{15}$	41	400	5.99	2400	**	Hexagonal
$Ba_5Ta_4O_{15}$	28	5700	5.55	31600	12	Hexagonal
$Ba_5Nb_4O_{15}$	39	5000	4.73	23700	78	Hexagonal
$Ba_4SrNb_4O_{15}$	48	3100	4.70	14600	140	Hexagonal
$Ba_3Sr_2Nb_4O_{15}$	50	3500	4.71	16500	232	Hexagonal
$Ba_2Sr_3Nb_4O_{15}$	51	4600	4.61	21200	117	Hexagonal
$BaSr_4Nb_4O_{15}$	45	5100	4.57	23300	82	Hexagonal
$Sr_5Nb_4O_{15}$	40	4000	4.84	19400	55	Hexagonal
5ZnO-2Nb ₂ O ₅	21	12600	6.98	88000	-73	Multiphase
5CaO-2Ta ₂ O ₅	41	1000	5.90	5900	140	Unknown
5CaO-2Nb ₂ O ₅	32	1000	6.48	6500	-37	Unknown

** τ_f could not measure due to poor quality factor

• Prepared by using heat treated MgO powder

The ceramics have ϵ_r in the range 11 to 51, $Q \times f$ in the range 2400 to 88000 GHz and τ_f in the range -73 to +232 ppm/ $^{\circ}$ C. The $\text{Ba}_5\text{Ta}_4\text{O}_{15}$ has a lower $\epsilon_r = 28$ than that of analogous $\text{Ba}_5\text{Nb}_4\text{O}_{15}$ which has $\epsilon_r = 39$. But this is in contrary to the expectation that the tantalum analogue is having higher dielectric constant than the niobium compound due to the larger ionic polarisability [23, 24] of tantalum while both the ceramics crystallise in the same symmetry group. Spectroscopic studies by Massa et al. [19, 20] shows that the lattice of $\text{Ba}_5\text{Ta}_4\text{O}_{15}$ is stable whereas that of $\text{Ba}_5\text{Nb}_4\text{O}_{15}$ is going to collapse to a lower symmetry state and there may be increased lattice anharmonicity in the compound. This may be reason for the higher dielectric constant of $\text{Ba}_5\text{Nb}_4\text{O}_{15}$. Interestingly the τ_f of the $\text{Ba}_5\text{Ta}_4\text{O}_{15}$ (+12 ppm/ $^{\circ}$ C) is considerably lower than that of $\text{Ba}_5\text{Nb}_4\text{O}_{15}$ (+78 ppm/ $^{\circ}$ C). Orthorhombic structured $\text{Mg}_5\text{Nb}_4\text{O}_{15}$ and $\text{Mg}_5\text{Ta}_4\text{O}_{15}$ showed a comparatively lower dielectric constant of 11 than the hexagonal phases with the general formula $\text{A}_5\text{B}_4\text{O}_{15}$. The lower dielectric constant may be due to the lower ionic polarisability of Mg ions and the different structure. The phase pure $\text{Mg}_5\text{Nb}_4\text{O}_{15}$ and $\text{Mg}_5\text{Ta}_4\text{O}_{15}$ ceramics have $Q \times f$ up to 37400 GHz and τ_f of -54 ppm/ $^{\circ}$ C each. In the case when uncalcined MgO is used, the Mg deficiency in the above ceramics leads to MgNb_2O_6 and MgTa_2O_6 as the secondary phases. Presence of MgTa_2O_6 whose $\epsilon_r = 30.3$, $Q \times f = 59600$ GHz and $\tau_f = +30$ ppm/ $^{\circ}$ C [25] increases dielectric constant of $\text{Mg}_5\text{Ta}_4\text{O}_{15}$ (prepared using uncalcined MgO) into 17 where as its τ_f decreases to -15 ppm/ $^{\circ}$ C. In a similar way, deficiency of Mg in $\text{Mg}_5\text{Nb}_4\text{O}_{15}$ (non-stoichiometry) leads to the formation of MgNb_2O_6 as the secondary phase which has $\epsilon_r = 21.4$, $Q \times f = 93800$ GHz and $\tau_f = -70$ ppm/ $^{\circ}$ C

[25]. The presence of the MgNb_2O_6 secondary phase increases the dielectric constant for 11 to 14 and τ_f from -54 to -58 ppm/ $^\circ\text{C}$, but decreases the quality factor as compared to the pure compounds. The phase pure $\text{Mg}_5\text{Ta}_4\text{O}_{15}$ could not densify more than 91%. Hence we have added 1 wt % Nd_2O_3 , Sm_2O_3 , Bi_2O_3 , CeO_2 , and MnO_2 into powders of $\text{Mg}_5\text{Nb}_4\text{O}_{15}$ and $\text{Mg}_5\text{Ta}_4\text{O}_{15}$ and then studied the densification and microwave dielectric properties. The results are summarised in Table 3. 2. In the case of $\text{Mg}_5\text{Nb}_4\text{O}_{15}$, the addition of Nd_2O_3 , Sm_2O_3 , Bi_2O_3 , CeO_2 , and MnO_2 all decreased the density but slightly increased the dielectric constant whereas the $Q \times f$ deteriorated. In the case of $\text{Mg}_5\text{Ta}_4\text{O}_{15}$ 1 wt % of Nd_2O_3 , Bi_2O_3 and MnO_2 increased the density but CeO_2 and Sm_2O_3 decreased the density. The presence of additives increased the dielectric constant. Addition of 1 wt % CeO_2 has increased the $Q \times f$ of 18600 GHz, but other additives decreased the quality factor. Though the addition of 1 wt % of Bi_2O_3 has increased density and dielectric constant it reduced the Q factor.

The $5\text{ZnO}-2\text{Nb}_2\text{O}_5$ composition does not give single-phase compounds analogous to $\text{A}_5\text{B}_4\text{O}_{15}$ ($\text{Zn}_5\text{Nb}_4\text{O}_{15}$). Instead they give a mixture of ZnNb_2O_6 and $\text{Zn}_3\text{Nb}_2\text{O}_8$. The ZnNb_2O_6 is reported to have $\epsilon_r = 25$, $Q \times f = 83700$ GHz and $\tau_f = -56$ ppm/ $^\circ\text{C}$ [25]. The $\text{Zn}_3\text{Nb}_2\text{O}_8$ has ϵ_r about 22, $Q \times f = 83300$ GHz and $\tau_f = -71$ ppm/ $^\circ\text{C}$ [26]. The $5\text{ZnO}-2\text{Nb}_2\text{O}_5$ showed $\epsilon_r = 21$, $Q \times f = 88000$ GHz and $\tau_f = -73$ ppm/ $^\circ\text{C}$. Similarly single phases analogous to $\text{A}_5\text{B}_4\text{O}_{15}$ could not be obtained for $5\text{CaO}-2\text{Nb}_2\text{O}_5$ and $5\text{CaO}-2\text{Ta}_2\text{O}_5$. However the ceramics show good microwave dielectric properties and are given in Table 3. 3. The $5\text{CaO}-2\text{Nb}_2\text{O}_5$ has $\epsilon_r = 32$,

$Q \times f = 6500$ GHz and $\tau_f = -37$ ppm/ $^{\circ}$ C whereas $5\text{CaO}-2\text{Ta}_2\text{O}_5$ has $\epsilon_r = 41$, $Q \times f = 5900$ GHz and $\tau_f = +140$ ppm/ $^{\circ}$ C.

3.3 FAR-INFRARED AND SUBMILLIMETER STUDIES OF $\text{A}_5\text{B}_4\text{O}_{15}$ (A=Ba, Sr, Mg, Ca, Zn; B=Nb, Ta) CERAMICS

3.3.1 Introduction

The important characteristics required for dielectric resonators are high permittivity ϵ' , high quality factor $Q = \epsilon'/\epsilon''$ and low temperature coefficient of resonant frequency τ_f . Unfortunately, these requirements cannot be fulfilled simultaneously. High ϵ' materials have generally higher dielectric loss ϵ'' (lower Q) and frequently also high τ_f [27]. The method of sample preparation has a pronounced influence on the value of ϵ'' in the MW region, while ϵ' is almost insensitive to it. MW losses can vary by several orders of magnitude between samples of the same chemical composition but with different amount of defects [28]. Usually, technologists try to reduce ϵ'' empirically. Then it is not sure if extrinsic losses were completely eliminated and if thus the intrinsic value of ϵ'' was reached. In this case the spectroscopic methods, which directly access the far infrared (FIR) and sub-millimeter (SMM) spectral regions, i.e. classical FIR

spectroscopy and time-domain terahertz transmission spectroscopy (TDTTS) [29], appear as powerful methods for direct estimates of intrinsic losses not only in FIR but also in MW region, because the intrinsic ε'' is simply proportional to the frequency well below the phonon frequencies ($f \leq 10^{12}$ Hz) [30]. Already in 1962, Rupprecht and Bell [31] experimentally confirmed that the relation $\varepsilon''(\omega) \propto \omega$ is fulfilled in SrTiO₃. The same frequency dependence can be theoretically obtained from the formula [32]

$$\varepsilon^*(\omega) = \varepsilon'(\omega) - i\varepsilon''(\omega) = \sum_{j=1}^n \frac{\Delta\varepsilon_j \omega_{TOj}^2}{\omega_{TOj}^2 - \omega^2 + i\omega\gamma_{TOj}} + \varepsilon_\infty \quad (1)$$

in the limit $\omega \ll \omega_{TOj}$. The formula (1) describes the complex dielectric function $\varepsilon^*(\omega)$ as a sum of classical harmonic oscillators with eigenfrequencies ω_{TOj} , dampings γ_{TOj} and oscillator strengths $\Delta\varepsilon_j \omega_{TOj}^2$. ε_∞ denotes high-frequency permittivity originating from electron transitions. Each oscillator describes an optical polar phonon mode contributing by $\Delta\varepsilon_j$ into static dielectric permittivity. The limit $\omega \ll \omega_{TOj}$ yields also frequency independent permittivity $\varepsilon' = \sum \Delta\varepsilon_j + \varepsilon_\infty$ in MW and SMM region.

Wakino *et al.* used for the first time the above described method for the determination of $\varepsilon''(\omega)$ in the MW region from infrared reflectivity spectra of Ba(Zr,Zn,Ta)O₃ ceramics [30]. The complex dielectric response can be obtained [33] from reflectivity using the Kramers-Kronig relations or by fitting the reflectivity with the formula (1) and

$$R(\omega) \equiv \left| \frac{\sqrt{\varepsilon^*(\omega)} - 1}{\sqrt{\varepsilon^*(\omega)} + 1} \right|^2 \quad (2)$$

However, FIR reflectivity spectra are little sensitive on weak modes in the SMM region ($10 - 100 \text{ cm}^{-1}$), therefore we have extended this method and used a combination of FIR reflection and a more sensitive FIR transmission spectroscopy in SMM region for determination of MW losses in many materials [27, 28, 34]. As an accurate determination of $\varepsilon^*(\omega)$ in the SMM region is very important for its extrapolation down to MW region and the above mentioned techniques give $\varepsilon^*(\omega)$ only from the model fit of the spectra, it is very useful to combine the FIR spectroscopy with TDTTS which can typically access the range of 3 to 80 cm^{-1} , and which is phase sensitive. So, it can provide independently both real and imaginary part of the permittivity without any fitting models [35].

Many defects as porosity, grain boundaries, micro-cracks etc. can break proportionality between ε'' and the frequency [28]. The presence of a second phase may cause even additional peaks in ε'' in the SMM region [28]. On the other hand, the theory [36] shows that not only intrinsic losses due to multi-phonon absorption, but also extrinsic losses by charged-defect induced one-phonon absorption of acoustic branches yield $\varepsilon''(\omega) \propto \omega$. Nevertheless, extrinsic losses can be well distinguished from intrinsic ones from the temperature dependences. The latter ones should decrease on cooling and disappear at low temperatures near liquid He temperature [27,36].

The crystal structure is known for six studied compounds only: $\text{Ba}_5\text{Ta}_4\text{O}_{15}$, $\text{Sr}_5\text{Ta}_4\text{O}_{15}$ and $\text{Ba}_5\text{Nb}_4\text{O}_{15}$ crystallize in trigonal space group $D_{3d}^3 - P\bar{3}m1$ ($Z=1$) [1,2, 4] Monoclinic symmetry $C_{2h}^1 - P2/m$ with $Z=2$ [7] was reported for $\text{Sr}_5\text{Nb}_4\text{O}_{15}$, but very recent paper [11] confirmed also trigonal symmetry $D_{3d}^4 - P\bar{3}c1$ with $Z=2$. The c -parameter is doubled due to an anti-tilting of TiO_6 octahedra ($\sim 15^\circ$) around the c axis [11]. The structure of all four above-mentioned compounds consists of five AO_3 close-packed layers with B ions located in corner-sharing octahedral holes between the layers. No B atom lies between the third and the fourth layer. The crystal structure of $\text{Mg}_5\text{Nb}_4\text{O}_{15}$ and $\text{Mg}_5\text{Ta}_4\text{O}_{15}$ is completely different and is isostructural with pseudobrookite Fe_2TiO_5 [15]. The space group is orthorhombic $D_{2h}^{17} - Cmcm$ with $Z = 4$. The structure consists of double chains of $(\text{Mg,B})\text{O}_6$ units, sharing edges of the bc plane, interconnected through common oxygen along the a axis to give a three-dimensional array [15].

Infrared (IR) reflectivity and Raman-scattering spectra of $\text{Ba}_5\text{Nb}_4\text{O}_{15}$ were recently published by Massa *et al.* [19]. According to these authors the spectra indicate that the lattice of this compound is close to collapsing into a lower symmetry structure. MW properties, X-ray diffraction, Raman scattering and FIR transmission spectra of $\text{Ba}_{5-x}\text{Sr}_x\text{Nb}_4\text{O}_{15}$ were published in Ref. [9]. Their data did not support the monoclinic symmetry of $\text{Sr}_5\text{Nb}_4\text{O}_{15}$ suggested by Weiden *et al.* [7]. The remaining three materials ($5\text{ZnO}-2\text{Nb}_2\text{O}_5$, $5\text{CaO}-2\text{Nb}_2\text{O}_5$ and $5\text{CaO}-2\text{Ta}_2\text{O}_5$), which are studied in this contribution, were never characterized by means of any physical method.

3.3.2 Experimental

All the ceramics are prepared as described in section 3.2.1. The IR reflectivity and transmission spectra were obtained at room temperature using the Fourier transform spectrometer Bruker IFS 113v in the frequency range 30 – 2000 cm^{-1} and 15 – 100 cm^{-1} (0.45 - 3 THz), respectively. The resolution of the reflectivity spectra was 2 cm^{-1} , an accurate determination of the interferences in the transmission spectra required a resolution of 0.5 cm^{-1} . Room temperature DTGS detectors were used for the reflectivity measurements, while highly sensitive helium cooled (1.5 K) Si bolometer was used for the transmission measurements.

3.3.3 Results and Discussion

3.3.3.1 Infrared and sub-millimeter spectra

IR reflectivity spectra of all the investigated ceramics together with the fits are shown in Fig. 3.5. Many samples show broad reflection bands, i.e. they exhibit large splitting of longitudinal optic $\omega_{\text{LO}j}$ and transverse optic $\omega_{\text{TO}j}$ phonon frequencies.

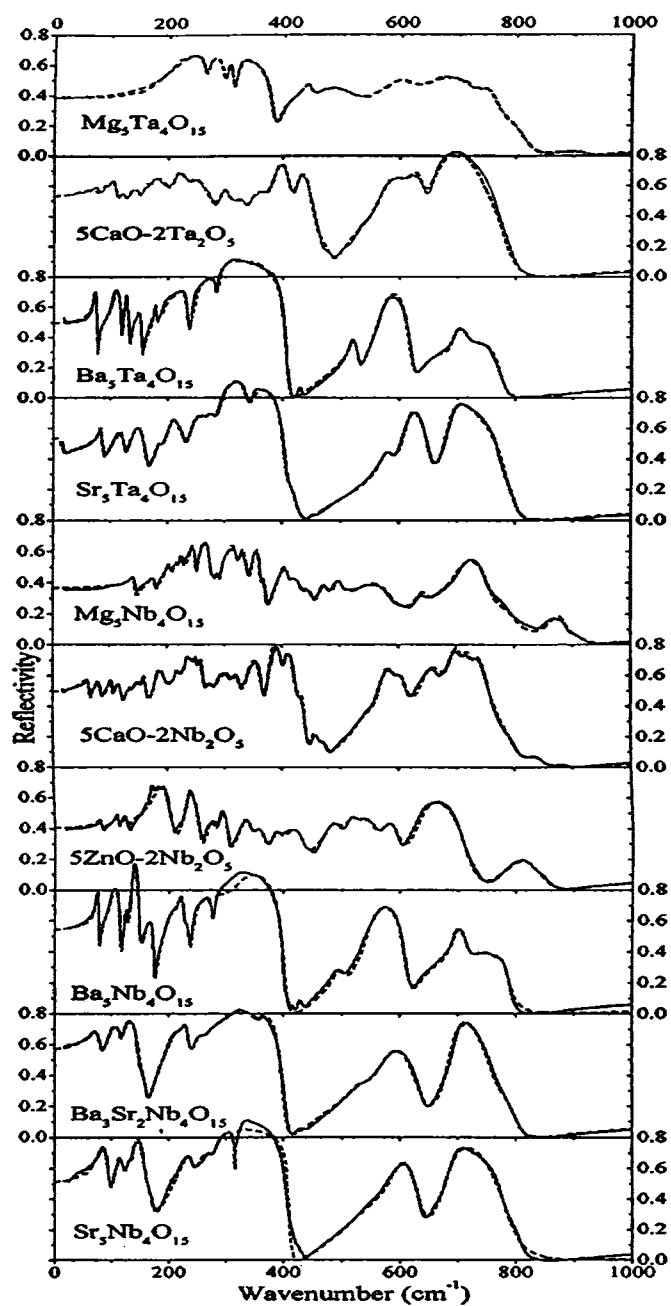


Fig. 3. 5 IR reflectivity spectra of the ceramics investigated.

**Solid and dashed curves are experimental
and fitted curves, respectively**

In this case their corresponding dampings γ_{LOj} and γ_{TOj} could substantially differ. Therefore, instead of Eq. (1) we have used the generalized factorized four-parameter oscillator model of the complex permittivity [33].

$$\varepsilon^*(\omega) = \varepsilon_\infty \prod_j \frac{\omega_{LOj}^2 - \omega^2 + i\omega\gamma_{LOj}}{\omega_{TOj}^2 - \omega^2 + i\omega\gamma_{TOj}}. \quad (3)$$

All the reflectivity spectra were fitted together with the transmission spectra. The reason of the simultaneous fitting was that in many cases the parameters of a good reflectivity fit did not fit the transmission spectra satisfactorily. Hence, in these cases we have added to the fit a weak and highly damped oscillator roughly describing the multiphonon absorption below the phonon frequencies. These weak additional features have no influence on reflectivity fits (reflectivity is not sensitive to weak absorption processes), but they markedly improved the transmission fit.

$\varepsilon'(\omega)$ and $\varepsilon''(\omega)$ obtained from the above fits were compared with the time resolved THz spectra and the MW data – see Fig. 3. 6 and Fig. 3. 7. One can see that the experimental $\varepsilon'(\omega)$ points agree very well with the calculated curves (obtained from reflectivity and transmission fits). No dispersion of $\varepsilon'(\omega)$ is seen below the phonon frequencies, a very good agreement of SMM ε' with the values in the MW region is observed. The accuracy of $\varepsilon'(\omega)$ obtained through TDTTS is

very high and depends practically only on the precision of the sample thickness determination.

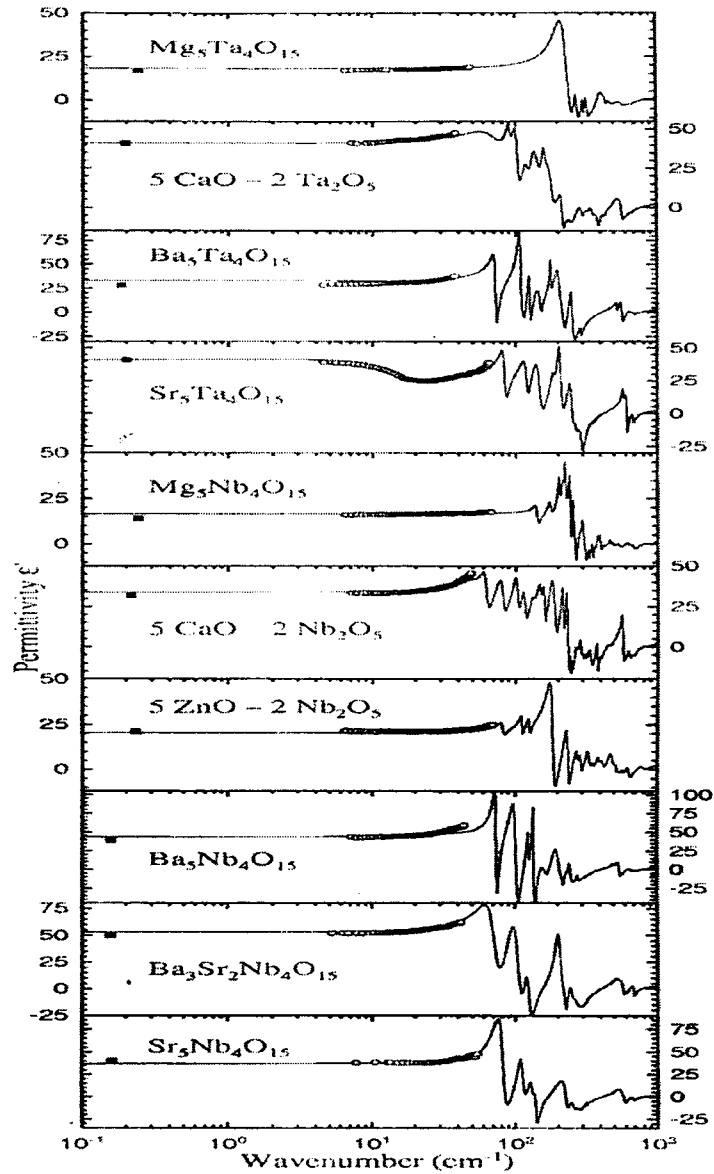


Fig. 3. 6 Permittivity ϵ' obtained from the fit of FIR transmission and reflectivity spectra (solid lines) compared with experimental values from the MW resonant cavity method (closed square) and TDTTS measurements (open circles).

R
519.641 537.226
JAW,1

G8776

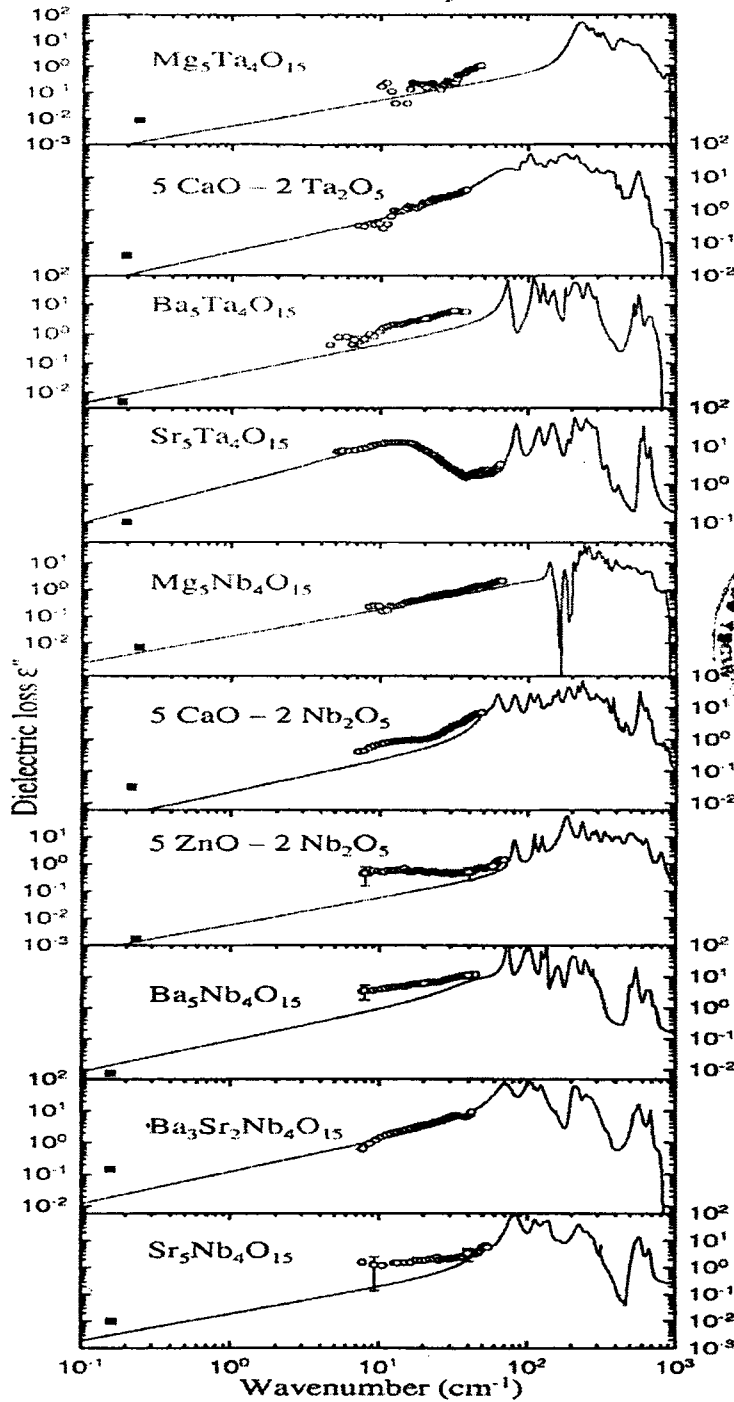


Fig. 3. 7 Dielectric loss ϵ'' obtained from the MW resonant cavity method (closed squares) and TDTTS measurements (open circles) compared with the result of the fit of FIR transmission and reflectivity spectra (solid lines). Note the log-log scale.

Experimental SMM values of $\epsilon''(\omega)$ are more noisy than $\epsilon'(\omega)$ because of a lower sensitivity of the method in case of low dielectric loss at low frequencies. The error bars are shown at the high and low frequency part of the spectra if they exceed the size of the points. The most of experimental $\epsilon''(\omega)$ values correspond to the calculated curves within the experimental error. Some deviation is seen mostly in several cases on multiphase samples. The linear extrapolation of SMM dielectric losses agrees rather well with the experimental MW data. Nevertheless, without cooling of the samples we cannot say, which kind of losses (extrinsic or intrinsic) predominates. Phonon spectra can also help us to distinguish which sample is single phase and which is not.

The experimental setup of TDTTS uses a biased large-aperture antenna (low-temperature grown GaAs) as a terahertz emitter and an electro-optic sampling detection technique.

The disc-shaped samples of diameter 9 mm and thickness of 1-2 mm were used for the reflectivity measurements. Well plane-parallel (about $200 \pm 1 \mu\text{m}$) thin plates were prepared for transmission measurements.

3.3.3.2 Phonon spectra and crystal structure

There is a close relationship between the features in IR reflectivity spectra and crystal structure of investigated ceramics. Number of atoms (s) in the primitive unit cell determines the number of different phonon modes N ($N=3s$) in

the Brillouin zone center (Γ -point of BZ). Not all optical phonons are infrared active, but the crystal structure determines the symmetry of vibrations and their activities in IR and Raman spectra.

$\text{Ba}_5\text{Ta}_4\text{O}_{15}$, $\text{Sr}_5\text{Ta}_4\text{O}_{15}$ and $\text{Ba}_5\text{Nb}_4\text{O}_{15}$ crystallize in the trigonal space group D_{3d}^3 with one formula unit ($Z=1$) per unit cell [1,2, 4, 15]. In this case 72 Γ -point modes are expected. Factor group analysis yields $A_{2u} + E_u$ acoustic modes (E_u is doubly degenerate) and $8A_{1g}(x^2+y^2, z^2) + 2A_{2g} + 10 E_g(x^2-y^2, xy, xz,yz) + 3A_{1u} + 10 A_{2u}(z) + 13E_u(x,y)$ optical modes in the Γ -point of BZ [19]. The letters in parenthesis give the mode activities in the spectra: x^2 , xy , xz etc. represent Raman activity in corresponding symmetry spectra. x,y,z mean infrared activity of the modes in $E||x$, $E||y$ and $E||z$ polarized spectra, respectively. In the ceramics, the $13E_u$ and $10A_{2u}$ symmetry modes cannot be distinguished in the IR spectra because of averaging over all grain orientations, therefore all 23 modes may be expected in the IR spectra. The fits of $\text{Ba}_5\text{Ta}_4\text{O}_{15}$ and $\text{Ba}_5\text{Nb}_4\text{O}_{15}$ ceramics spectra yield 17 and 18 phonon modes, respectively. It is a rather common case that not all predicted modes are seen in the spectra, the phonons can be weak or heavy damped in room temperature (RT) spectra and reflection bands can be overlapped.

The spectra of $\text{Ba}_5\text{Nb}_4\text{O}_{15}$ agree very well with the spectra published by Massa *et al.* [19].

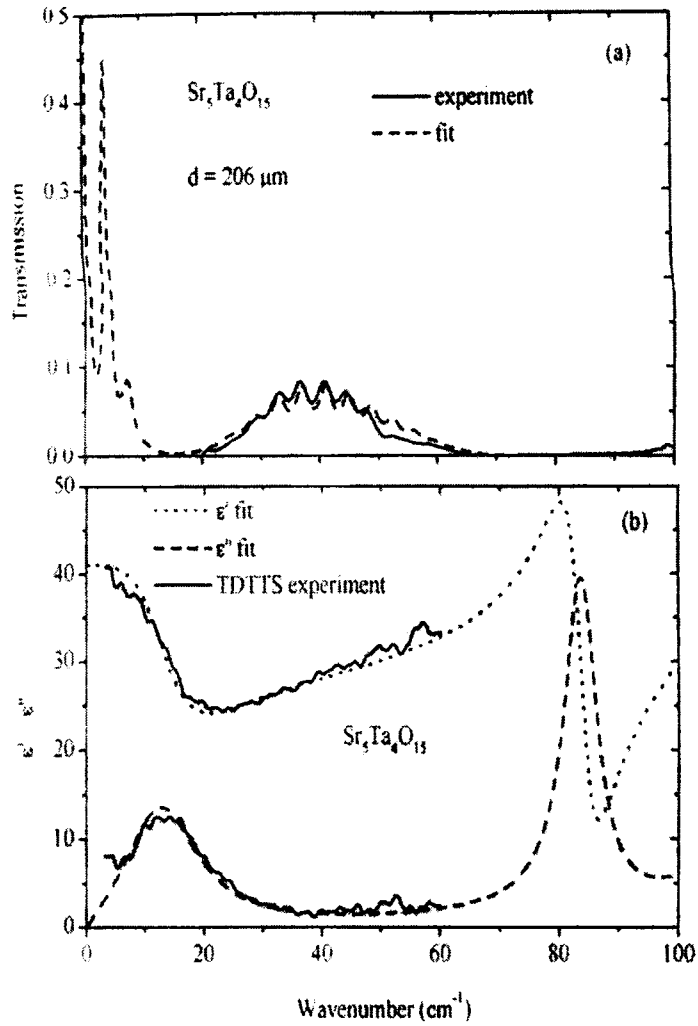


Fig. 3. 8 (a) Experimental and fitted FIR transmission spectra of $\text{Sr}_5\text{Ta}_4\text{O}_{15}$. (b) Complex dielectric spectra obtained from the TDTTS measurement compared with the result of FIR transmission and reflectivity spectra.

$\text{Sr}_5\text{Ta}_4\text{O}_{15}$ exhibits an unusual low-frequency heavily damped excitation at 15 cm^{-1} . This mode is partially seen in reflectivity and is very well evident in both THz and FIR transmission spectra (see Fig. 3. 8). Excellent agreement of TDTTS experiment with the result of FIR transmission and reflectivity spectra fit is

noticeable and illustrates the accuracy of our measurements. If $\text{Sr}_5\text{Ta}_4\text{O}_{15}$ sample could contain some traces of a second phase with complicated structure (more formula units per unit cell), the folded acoustic phonons can become IR active at such a low frequency. However, our XRD measurement confirmed only single-phase composition. So the excitation at 15 cm^{-1} is probably a phonon and its frequency is so low that it could be a soft optical mode. This could indicate the lattice instability and possibility of some structural phase transition. However, in our differential thermal scanning measurement we could not observe any phase transition in the range of 95 and 920 K. The low temperature dielectric measurement below 95 K is needed for a detection of the possible ferroelectric phase transition.

Two structures were reported for $\text{Sr}_5\text{Nb}_4\text{O}_{15}$ - monoclinic and trigonal. If the sample would crystallize in the monoclinic space group C_{2h}^1 with $Z=2$ [7], the factor group analysis yields A_u and $2B_u$ acoustic modes and $39A_g(x^2, y^2, z^2, xy) + 30A_u(z) + 27B_g(xz, yz) + 46B_u(x, y)$ optical modes. It means that totally 76 phonon modes could be expected in IR spectra. If the sample crystallize in the recently reported D_{3d}^4 space group with $Z=2$ [11], the group analysis yields $A_{2u} + E_u$ acoustic modes and $11A_{1g}(x^2+y^2, z^2) + 13A_{2g} + 24E_g(x^2-y^2, xy, xz, yz) + 11A_{1u} + 12A_{2u}(z) + 23E_u(x, y)$ optical modes in the Γ -point of BZ. So, overall 35 optical modes can be expected in IR spectra. In our case, only 13 modes were sufficient for the reflectivity spectra fitting, so the trigonal structure of the sample is more probable. Again, not all symmetry allowed modes are seen in the spectra due to their overlapping and high damping. Our result is consistent with the conclusion

in Ref. [9], who also could not confirm monoclinic structure of $\text{Sr}_5\text{Nb}_4\text{O}_{15}$ with $Z = 2$. One can see that the spectra of $\text{Ba}_{5-x}\text{Sr}_x\text{Nb}_4\text{O}_{15}$ are very similar to those of pure compounds with $x = 0$ and $x = 5$, so the structure of $\text{Sr}_5\text{Nb}_4\text{O}_{15}$ seems to be similar to $\text{Ba}_5\text{Nb}_4\text{O}_{15}$ with $Z = 1$. Phonon dispersion branches of optical phonons have probably only small dispersion in the BZ, therefore newly activated modes in the folded BZ have similar frequencies as already active modes. Therefore they are not resolved in reflectivity spectra but cause effectively higher damping of most of the modes.

The reflectivity spectra of $\text{Mg}_5\text{Ta}_4\text{O}_{15}$ and $\text{Mg}_5\text{Nb}_4\text{O}_{15}$ are completely different from previously discussed spectra giving the evidence about the different crystal structure. Both materials crystallize in orthorhombic D_{2h}^{17} space group with $Z = 4$ in the centered unit cell [15]. Their chemical formula can be rewritten as $\text{Mg}_{5/3}\text{B}_{4/3}\text{O}_5$ ($\text{B}=\text{Nb}$ or Ta) in order to be compared with the stoichiometry of the pseudo-brookite Fe_2TiO_5 . Necessarily, there must be a mixed occupancy of both metal positions, so the most general formula is $(\text{Mg}_{1-m}\text{B})_{4c}(\text{Mg}_{2/3+m}\text{B}_{4/3-m})_{8f}\text{O}_5$ in which both 4c and 8f positions are occupied by both cations $\text{Mg}(\text{II})$ and $\text{Nb}(\text{V})$ or $\text{Ta}(\text{V})$, randomly distributed. The group analysis yields $\text{B}_{1u}+\text{B}_{2u}+\text{B}_{3u}$ acoustic modes and $8\text{A}_g(x^2, y^2, z^2) + 3\text{A}_u + 5\text{B}_{1g}(xy) + 7\text{B}_{1u}(z) + 3\text{B}_{2g}(xz) + 7\text{B}_{2u}(y) + 8\text{B}_{3g}(yz) + 4\text{B}_{3u}(x)$ optical modes. It means that only 18 IR active modes are expected in the spectra of orthorhombic ceramics with pseudo-brookite structure. 14 modes were observed in reflectivity spectrum of $\text{Mg}_5\text{Ta}_4\text{O}_{15}$, however, 28 modes are distinguished in $\text{Mg}_5\text{Nb}_4\text{O}_{15}$ spectrum giving the evidence about the traces of a secondary phases in the sample.

IR reflectivity spectrum of $5\text{ZnO}-2\text{Nb}_2\text{O}_5$ with 18 modes is very similar to $\text{Mg}_5\text{Nb}_4\text{O}_{15}$ spectrum, giving the evidence about multiphase composition of the ceramics. The XRD analysis revealed that the ceramics is a mixture containing ZnNb_2O_6 and $\text{Zn}_2\text{Nb}_3\text{O}_8$ as the major phases.

$5\text{CaO}-2\text{Nb}_2\text{O}_5$ and $5\text{CaO}-2\text{Ta}_2\text{O}_5$ also display completely different reflectivity spectra compared with other samples supporting the results of XRD measurements that the ceramics do not form single phases but consist of more phases like CaB_2O_6 , $\text{Ca}_2\text{B}_2\text{O}_7$, etc (B=Nb, Ta). Multiphase composition of the ceramics is probably responsible for their relatively low Q factor.

3.3.4 Conclusion

New MW dielectrics with a general chemical formula $\text{A}_5\text{B}_4\text{O}_{15}$ (A=Ba, Sr, Mg, Zn, Ca; B=Nb, Ta) were studied by means of the FIR reflection, transmission and TDTTS. The last technique allowed us to determine directly ϵ' and ϵ'' in the range of $5 - 60 \text{ cm}^{-1}$ ($0.15 - 1.8 \text{ THz}$). The experimental THz data correspond very well to the results of the fits of FIR transmission and reflection spectra. Some exceptions are seen only in multiphase samples. It is shown that the MW ϵ' of our ceramic samples is determined by the polar phonon contributions and therefore ϵ' is dispersionless below the phonon frequencies. In single-phase samples, dielectric loss ϵ'' extrapolated from the SMM down to the MW region according to the simple proportionality $\epsilon''(\omega) \propto \omega$ corresponds satisfactorily to the MW data.

The number of phonon modes observed in IR reflectivity spectra brings information about the symmetry of crystal structure of the investigated ceramics, particularly about the number of formula units in the primitive unit cell. The spectra of $\text{Ba}_5\text{Nb}_4\text{O}_{15}$, $\text{Ba}_5\text{Ta}_4\text{O}_{15}$ and $\text{Sr}_5\text{Ta}_4\text{O}_{15}$ support the same trigonal symmetry with $Z = 1$. The low-frequency excitation at 15 cm^{-1} in $\text{Sr}_5\text{Ta}_4\text{O}_{15}$ suggest a ferroelectric soft mode, however, low-temperature measurements are needed to confirm it. IR spectrum of $\text{Sr}_5\text{Nb}_4\text{O}_{15}$ does not confirm the previously published monoclinic symmetry with $Z = 2$. The spectrum is similar to previous three samples with trigonal symmetry and $Z = 1$. Spectra of $\text{Mg}_5\text{Nb}_4\text{O}_{15}$ and $\text{Mg}_5\text{Ta}_4\text{O}_{15}$ confirm the known pseudobrookite structure, however the higher number of modes in $\text{Mg}_5\text{Nb}_4\text{O}_{15}$ indicate some traces of a second phase in the sample. The spectra of $5\text{ZnO}-2\text{Nb}_2\text{O}_5$, $5\text{CaO}-2\text{Nb}_2\text{O}_5$ and $5\text{CaO}-2\text{Ta}_2\text{O}_5$ differ from the spectra of all the above-investigated samples because of their multiphase compositions.

3. 4. $\text{Ba}_{5-x}\text{Sr}_x\text{Ta}_4\text{O}_{15}$, $\text{Ba}_5\text{Nb}_x\text{Ta}_{4-x}\text{O}_{15}$ AND $\text{Sr}_5\text{Nb}_x\text{Ta}_{4-x}\text{O}_{15}$ SOLID SOLUTION PHASES

3. 4. 1 Introduction

The far infrared and Raman studies of $\text{Ba}_5\text{Nb}_4\text{O}_{15}$ and $\text{Ba}_5\text{Ta}_4\text{O}_{15}$ [19, 20] have shown that the ceramics have difference in spectra even though both the ceramics crystallize within $D_{3d}^3 - P3m1$ space group with hexagonal structure. $\text{Ba}_5\text{Ta}_4\text{O}_{15}$ has shown the phonon activity of a stable lattice. The Raman spectra were in conformity with the proposed structure. However the $\text{Ba}_5\text{Nb}_4\text{O}_{15}$ has shown anomalous behaviour of the Raman spectra and is attributed to the small local departure of crystal structure from the proposed symmetry. On the basis of above results Massa et al. [19] has postulated that the structure is at the edge of collapsing into a lower symmetry state. Most of the phonons are hardened when the niobium is replaced by tantalum. The $\text{Ba}_5\text{Nb}_4\text{O}_{15}$ is characterized by a higher dielectric constant of 39 and higher τ_f of 78 ppm/ $^\circ\text{C}$ than those of $\text{Ba}_5\text{Ta}_4\text{O}_{15}$ where the values are 28 and 12 ppm/ $^\circ\text{C}$ respectively. At the same time $\text{Ba}_5\text{Ta}_4\text{O}_{15}$ showed higher quality factor than $\text{Ba}_5\text{Nb}_4\text{O}_{15}$ that may be due to its stable structure. Despite their similar structure and space group the two compounds have shown entirely different microwave dielectric properties. Hence the small local departure in the crystal structure of $\text{Ba}_5\text{Nb}_4\text{O}_{15}$ has to be ascribed to this anomaly.

$\text{Sr}_5\text{Nb}_4\text{O}_{15}$ has been established to be of the hexagonal structure based on X-ray, neutron diffraction and Raman spectroscopy and has a dielectric constant of 40 with τ_f of 55 ppm/ $^{\circ}\text{C}$ and is comparable to those values of its barium counterpart. $\text{Sr}_5\text{Ta}_4\text{O}_{15}$ has dielectric constant of 41 (at 10 MHz) and shows high dielectric loss at microwave frequencies. Hence an investigation of the microwave dielectric properties of the intermediate solid solutions phases should reveal some information of their structure. Further more in order to tune the microwave dielectric properties the solid solution phases were prepared by partially replacing Ba by Sr, Nb by Ta in $\text{Ba}_5\text{Nb}_4\text{O}_{15}$. Accordingly the microwave dielectric properties of $\text{Ba}_{5-x}\text{Sr}_x\text{Ta}_4\text{O}_{15}$, $\text{Ba}_5\text{Nb}_x\text{Ta}_{4-x}\text{O}_{15}$ and $\text{Sr}_5\text{Nb}_x\text{Ta}_{4-x}\text{O}_{15}$ solid solutions are investigated.

3.4.2 Experimental

The ceramics are prepared through the solid-state ceramic route. High purity BaCO_3 (99+ %) and SrCO_3 (99.9 %) (Aldrich Chemicals, USA) and Nb_2O_5 (99.9%) and Ta_2O_5 (>99.5%) (NFC, Hyderabad, India) are used as the starting oxide powders. The powders are weighed according to the stoichiometry, mixed in an agate mortar with pestle for 1 hour using distilled water as the medium. The wet mixed powder is dried and calcined at 1250- 1400 $^{\circ}\text{C}$ for 4-10 h with intermediate grindings. The calcined mixture is ground well for 1 hour, 3 wt% PVA is added as the binder, mixed, dried and again ground. The resultant fine

powder is uni-axially pressed in a tungsten carbide die under a pressure of 150 MPa such that the pressed disks have 6-8 mm height and 14 mm diameter. Stearic acid dissolved in iso-propanol is used as a lubricant. The green pellets are sintered at different temperatures in the range 1400-1625°C for 2 to 4 hours. The sintered pellets are polished well. The ceramics are characterised as described in chapter 2.

3.4.3 Results and discussion

3.4.3.1 Density

The calcination and sintering temperatures and percentage densities of the ceramics are given in Tables 3.4, 3.5 and 3.6.

Table 3.4
The microwave dielectric properties of $Ba_{5-x}Sr_xTa_4O_{15}$

x	% Density	Calcination Temp (°C)	Sint. Temp (°C)	ϵ_r	ϵ_r (corr)	τ_f ppm/°C	Q	f GHz
0	95	1325	1550	28.0	30.2	12	5700	5.55
1	96.2	1350	1575	31.1	32.9	49	1827	5.185
2	97.7	1350	1575	33.2	34.3	20	830	5.22
3	97.0	1375	1600	33.7	35.2	-25	490	5.05
4	97.0	1375	1600	31.7	33.2	-60	525	5.34
5	96	1400	1610	*	*	*	400	5.99

* Could not measure due to high dielectric loss.

Table 3. 5

The microwave dielectric properties of Ba₅Ta_{4-x}Nb_xO₁₅

x	% Den sity	Calcin- ation Temp. (°C)	Sint. Temp (°C)	ε _r	ε _r (corr)	τ _f (ppm/°C)	Q	f GHz
0	95.0	1325	1550	28.0	30.2	12	5700	5.55
1	86.7	1300	1500	25.7	31.7	16	4390	4.928
2	85.3	1300	1475	27.0	34.2	22	2250	4.726
3	90.4	1275	1435	32.2	37.2	35	1070	4.408
4	96.0	1250	1380	39.0	42.0	78	5000	4.73

Table 3. 6

**The % density, Calcination and sintering temperatures and
microwave dielectric properties of Sr₅Ta_{4-x}Nb_xO₁₅**

x	% Den sity	Calci- nation Temp (°C)	Sint. Temp (°C)	ε _r	ε _r (corre cted)	τ _f (ppm/°C)	Q GHz	f GHz
0	96	1400	1610	*	*	*	400	5.99
0.50	95.0	1400	1600	32.5	34.9	*	*	*
0.75	96.2	1400	1600	32.4	34.3	*	*	*
1.0	96.7	1400	1600	31.6	33.2	-32	*	*
1.5	95.0	1400	1575	32.2	34.5	*	*	*
2.0	97.8	1400	1575	33.2	34.3	-2	507	5.65
3.0	96.2	1300	1575	36.2	38.2	31	1340	5.17
4.0	93.0	1250	1400	40.0	45.2	55	4000	4.84

* The parameters could not measure due to high dielectric loss

In general the calcination and sintering temperatures increases when Sr is substituted at the Ba site and Ta is substituted at Nb site. The ceramics were sintered into dense bodies under the sintering conditions. The Ba_{5-x}Sr_xTa₄O₁₅ ceramics were sintered to 95 to 97.7 % of their theoretical densities when sintered in the range 1550°C to 1610°C for 4 hours. The Ba₅Nb_xTa_{4-x}O₁₅ ceramics were sintered to 85.3 to 96 % of their theoretical densities in the temperature range

1380 to 1550°C for 2 to 4 hours. The $\text{Sr}_5\text{Nb}_x\text{Ta}_{4-x}\text{O}_{15}$ ceramics were sintered to 93 to 97.8 % of their theoretical densities at 1575°C –1600°C for 4 hours.

3. 4. 3. 2 X-ray Diffraction Analysis

The structure and lattice parameters of the end members $\text{Ba}_5\text{Nb}_4\text{O}_{15}$ and $\text{Ba}_5\text{Ta}_4\text{O}_{15}$, $\text{Sr}_5\text{Nb}_4\text{O}_{15}$ and $\text{Sr}_5\text{Ta}_4\text{O}_{15}$ are already reported [6, 11, 38, 39]. All these compounds crystallize with hexagonal structure. $\text{Ba}_5\text{Nb}_4\text{O}_{15}$ and $\text{Ba}_5\text{Ta}_4\text{O}_{15}$ belong to the $D_{3d}^3 - P3m1$ space group [23,24]. $\text{Sr}_5\text{Nb}_4\text{O}_{15}$ possesses hexagonal structure and crystallize in the $P3c1$ space group where doubling of c axis occur such that $Z = 2$ [9,11]. Galasso and Katz [1] suggested Hexagonal structure with $a = 5.67 \text{ \AA}$ and $c = 11.42 \text{ \AA}$ for $\text{Sr}_5\text{Ta}_4\text{O}_{15}$. The calculated lattice parameters closely agree with the reported values except for $\text{Sr}_5\text{Ta}_4\text{O}_{15}$ where we have got $a = 5.646 \text{ \AA}$ and $c = 11.475 \text{ \AA}$. The substitution of Ba by Sr in $\text{Ba}_5\text{Ta}_4\text{O}_{15}$ is possible and the X-ray diffraction studies of the $\text{Sr}_x\text{Ba}_{5-x}\text{Ta}_4\text{O}_{15}$ compounds show single-phase nature.

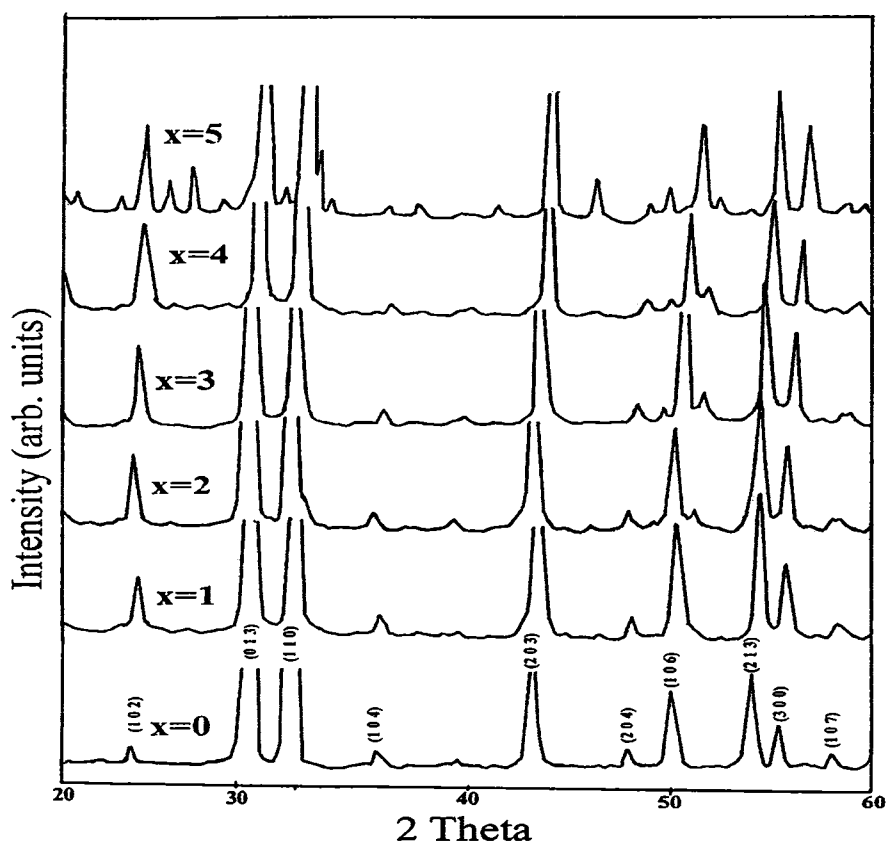


Fig. 3.9 The X-ray Diffraction Patterns of Ba_{5-x}Sr_xTa₄O₁₅ (x = 0, 1, 2, 3, 4, 5)

The XRD pattern of the compounds is given in Fig. 3.9. The solid solution phases are indexed based on Ba₅Ta₄O₁₅. The cell parameters a, c, c/a, and cell volume are given in Table 3.7.

Table 3.7
The cell parameters of Ba_{5-x}Sr_xTa₄O₁₅

Compound	A (Å)	c (Å)	c/a	V _m Å ³	D _x
0	5.79	11.802	2.038	342.63	7.990
1	5.76(5)	11.78(4)	2.044	339.05	7.83(9)
2	5.72(9)	11.78(5)	2.057	334.97	7.68(8)
3	5.710	11.719	2.052	330.89	7.533
4	5.69(0)	11.64(6)	2.047	326.53	7.380
5	5.646	11.475	2.032	316.78	7.347

The $\text{Ba}_5\text{Ta}_4\text{O}_{15}$ has a cell volume of 342.63 \AA^3 whereas that of $\text{Sr}_5\text{Ta}_4\text{O}_{15}$ is 316.78 \AA^3 . The cell parameter 'a' decreases from 5.79 \AA to 5.646 \AA and c decreases from 11.802 \AA to 11.475 \AA upon increasing x from 0 to 5. As a result the cell volume gradually decreases with x. The variation of a, c, c/a and cell volume are given in Fig 3.10 and 3.11 respectively.

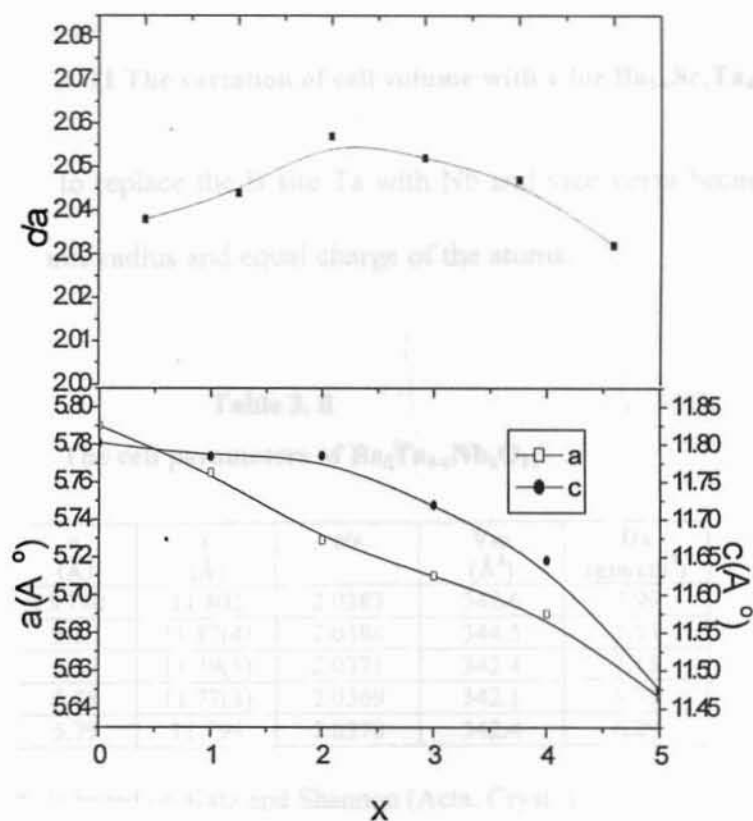


Fig. 3.10 The variation of cell parameters a, c, c/a for $\text{Ba}_{5-x}\text{Sr}_x\text{Ta}_4\text{O}_{15}$

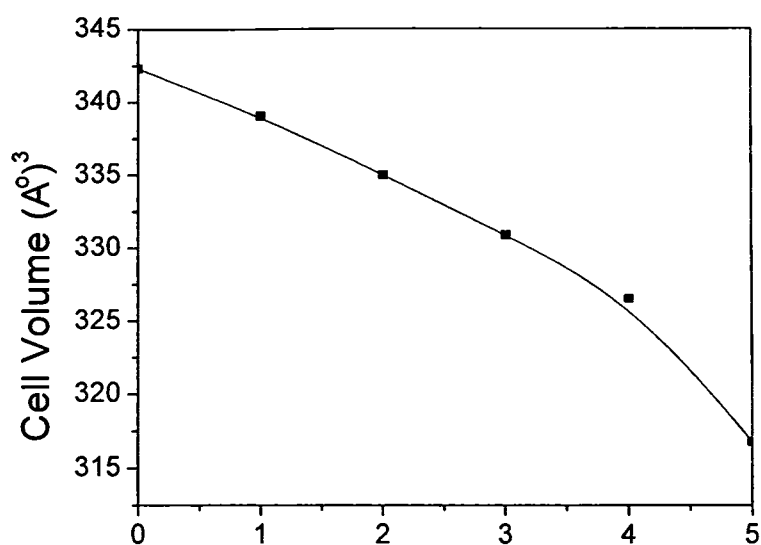


Fig. 3. 11 The variation of cell volume with x for $Ba_{5-x}Sr_xTa_4O_{15}$

It is also possible to replace the B site Ta with Nb and vice versa because of the nearly the same ionic radius and equal charge of the atoms.

Table 3. 8
The cell parameters of $Ba_5Ta_{4-x}Nb_xO_{15}$

X	a (Å)	c (Å)	c/a	Vm (Å³)	Dx (gm/cm³)
0*	5.790	11.802	2.0383	342.6	7.99
1.0	5.80	11.82(4)	2.0386	344.5	7.53
2.0	5.79	11.79(5)	2.0371	342.4	7.15
3.0	5.78	11.77(3)	2.0369	342.1	6.73
4.0	5.79	11.794	2.0370	342.4	6.29

* The data is based on Katz and Shannon (Acta. Cryst.)

The replacement of the B sites of $Ba_5Ta_4O_{15}$ with Nb gives the solid solution phases $Ba_5Nb_xTa_{4-x}O_{15}$. The XRD pattern is given in Fig. 3. 12. The XRD analysis shows single-phase nature of the ceramics. The intermediate

compounds were indexed based on $\text{Ba}_5\text{Ta}_4\text{O}_{15}$. The lattice parameters and cell volume are given in Table 3. 8.

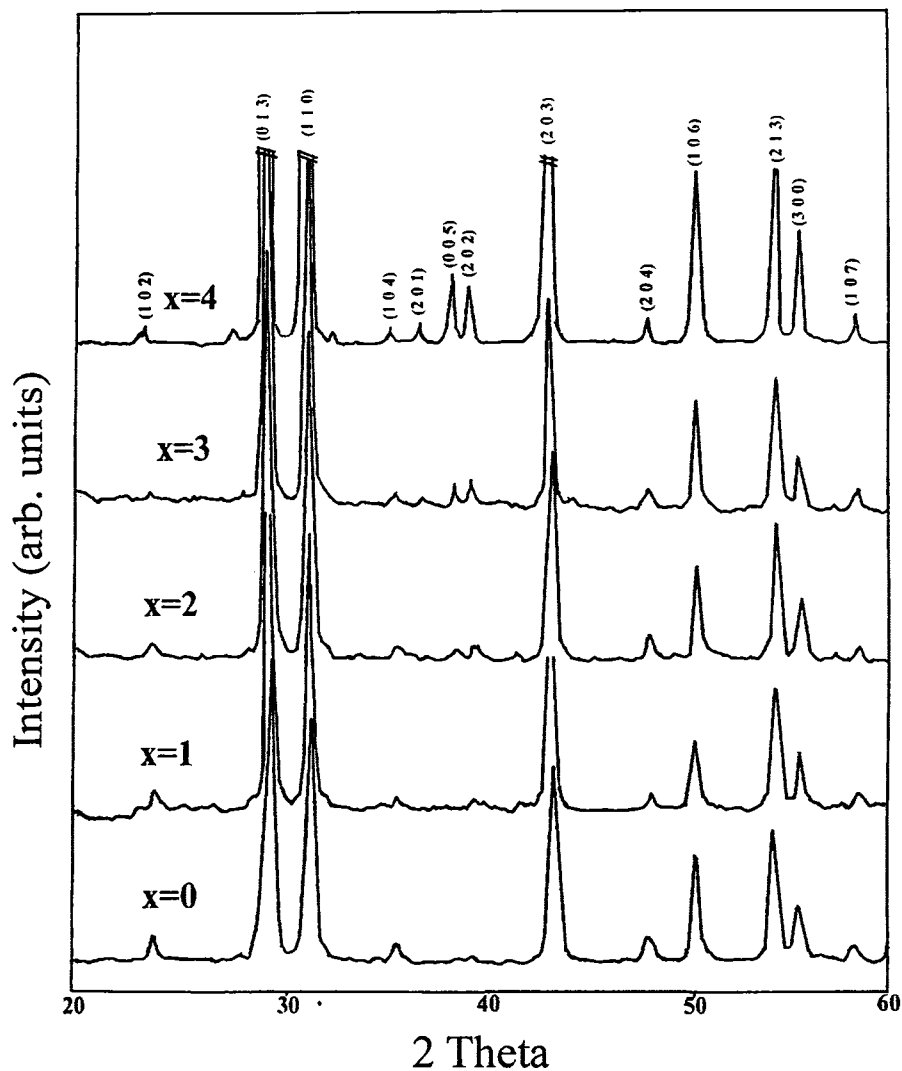


Fig. 3. 12 The X-ray diffraction patterns for $\text{Ba}_5\text{Nb}_x\text{Ta}_{4-x}\text{O}_{15}$ ($x = 0, 1, 2, 3, 4$)

The variation of a , c , c/a are plotted in Fig. 3. 13. The variation of cell volume with x is shown in Fig. 3. 14. The end compounds have nearly the same cell volume. There is no significant change in the lattice parameters or the cell

volume for the intermediate compounds although initially for $x = 1$, there is small increase in cell volume and lattice parameter 'c'.

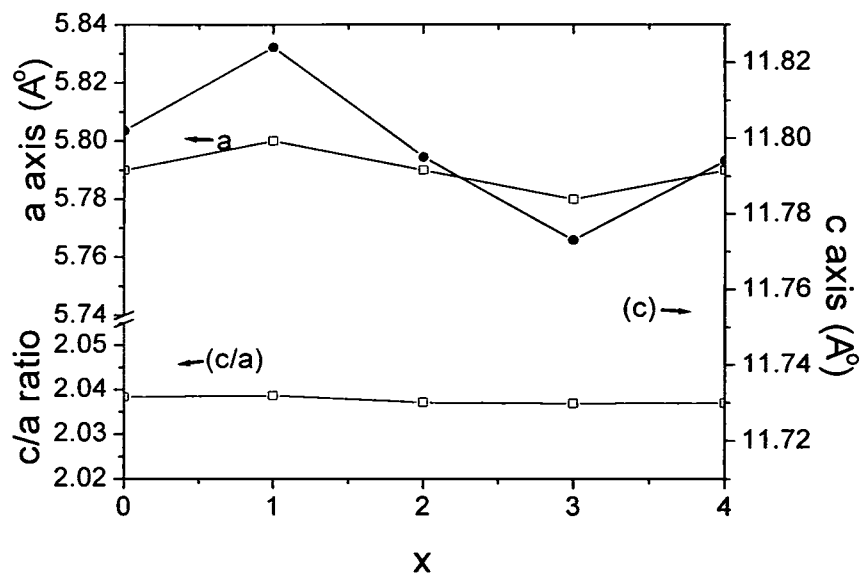


Fig. 3. 13 The variation of a, c and c/a with x for $Ba_5Nb_xTa_{4-x}O_{15}$

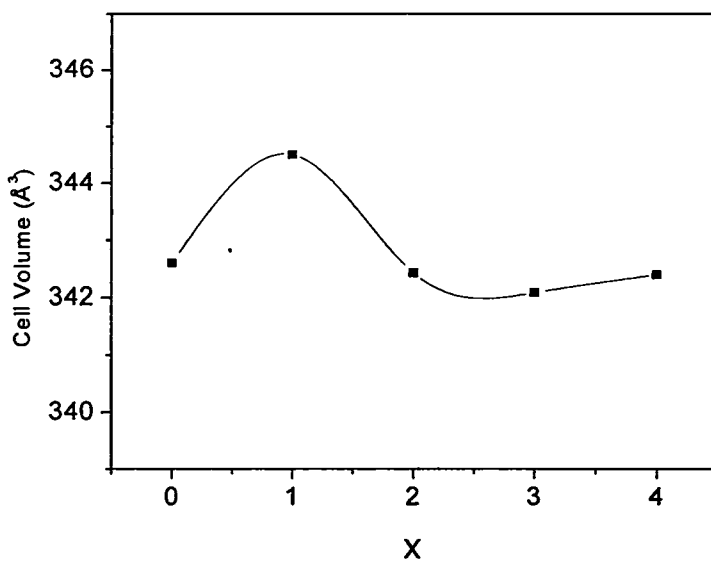


Fig. 3. 14 The variation of cell volume with x for $Ba_5Nb_xTa_{4-x}O_{15}$

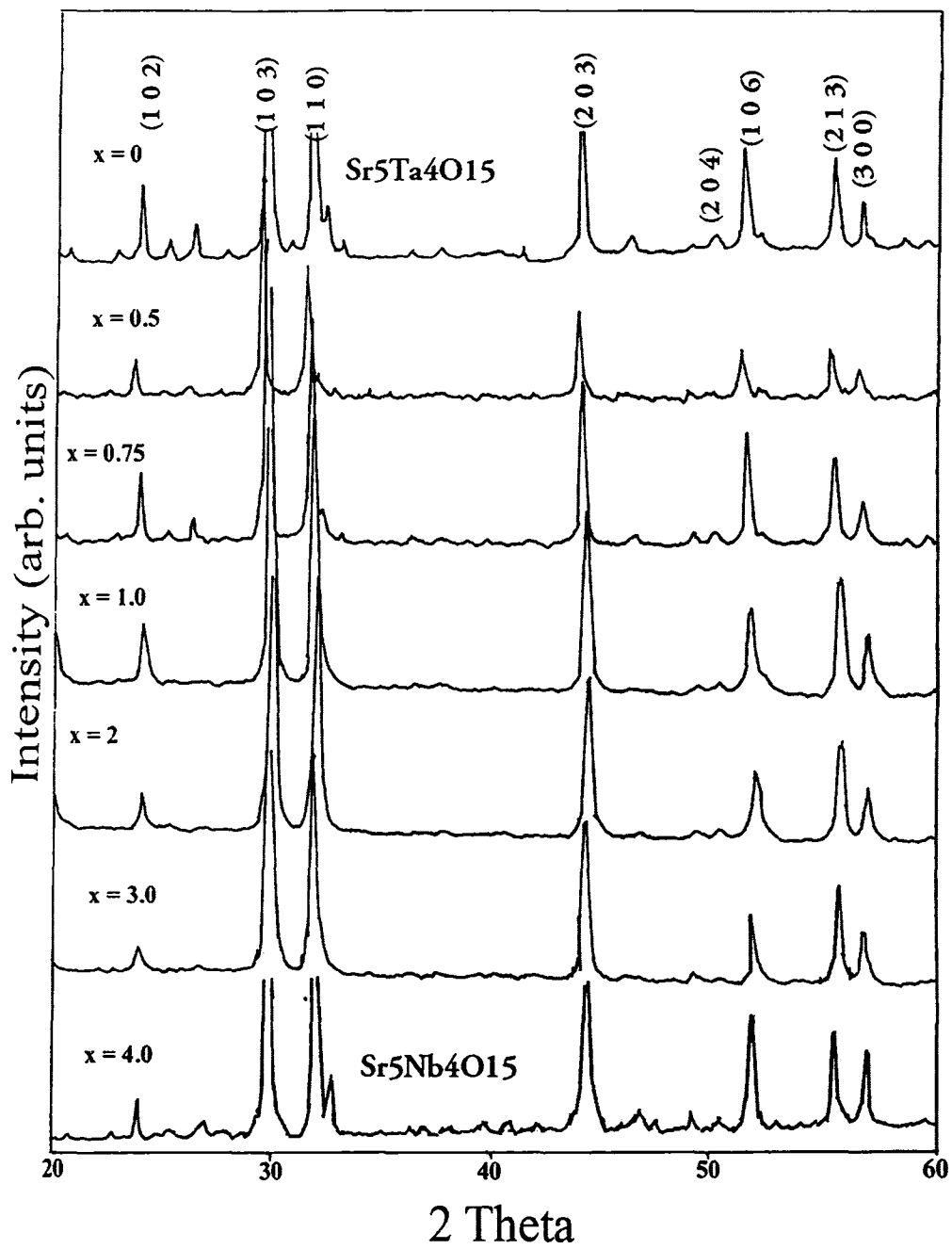


Fig. 3. 15 The X-ray diffraction patterns for $\text{Sr}_5\text{Nb}_x\text{Ta}_{4-x}\text{O}_{15}$ ($x=0, 1, 2, 3, 3.25, 3.5, 4.0$)

The $\text{Sr}_5\text{Nb}_x\text{Ta}_{4-x}\text{O}_{15}$ ceramics also give single-phase solid solutions. The XRD patterns are given in Fig. 3. 15. The variation of a , c , and c/a are shown in Fig. 3. 16. Upon substituting Nb up to $x = 0.5$, the cell volume increases from 316.78 to 319.31 (\AA^3) (Fig. 3. 17).

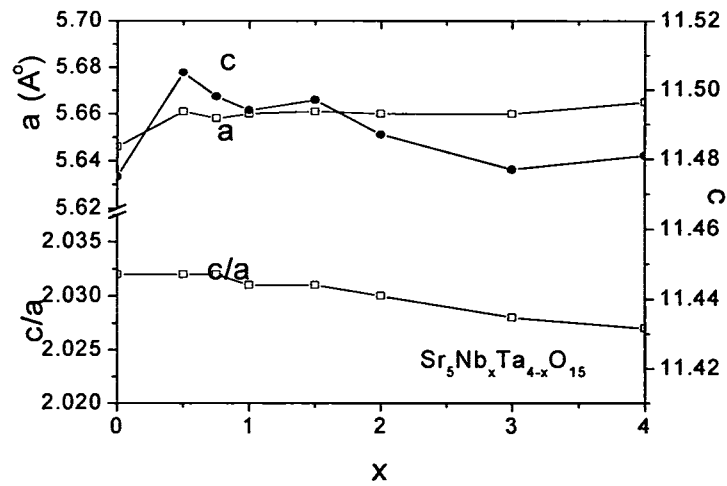


Fig. 3. 16 The variation of lattice parameters a , c and c/a with x for $\text{Sr}_5\text{Nb}_x\text{Ta}_{4-x}\text{O}_{15}$

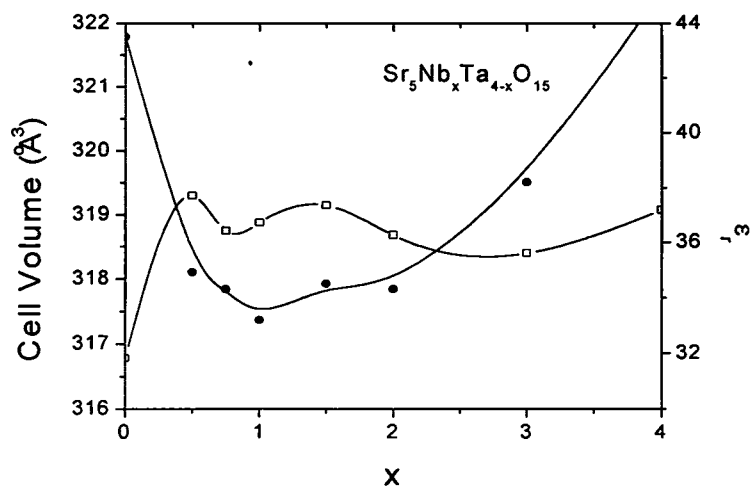


Fig. 3. 17 The variation of cell volume and ϵ_r with x for $\text{Sr}_5\text{Nb}_x\text{Ta}_{4-x}\text{O}_{15}$

Thereafter it remains more or less the same. After the initial increase, with increase in the value of x , the cell parameter 'a' increases slightly whereas 'c' decreases such that c/a remains almost a constant.

3.4.3.3 Microwave dielectric properties

3.4.3.3.1 $Ba_{5-x}Sr_xTa_4O_{15}$

The microwave dielectric properties of the $Ba_{5-x}Sr_xTa_4O_{15}$ ceramics are shown in Table 3.4 and Fig. 3.18.

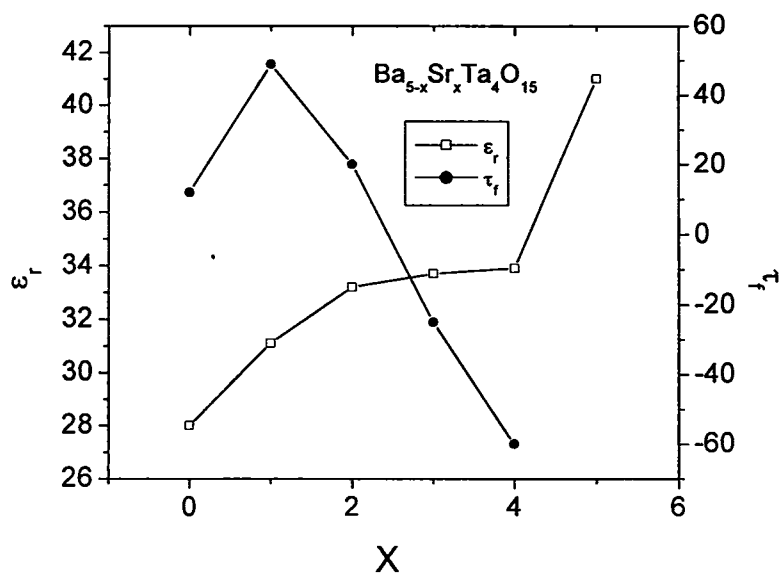


Fig. 3.18 The variation of ϵ_r and τ_f with x for $Ba_{5-x}Sr_xTa_4O_{15}$

The substitution of Sr at the Ba site increases the dielectric constant. The resonance become weak when $x > 3$. The microwave dielectric constant of $\text{Sr}_5\text{Ta}_4\text{O}_{15}$ could not be measured due to high loss of the samples even though the samples were sintered to $> 96\%$ densities. The low frequency dielectric constant is given in Table 3. 9.

Table 3. 9
The low frequency dielectric properties of the
 $\text{Ba}_{5-x}\text{Sr}_x\text{Ta}_4\text{O}_{15}$ ceramics (at 10 MHz)

Material	% density	ϵ_r	ϵ_r (corr)
$\text{Ba}_2\text{Sr}_3\text{Ta}_4\text{O}_{15}$	95.0	30.7	33.1
$\text{BaSr}_4\text{Ta}_4\text{O}_{15}$	96.3	29.7	31.4
$\text{Sr}_5\text{Ta}_4\text{O}_{15}$	96.0	41.0	43.5

The low frequency dielectric constants (measured at 10 MHz) are found to be lower than those measured at microwave frequencies. The dielectric constant (at 10 MHz) undergoes a sudden increase to 41 for $x = 5$ measured for a 96 % dense sample of $\text{Sr}_5\text{Ta}_4\text{O}_{15}$. The compound $\text{Ba}_5\text{Ta}_4\text{O}_{15}$ shows high quality factor of 5700 at 5.5 GHz whereas $\text{Sr}_5\text{Ta}_4\text{O}_{15}$ shows very weak resonance or low Q. The substitution of Sr at the Ba sites drastically reduces the quality factor. The higher dielectric loss of $\text{Sr}_5\text{Ta}_4\text{O}_{15}$ is established by the far infrared spectroscopic studies by high frequency method as described in Section 3. 3. As x increases the τ_f initially increases and then decreases and becomes negative.

3.4.3.3.2 Ba₅Nb_xTa_{4-x}O₁₅

The dielectric constant of the solid solutions phases Ba₅Nb_xTa_{4-x}O₁₅ is shown in Table 3. 5. The dielectric constant increases with niobium content. The variation of ϵ_r and τ_f with x are shown in Fig. 3. 19.

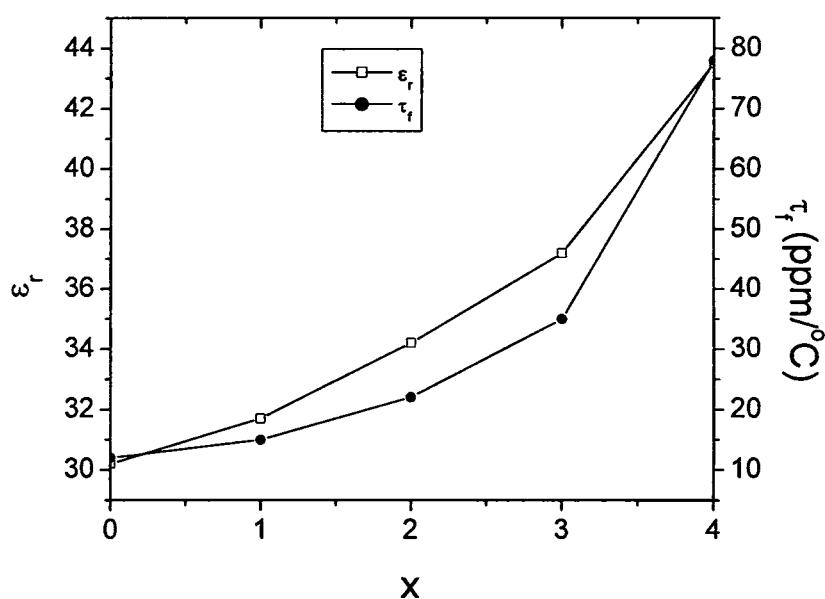


Fig. 3. 19 The variation of ϵ_r and τ_f with x for Ba₅Nb_xTa_{4-x}O₁₅

The variation in τ_f and ϵ_r with x are found to be continuous and gradual. The Ba₅Ta₄O₁₅ and Ba₅Nb₄O₁₅ are characterized with high quality factors. There is a lowering of quality factors for the intermediate compounds when compared to the end compounds, which is attributed to porosity. Though both Ba₅Nb₄O₁₅ and Ba₅Ta₄O₁₅ crystallize within $D_{3d}^3 - P3m1$ space group with hexagonal structure, their Raman spectra were different. The Ba₅Ta₄O₁₅ shows the features of a hardened phonon spectra and hence a stable structure. Hence according to Massa

et al. [20], there may be a small local departure from the suggested structure for $\text{Ba}_5\text{Nb}_4\text{O}_{15}$ and is at the edge of collapsing into a lower symmetry state. $\text{Ba}_5\text{Ta}_4\text{O}_{15}$ has a comparatively lower ϵ_r of 28 and τ_f of 12 ppm/ $^\circ\text{C}$ than $\text{Ba}_5\text{Nb}_4\text{O}_{15}$, which has ϵ_r of 39, and τ_f of +78 ppm/ $^\circ\text{C}$. The increase in dielectric constant of $\text{Ba}_5\text{Nb}_4\text{O}_{15}$ may be due to the local variations in the structure from the proposed symmetry. Ratheesh et al. [40] has suggested larger short-range interaction parameter in O-Ta-O bond as the cause of lowering of dielectric constant and lower dielectric loss for tantalum compounds than the niobium compounds. The gradual increase in ϵ_r and τ_f of the intermediate compound within $\text{Ba}_5\text{Ta}_{4-x}\text{Nb}_x\text{O}_{15}$ system suggest that this local departure may be gradual from the D^3_{3d} space group and with increase in the niobium content the structure may be approaching to that of $\text{Ba}_5\text{Nb}_4\text{O}_{15}$. No abrupt variation in microwave dielectric properties is observed for the above compounds.

3. 4. 3. 3. 3 $\text{Sr}_5\text{Nb}_x\text{Ta}_{4-x}\text{O}_{15}$ ceramics

The microwave dielectric properties of the ceramics are shown in Table 3. 6. The variation of ϵ_r and τ_f with x is shown in Fig. 3. 20. The $\text{Sr}_5\text{Nb}_x\text{Ta}_{4-x}\text{O}_{15}$ have ϵ_r in the range 30-45. For x = 0, ($\text{Sr}_5\text{Ta}_4\text{O}_{15}$) the loss is very high and do not resonate. Hence low frequency measurements using LCR meter is done and the results are given in Table 3. 10, Fig. 3. 21 and Fig. 3. 22. The porosity corrected ϵ_r for $\text{Sr}_5\text{Ta}_4\text{O}_{15}$ at 10 MHz is 43.5. For x = 0.5 the microwave dielectric constant

decreases to 34.9. The dielectric constant remains steady at 34 ± 1 in the range $0.5 < x < 2.0$ and thereafter increases to 45.2 when $x = 4$.

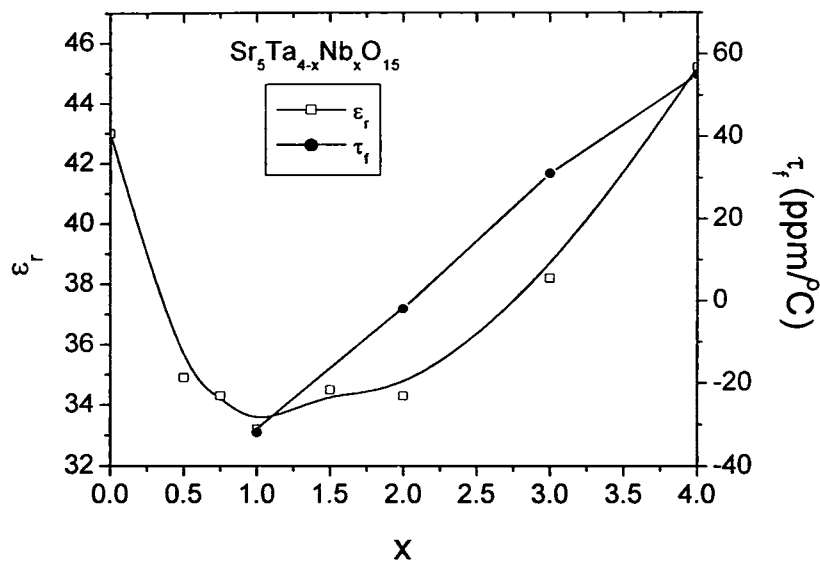


Fig. 3.20 The variation of ϵ_r and τ_f with x for $\text{Sr}_5\text{Ta}_{4-x}\text{Nb}_x\text{O}_{15}$ at microwave frequencies

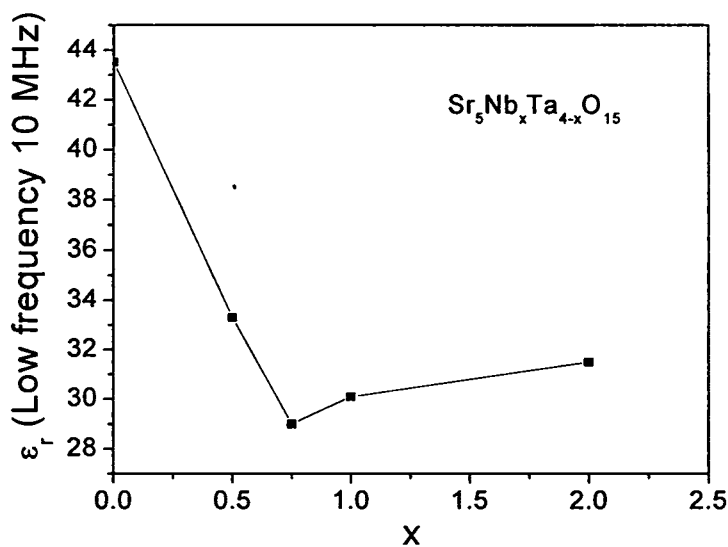


Fig. 3.21 The variation of ϵ_r and τ_f with x for $\text{Sr}_5\text{Ta}_{4-x}\text{Nb}_x\text{O}_{15}$ at 10 MHz

Table 3. 10
The RF dielectric properties of the $\text{Sr}_5\text{Ta}_{4-x}\text{Nb}_x\text{O}_{15}$
ceramics (at 10 MHz)

X	% density	ϵ_r	ϵ_r (corr)
0	96.0	41.0	43.5
0.5	93.5	30.2	33.3
0.75	96.0	27.3	29.0
1.0	94.7	27.8	30.1
2.0	96.3	29.8	31.5

The dielectric constants of the ceramics measured at low frequencies are found to be lower than the values measured at microwave frequencies. The intermediate solid solution phases have comparatively lower dielectric constant compared to the end compounds. The τ_f varies from -32 to 55 when x varies from 1.0 to 5.0. The τ_f values could not be determined for samples with $x \leq 1$ due to their high dielectric loss. The τ_f of solid solution is negative at the Ta rich end and increases to +ve value with increase in Nb content. The intermediate solid solutions show higher dielectric loss up to $x \geq 1$ such that the quality factors of the compounds could not be measured even though the samples were very dense. The quality factor increases with $x = 2$. The quality factor improves as the niobium content increases. No noticeable change in cell volume takes place in this range (See Table 3.11). The dielectric constant sharply increased to 38.2 for $x = 3$ without any significant change in cell volume and further increases to 45.2 for $x = 4$. The associated change in the cell volume is small. This may be due to some phase change from one symmetry group to another as the substitution of Nb progresses and contribute to the sudden increase in dielectric constant when the composition approaches toward the niobium rich end.

3. 4. 4 Conclusion

The $Ba_{5-x}Sr_xTa_4O_{15}$, $Ba_5Nb_xTa_{4-x}O_{15}$ and $Sr_5Nb_xTa_{4-x}O_{15}$ are obtained in phase pure form with high densities using the solid-state ceramic route. The structure of the compounds is studied through X-ray diffraction technique and dielectric properties by low frequency and microwave methods. The lattice parameters and cell volumes are determined for the solid solutions. All the ceramics crystallize with hexagonal symmetry. The substitution of Sr at the Ba site in $Ba_{5-x}Sr_xTa_4O_{15}$ increases the dielectric constant with increase in the value of x. The loss is very high when $x > 3$. The $Ba_5Nb_xTa_{4-x}O_{15}$ system shows intermediate dielectric properties of the end compounds. The $Sr_5Nb_xTa_{4-x}O_{15}$ solid solutions show lower dielectric constant than the end members and the dielectric constant remains more or less the same in the range $0.5 < x < 2.0$. The trend in variation of ϵ_r is further confirmed by low frequency measurements. The dielectric loss for the ceramics is increasing drastically when the solid solutions approach to $Sr_5Ta_4O_{15}$ by the substitution at the A and B site. No significant anomaly in cell volume change is noticed for the systems. Hence the abnormal dielectric properties of the systems may be due to change in symmetry or the local variations in structure of the compounds. Though the ceramics do not give any useful materials for practical applications the interesting dielectric properties can give insight into the dielectric phenomena for the cation deficient perovskites at the phase transition region.

3.5 THE MICROWAVE DIELECTRIC PROPERTIES OF $(1-x)\text{ZnNb}_2\text{O}_6 - x\text{Zn}_3\text{Nb}_2\text{O}_8$ MIXTURES

3.5.1 Introduction

In Section 3.2, we have attempted to prepare $\text{Zn}_5\text{Nb}_4\text{O}_{15}$ in analogy with compounds of $\text{A}_5\text{B}_4\text{O}_{15}$. But $\text{Zn}_5\text{Nb}_4\text{O}_{15}$ did not form, instead a mixture of ZnNb_2O_6 and $\text{Zn}_3\text{Nb}_2\text{O}_8$. In section 3.2 we have seen that the mixture phases have high dielectric constant of 22, high $Q \times f$ of 88000 GHz and τ_f of $-73 \text{ ppm}/^\circ\text{C}$. The X-ray diffraction analysis revealed that the ceramic is a mixture of ZnNb_2O_6 and $\text{Zn}_3\text{Nb}_2\text{O}_8$. The ZnNb_2O_6 has ϵ_r of 25 with high $Q \times f$ of 83700 GHz and τ_f of $-56 \text{ ppm}/^\circ\text{C}$ [25]. During the course of this work the Kim et al. [26] has reported the microwave dielectric properties of $\text{Zn}_3\text{Nb}_2\text{O}_8$ with $Q \times f$ 83300 GHz and τ_f of $-71 \text{ ppm}/^\circ\text{C}$. The higher quality factor of the mixture $5\text{ZnO}-2\text{Nb}_2\text{O}_5$ (mixture of ZnNb_2O_6 and $\text{Zn}_3\text{Nb}_2\text{O}_8$) than its components stimulated us for a systematic investigation of the mixture phases between ZnNb_2O_6 and $\text{Zn}_3\text{Nb}_2\text{O}_8$. In this section the preparation and microwave dielectric properties of $(1-x)\text{ZnNb}_2\text{O}_6+x\text{Zn}_3\text{Nb}_2\text{O}_8$ mixtures are investigated.

3.5.2 Experimental

The ceramics are prepared through the solid-state ceramic route. Two methods are used for the preparation of $(1-x)\text{ZnNb}_2\text{O}_6 + x\text{Zn}_3\text{Nb}_2\text{O}_8$. In first method, the mixture phases were directly obtained from the composition $(1-x)\text{ZnNb}_2\text{O}_6 + x\text{Zn}_3\text{Nb}_2\text{O}_8$ ($x=0.2, 0.4, 0.5, 0.6, 0.8, 0.9$) by mixing ZnO and Nb₂O₅ according to the formula. High purity ZnO (99.9%, Aldrich Chemicals) and Nb₂O₅ (99.9 %, NFC, India) are used as starting oxide powders. The stoichiometrically weighed powders were mixed by ball milling for 24 h using zirconia balls using distilled water as the mixing medium. The slurry is dried and calcined at 1050°C for 4 hours. The calcined powder is ground well in an agate mortar for 1 hour. 3 wt% PVA is used as the binder. Stearic acid is used as the lubricant. The dried powder is ground well and formed into cylindrical compact in a tungsten carbide die having 14 mm diameter under a pressure of 200 MPa. The aspect ratio of the pellet has to be 2 to 2.5 for best performance. The green compacts were sintered at 1190°C for 2 hours. In the second method the ZnNb₂O₆ and Zn₃Nb₂O₈ were separately prepared through the solid state ceramic route as described above and fine powders of ZnNb₂O₆ and Zn₃Nb₂O₈ were mixed together in the molar ratios $(1-x)\text{ZnNb}_2\text{O}_6-x\text{Zn}_3\text{Nb}_2\text{O}_8$ ($x= 0.2, 0.4, 0.50, 0.6, 0.8$), 3 wt% PVA is added, dried, again ground, shaped into pellets as described above and sintered at appropriate temperatures and polished the surfaces. The bulk densities of all samples were measured using Archimedes method. The microwave characterization was done as described in chapter 2.

3.5.3 Results and discussion

3.5.3.1 Density

The ceramics were sintered well near to their theoretical densities. The individual members ZnNb_2O_6 , $\text{Zn}_3\text{Nb}_2\text{O}_8$ and the mixed phases were sintered to their optimum densities in the temperature range 1175 to 1190°C. The mixed phases showed higher sinterability than the constituent phases i.e., ZnNb_2O_6 and $\text{Zn}_3\text{Nb}_2\text{O}_8$. The theoretical densities for ZnNb_2O_6 and $\text{Zn}_3\text{Nb}_2\text{O}_8$ are 5.65 and 5.82 respectively. Using these data, the theoretical densities of the mixture were calculated according to the equation

$$\rho_m = x\rho_{z_3} + (1-x)\rho_z$$

where ρ_m is the calculated theoretical density and ρ_{z_3} and ρ_z are the theoretical densities of $\text{Zn}_3\text{Nb}_2\text{O}_8$ and ZnNb_2O_6 respectively. Table 3.12 and Table 3.13 show the densities and percentage densities of ceramics prepared through both methods. Fig. 3.23 shows the plot of the densities and percentage densities of the ceramics. The ceramics prepared through the $\text{ZnO-Nb}_2\text{O}_5$ route is denser than the other. The calculated theoretical densities by mixture rule are also shown. The density of the mixture increases with $\text{Zn}_3\text{Nb}_2\text{O}_8$.

Table 3. 12

**The microwave dielectric properties of $x\text{Zn}_3\text{Nb}_2\text{O}_8 - (1-x)\text{ZnNb}_2\text{O}_6$
(prepared through ZnO-Nb₂O₅ route)**

x	ρ g/cm³	Theor. Density	% dens ity	ϵ_r	ϵ_r (corr)	τ_f (ppm/°C)	Qxf GHz
0.0	5.50	5.645	97.4	23.7	24.8	-55	51300
0.2	5.56	5.688	97.7	23.7	24.5	-61	85580
0.4	5.64	5.725	98.5	23.6	24.1	-63	86152
0.6	5.66	5.757	98.3	23.2	23.8	-64	87725
0.8	5.68	5.785	98.2	23.0	23.6	-68	84590
1.0	5.57	5.810	95.8	21.2	22.6	-72	64800

Table 3. 13

**The microwave dielectric properties of $x\text{Zn}_3\text{Nb}_2\text{O}_8 - (1-x)\text{ZnNb}_2\text{O}_6$
(prepared through ZnNb₂O₆-Zn₃Nb₂O₈ route)**

x	ρ g/cm³	Theor. Density g/cm³	% density	ϵ_r	ϵ_r (corr)	τ_f ppm/°C	Qxf GHz
0.0	5.50	5.645	97.6	23.7	24.8	-55	51300
0.2	5.52	5.688	97.5	23.5	24.3	-61	92100
0.4	5.58	5.725	97.2	22.8	23.7	-64	93100
0.5	5.59	5.742	97.2	22.7	23.6	-65	91200
0.6	5.62	5.757	97.6	22.7	23.5	-67	89500
0.8	5.60	5.785	96.8	22.0	23.0	-71	89900
1.0	5.57	5.81	95.8	21.2	22.6	-73	64800

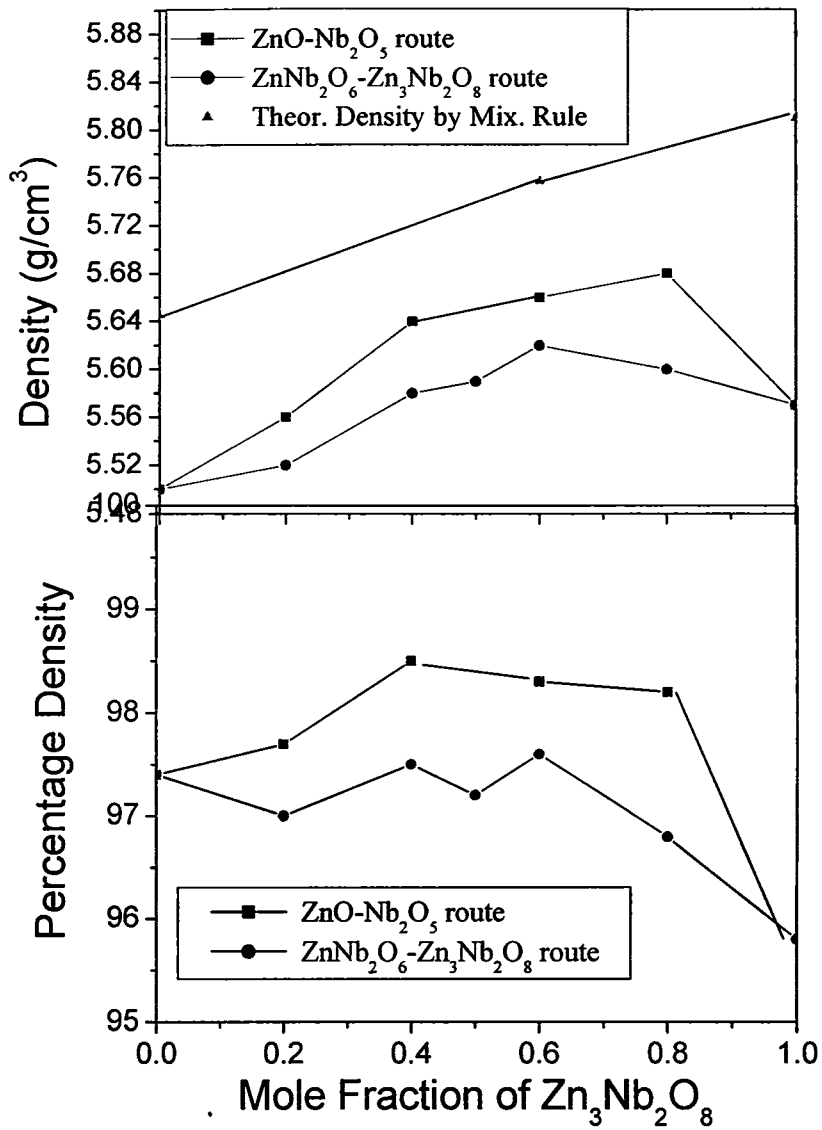


Fig. 3. 23 The variation of density and percentage density with mole fraction of $Zn_3Nb_2O_8$

3.5.3.2 X-ray diffraction analysis

Fig. 3. 24 shows the XRD pattern of $(1-x)\text{ZnNb}_2\text{O}_6 - x\text{Zn}_3\text{Nb}_2\text{O}_8$ (prepared through the $\text{ZnO-Nb}_2\text{O}_5$ route) where as Fig. 3. 25 shows XRD patterns of $(1-x)\text{ZnNb}_2\text{O}_6-x\text{Zn}_3\text{Nb}_2\text{O}_8$ (prepared through $\text{ZnNb}_2\text{O}_6\text{-Zn}_3\text{Nb}_2\text{O}_8$ route).

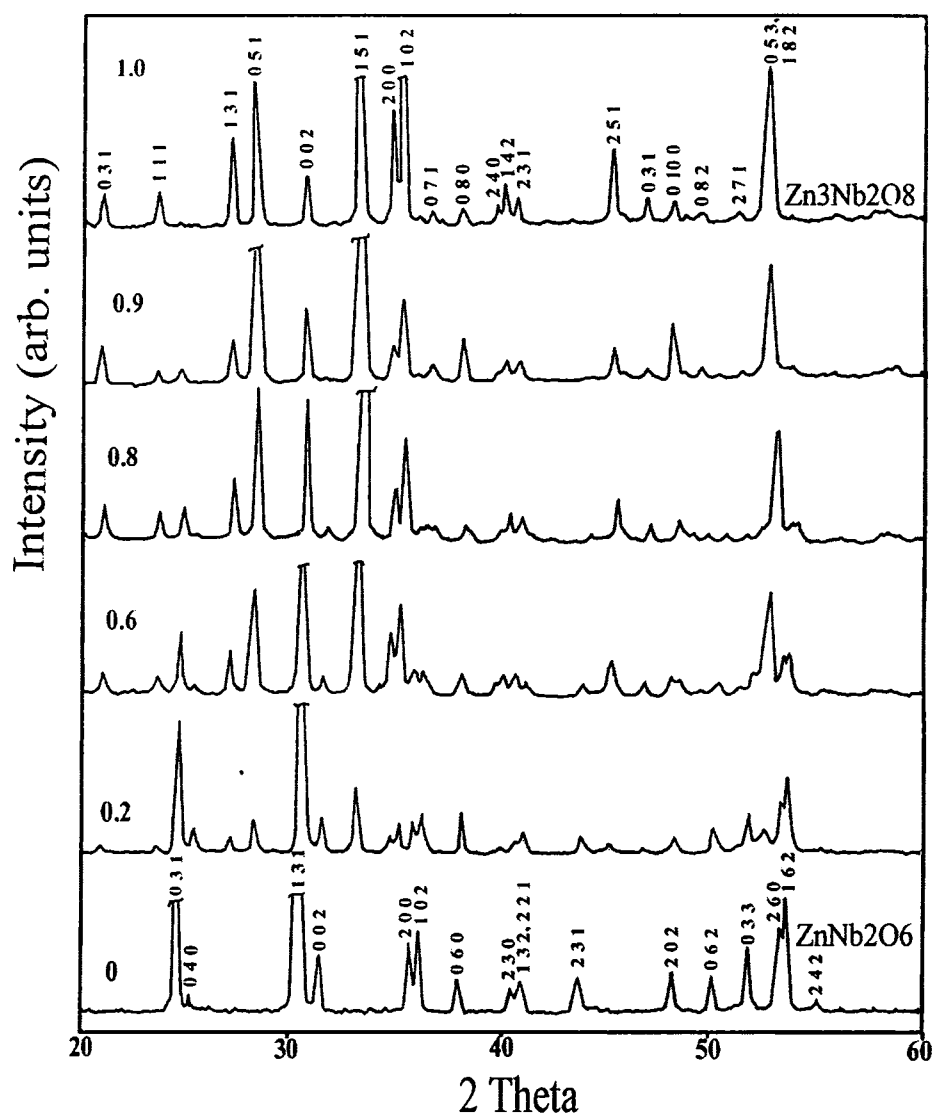


Fig 3. 24 The XRD of $x\text{Zn}_3\text{Nb}_2\text{O}_8 - (1-x)\text{ZnNb}_2\text{O}_6$ ($\text{ZnO-Nb}_2\text{O}_5$ route)

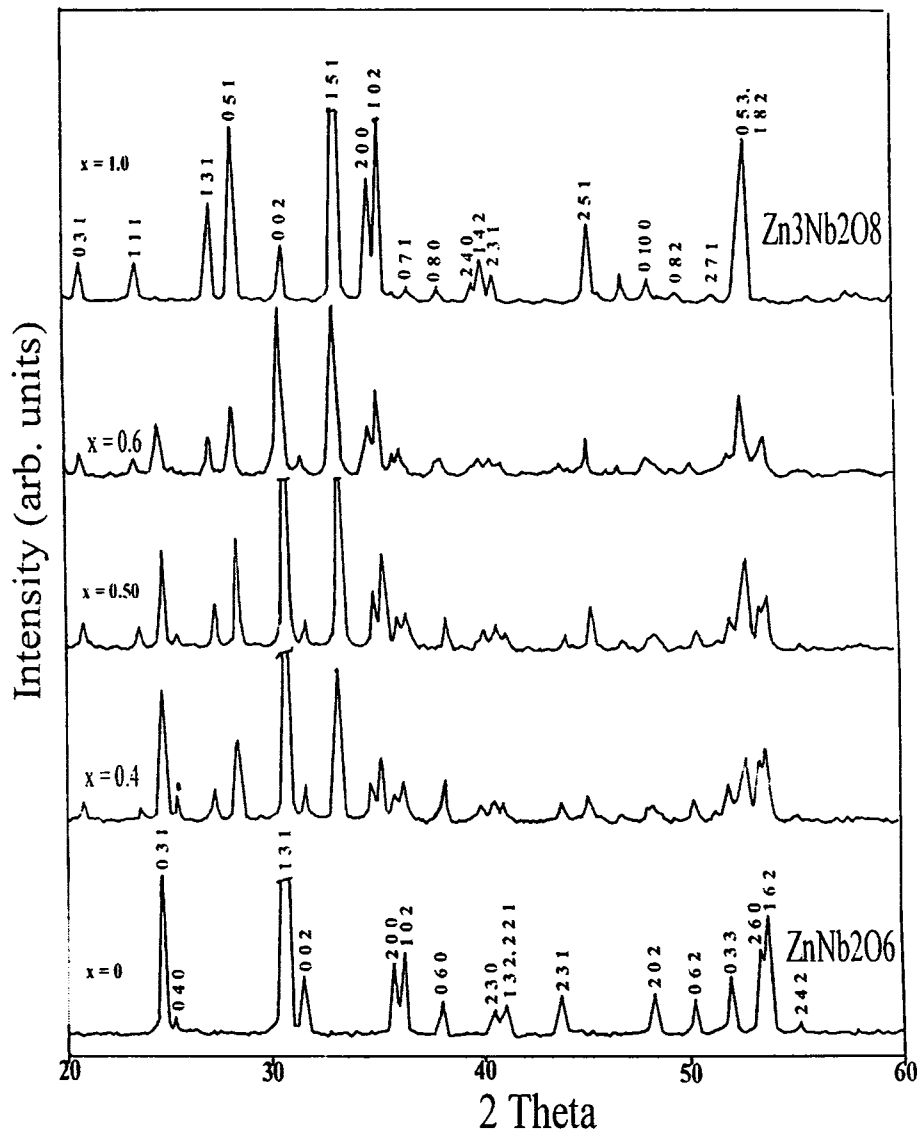


Fig. 3. 25 The XRD of $x\text{Zn}_3\text{Nb}_2\text{O}_8 - (1-x)\text{ZnNb}_2\text{O}_6$ mixtures ($\text{ZnNb}_2\text{O}_6\text{-Zn}_3\text{Nb}_2\text{O}_8$ route)

The XRD patterns of ZnNb_2O_6 and $\text{Zn}_3\text{Nb}_2\text{O}_8$ are compared with the standard JCPDS file and confirmed that the expected phases are formed. (Ref.

File Card No. 37-1371 for ZnNb_2O_6 and 26-1026 for $\text{Zn}_3\text{Nb}_2\text{O}_8$). The XRD patterns shows that the $(1-x)\text{ZnNb}_2\text{O}_6-x\text{Zn}_3\text{Nb}_2\text{O}_8$ ceramics is a mixture of ZnNb_2O_6 and $\text{Zn}_3\text{Nb}_2\text{O}_8$. A plot of the ratio of relative intensity of $\text{Zn}_3\text{Nb}_2\text{O}_8$ for the strongest peak to the sum of relative intensities of strongest peaks of ZnNb_2O_6 and $\text{Zn}_3\text{Nb}_2\text{O}_8$ is shown in Fig. 3. 26. It is evident that the proportion of the $\text{Zn}_3\text{Nb}_2\text{O}_8$ in the mixture is increasing with x.

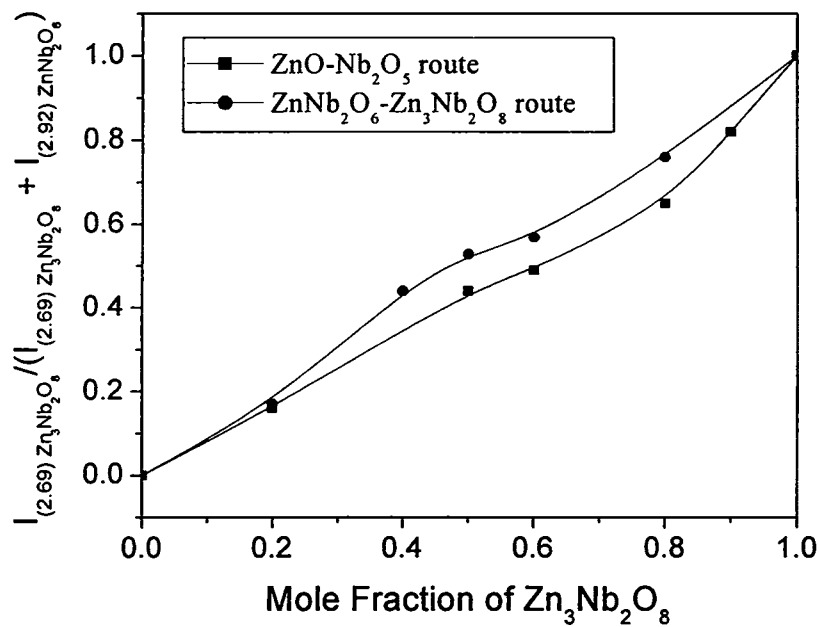


Fig. 3. 26 variation of relative intensities of prominent peak of $\text{Zn}_3\text{Nb}_2\text{O}_8$ with mole fraction of $\text{Zn}_3\text{Nb}_2\text{O}_8$

3.5.3.3 Microwave dielectric properties

Fig. 3. 27 shows the variation of ϵ_r with volume fraction of $\text{Zn}_3\text{Nb}_2\text{O}_8$. Dielectric constant of $(1-x)\text{ZnNb}_2\text{O}_6-x\text{Zn}_3\text{Nb}_2\text{O}_8$ ceramics prepared through ZnO-

Nb_2O_5 shows a higher value than that prepared through the $\text{ZnNb}_2\text{O}_6\text{-Zn}_3\text{Nb}_2\text{O}_8$ route. The dotted line in Fig. 3.27 represents the dielectric constant obtained through mixture rule,

$$\varepsilon_{r,mixture} = V_1\varepsilon_{r1} + V_2\varepsilon_{r2}$$

ε_{r1} and ε_{r2} are the dielectric constant for the constituent phases and $\varepsilon_{r,mixture}$ is the dielectric constant of the mixed phase ceramic. The ceramic prepared through $\text{ZnNb}_2\text{O}_6\text{-Zn}_3\text{Nb}_2\text{O}_8$ route agrees with the expression where as that prepared through $\text{ZnO-Nb}_2\text{O}_5$ route shows a higher value.

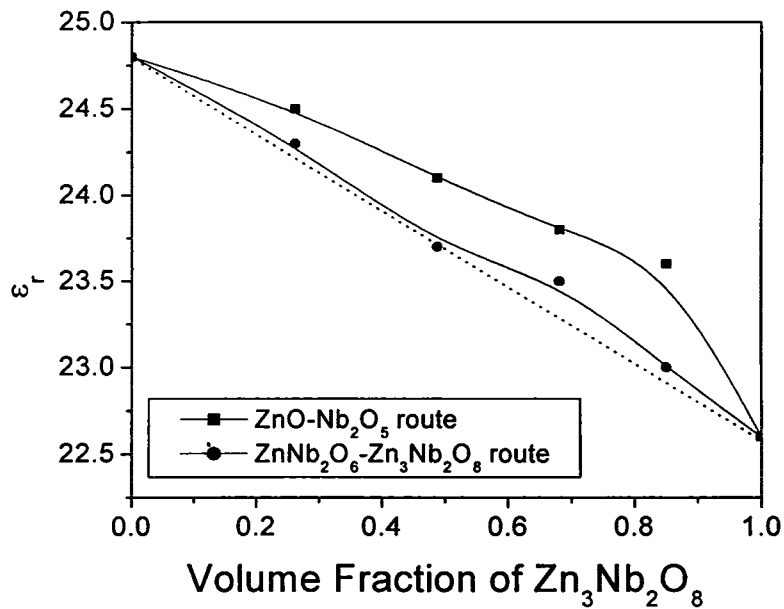


Fig. 3. 27 The variation of ε_r with volume fraction of $\text{Zn}_3\text{Nb}_2\text{O}_8$

Fig. 3. 28 shows the variation of τ_f with volume fraction of $\text{Zn}_3\text{Nb}_2\text{O}_8$ for the ceramics prepared through both the methods. The dotted line shows the mixing model according to the expression

$$\tau_{f,mixture} = V_1 \tau_{f1} + V_2 \tau_{f2}$$

where τ_{f1} and τ_{f2} are the temperature coefficient of resonant frequencies of the constituent phases and $\tau_{f,mixture}$ is the temperature coefficient of resonant frequency of the mixed phases. The τ_f of the ceramic prepared through the ZnO-Nb₂O₅ route shows lower value than the mixing model values whereas the ceramics prepared through ZnNb₂O₆-Zn₃Nb₂O₈ shows higher values.

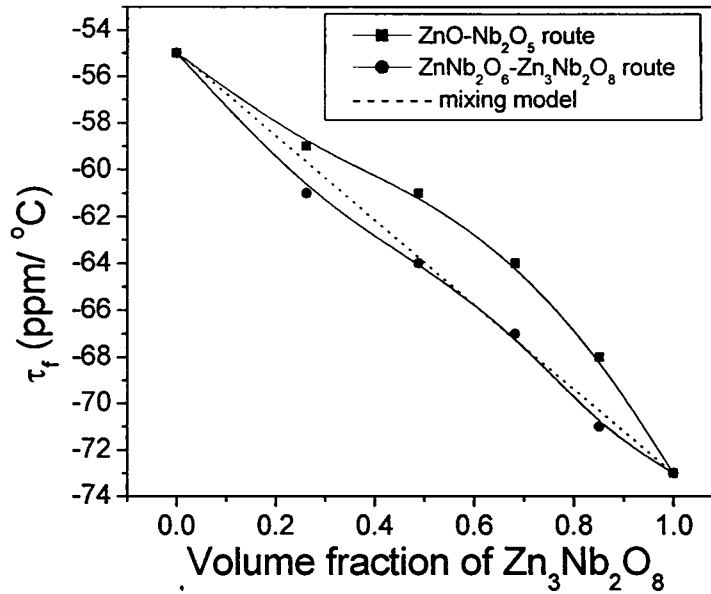


Fig.3. 28 Variation of τ_f with the volume fraction of Zn₃Nb₂O₈.

Fig. 3. 29 shows the variation of $Q \times f$ with volume fraction of Zn₃Nb₂O₈.

The line shows theoretical Q factor according to the mixing relation

$$\frac{1}{Q_{mixture}} = \frac{V_1}{Q_1} + \frac{V_2}{Q_2}$$

where Q_1 and Q_2 are the quality factors for the constituent phases and Q_{mixture} is the quality factor of the mixed phases.

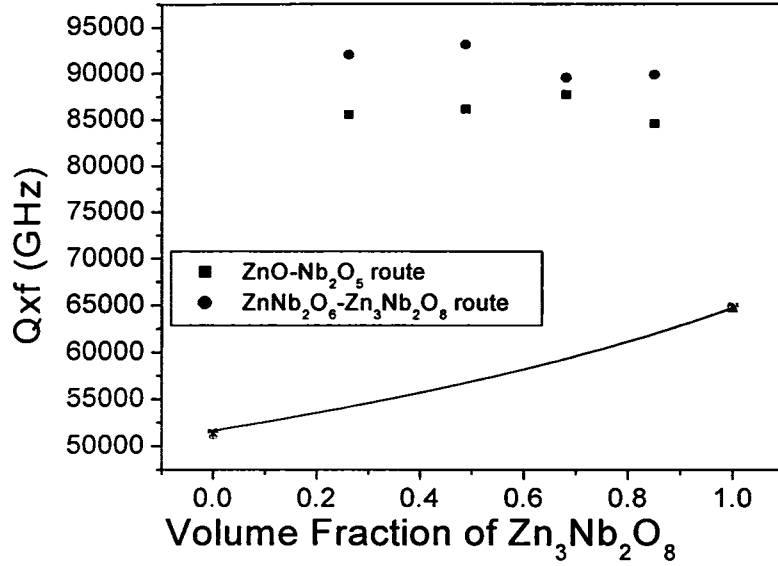
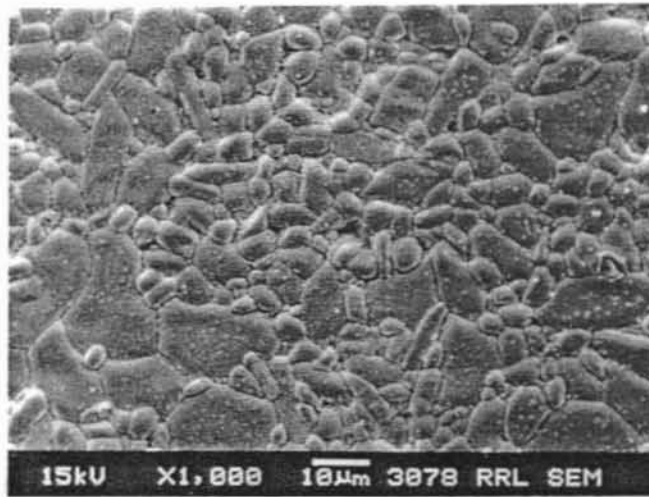
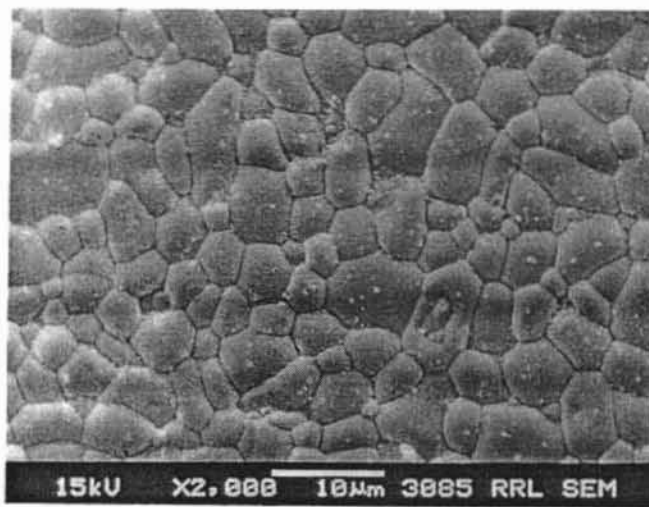


Fig. 3. 29 The variation of $Q \times f$ with volume fraction of $Zn_3Nb_2O_8$

The quality factor of the mixed phases prepared through both methods showed values higher than the values obtained from the mixture relation. Fig 3. 30 shows the typical SEM recorded for $0.5ZnNb_2O_6-0.5Zn_3Nb_2O_8$ and $0.6ZnNb_2O_6-0.4Zn_3Nb_2O_8$. There are smaller and bigger grains in $0.5ZnNb_2O_6-0.5Zn_3Nb_2O_8$ (Fig. 3.30a). This may be due to certain amount of melting due to higher sintering temperature. The SEM picture recorded for $0.6ZnNb_2O_6-0.4Zn_3Nb_2O_8$ (Fig. 3. 30b) shows regular grains of hexagonal shape. The grains are having a size of less than $10 \mu\text{m}$.



(a) $0.5\text{ZnNb}_2\text{O}_6\text{-}0.5\text{Zn}_3\text{Nb}_2\text{O}_8$



(b) $0.6\text{ZnNb}_2\text{O}_6\text{-}0.4\text{Zn}_3\text{Nb}_2\text{O}_8$

Fig 3. 30 The SEM pictures of $0.5\text{ZnNb}_2\text{O}_6\text{-}0.5\text{Zn}_3\text{Nb}_2\text{O}_8$
and $0.6\text{ZnNb}_2\text{O}_6\text{-}0.4\text{Zn}_3\text{Nb}_2\text{O}_8$

3. 5. 4 Conclusion

The $(1-x)\text{ZnNb}_2\text{O}_6 - x\text{Zn}_3\text{Nb}_2\text{O}_8$ mixed phase ceramics are prepared through $\text{ZnO-Nb}_2\text{O}_5$ and $\text{ZnNb}_2\text{O}_6\text{-Zn}_3\text{Nb}_2\text{O}_8$ routes. Dense ceramics are obtained through both the methods. The mixed phase nature of the ceramics is confirmed through XRD. The ceramics shows intermediate dielectric constant and τ_f of the end members. The quality factors of the mixed phase ceramics are higher than the values of the constituent phases prepared under similar conditions. The samples prepared by mixing ZnO and Nb_2O_5 gave higher density, high dielectric constant and better τ_f as compared to those prepared by mixing ZnNb_2O_6 and $\text{Zn}_3\text{Nb}_2\text{O}_8$. The quality factors of the samples prepared by mixing ZnNb_2O_6 and $\text{Zn}_3\text{Nb}_2\text{O}_8$ is slightly higher than those prepared by mixing ZnO and Nb_2O_5 .

3. 6 THE MICROWAVE DIELECTRIC PROPERTIES OF $x\text{ZnO-(5-x)}\text{MgO-2Nb}_2\text{O}_5$

3. 6. 1 Introduction

In section 3.2 where the microwave dielectric properties of $\text{A}_5\text{B}_4\text{O}_{15}$ are discussed, the compound $\text{Mg}_5\text{Nb}_4\text{O}_{15}$ is found to crystallise with orthorhombic structure and showed very high quality factor. In this section a

systematic attempt is made to substitute Mg by Zn in order to tune the dielectric properties.

3. 6. 2 Experimental

The ceramics are prepared through the solid-state ceramic route. High purity MgO (CDH, India, AR grade), ZnO (99.9%, Aldrich Chemicals) and Nb₂O₅ (99.9 %, NFC, India) are used as starting oxide powders. MgO is heated to 1000°C for 3 hours to remove any carbonates or hydroxides. The stoichiometrically weighed powders were mixed in agate mortar for 1 hour with distilled water as the medium. The slurry is dried and calcined at 1100 to 1250°C for 4 hours. The calcined powder is ground well in an agate mortar for 1 hour. 3 wt% PVA is used as the binder. Stearic acid is used as the lubricant. The dried powder is ground well and formed into cylindrical compact in a tungsten carbide die having 14 mm diameter under a pressure of 200 MPa. The aspect ratio of the pellet has to be 2 to 2.5 for best performance. The green compacts were sintered at 1250 to 1400°C for 2 hours. The samples are polished well. The bulk densities of all samples were measured using Archimedes method. The microwave characterization was done as described in chapter 2.

3. 6. 3 Results and discussion

3. 6. 3. 1 Density and XRD

The ceramics are sintered well at their respective sintering temperatures.

The density with x is shown in Table 3. 14.

Table 3.14
The sintering temperature, density and microwave dielectric properties of $x\text{ZnO}-(5-x)\text{MgO}-2\text{Nb}_2\text{O}_5$ ceramics

x	Sint Temp (°C)	Density (g/cm ³)	ϵ_r	τ_f ppm/°C	Q	F GHz	Qxf GHz
0	1475	3.90	11.0	-54	4500	8.3	37350
0.5	1385	4.20	14.0	-55	2400	7.71	18500
1.0	1300	4.67	15.5	-56	2800	7.26	20300
1.5	1275	4.72	17.5	-57	4900	7.43	36400
2.0	1275	4.84	17.5	-57	12700	7.0	88900
2.25	1275	4.85	17.5	-56	7500	7.20	54000
2.5	1275	4.84	17	-57	8300	7.17	59600
2.75	1275	4.93	17.5	-57	4500	7.10	31900
3.0	1275	4.97	18	-60	4900	6.88	33700
3.5	1275	5.02	19	-64	6700	7.16	48000
4.0	1250	5.20	19.5	-65	9100	6.62	60000
4.5	1250	5.29	20	-66	7000	6.56	46000
5.0	1220	5.61	21	-73	12600	6.98	88000

The variation of density with x is plotted in Fig. 3. 31. The density increases as the value of x increases. The X-Ray diffraction pattern of the ceramics is shown in Fig. 3. 32. The pattern shows multiphase nature. The $Mg_5Nb_4O_{15}$ type phase is present in trace amount as secondary phase up to $x = 1$. Thereafter the XRD spectra are analogous to the pattern recorded for $5ZnO-2Nb_2O_5$, which is a mixture of $ZnNb_2O_6$ and $Zn_3Nb_2O_8$. Hence the intermediate ceramics may be a mixture of $(Zn, Mg)Nb_2O_6$ and $(Zn,Mg)_3Nb_2O_8$ phases.

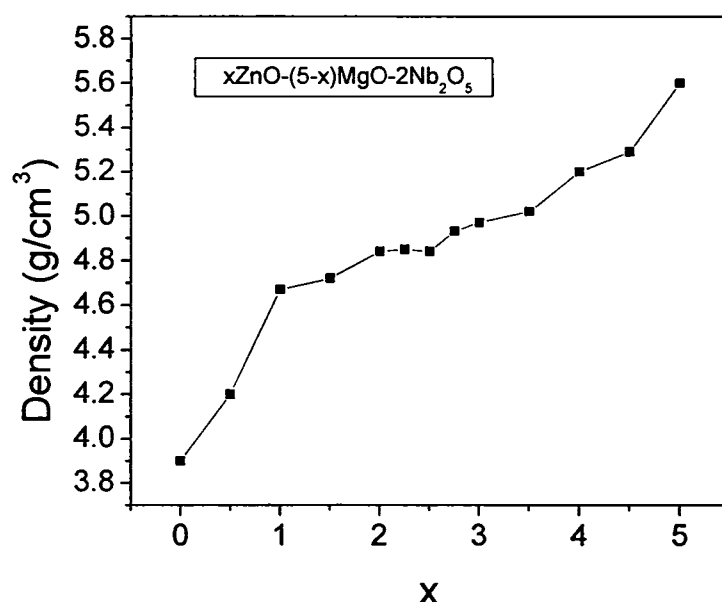


Fig. 3. 31 The variation of density with x for $xZnO - (5-x)MgO-2Nb_2O_5$

Fig. 3. 33 shows the typical SEM pictures recorded for $5ZnO-2Nb_2O_5$ and $4ZnO-MgO-2Nb_2O_5$. The grains of the mixture phases are about 10 to 20 μm , where as the average grain size of $5ZnO-2Nb_2O_5$ is greater than 20 μm . The presence of Mg reduces the grain growth.

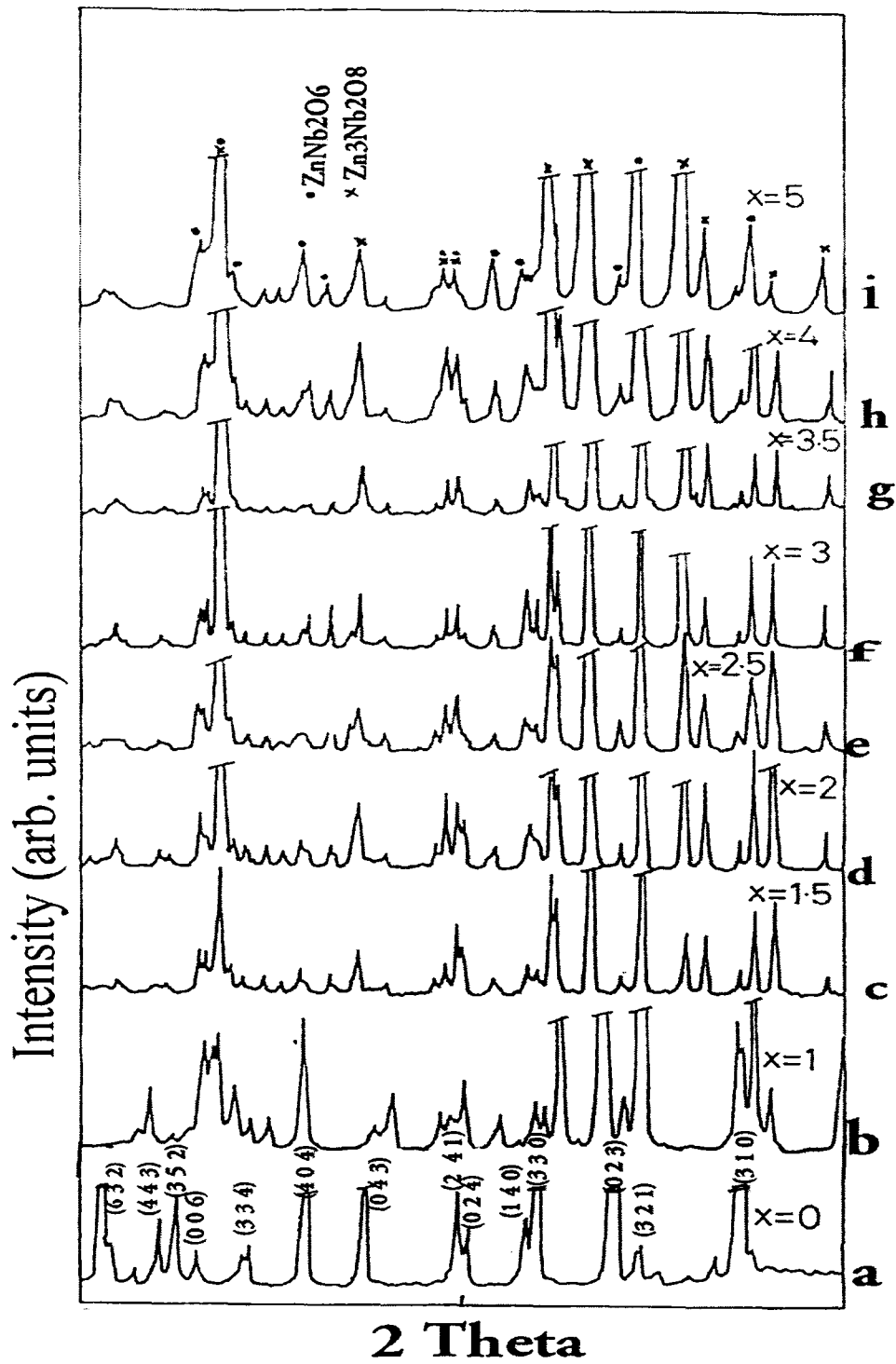
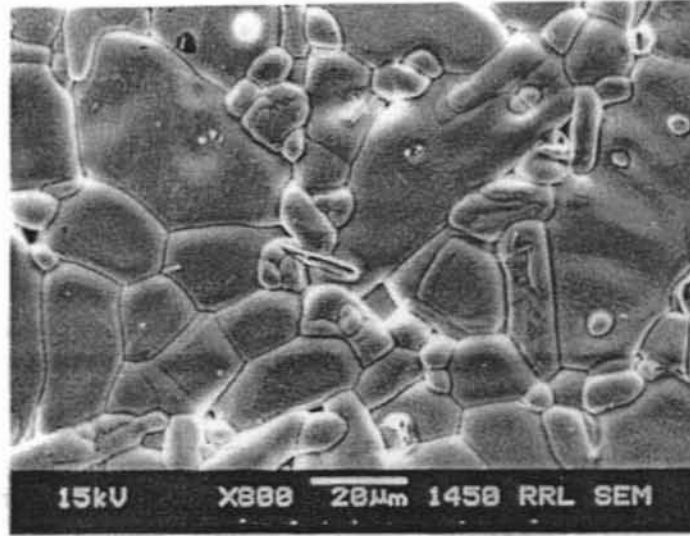
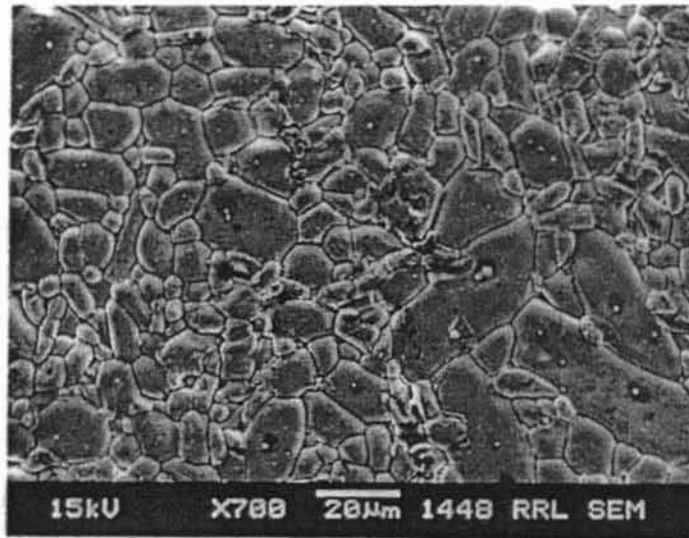


Fig.3. 32 The X-ray diffraction pattern of $x\text{ZnO} - (5-x)\text{MgO} - 2\text{Nb}_2\text{O}_5$



5ZnO-2Nb₂O₅



4ZnO-MgO-2Nb₂O₅

Fig. 3. 33 The SEM pictures of 5ZnO-2Nb₂O₅
and 4ZnO-MgO-2Nb₂O₅

3.6.3.2 Microwave dielectric properties

The microwave dielectric properties are given in Table 3. 14. Fig 3. 34 shows the variation of ϵ_r and τ_f with x. The dielectric constant increases from 11 to 21.

Table 3.14

The sintering temperature, density and microwave dielectric properties of $x\text{ZnO}-(5-x)\text{MgO}-2\text{Nb}_2\text{O}_5$ ceramics

x	Sint Temp (°C)	Density (g/cm ³)	ϵ_r	τ_f ppm/°C	Q	F GHz	Qxf GHz
0	1475	3.90	11.0	-54	4500	8.3	37350
0.5	1385	4.20	14.0	-55	2400	7.71	18500
1.0	1300	4.67	15.5	-56	2800	7.26	20300
1.5	1275	4.72	17.5	-57	4900	7.43	36400
2.0	1275	4.84	17.5	-57	12700	7.0	88900
2.25	1275	4.85	17.5	-56	7500	7.20	54000
2.5	1275	4.84	17	-57	8300	7.17	59600
2.75	1275	4.93	17.5	-57	4500	7.10	31900
3.0	1275	4.97	18	-60	4900	6.88	33700
3.5	1275	5.02	19	-64	6700	7.16	48000
4.0	1250	5.20	19.5	-65	9100	6.62	60000
4.5	1250	5.29	20	-66	7000	6.56	46000
5.0	1220	5.61	21	-73	12600	6.98	88000

The τ_f slowly increases from -54 to -60 ppm/ $^{\circ}\text{C}$ when x increases up to 3 and thereafter it increases up -73 ppm/ $^{\circ}\text{C}$ when x increases from 3 to 5. The mixture-phased ceramics shows $Q \times f$ in the range 8400 to 88900 GHz (Table 3.14). The intermediate compound at $x = 0$ shows $\epsilon_r = 17.5$, $\tau_f = -57$ ppm/ $^{\circ}\text{C}$ and $Q \times f = 88900$ GHz.

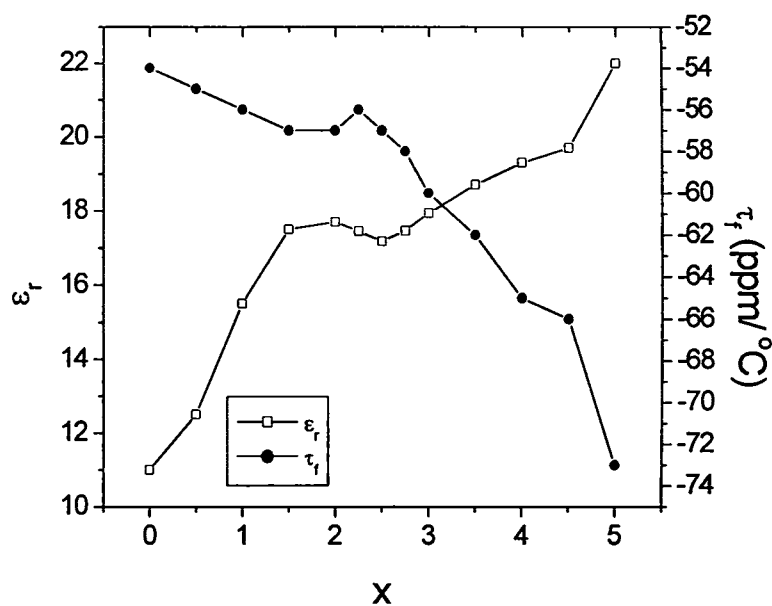


Fig. 3. 34 The variation of ϵ_r and τ_f as a function of x

3.7 CONCLUSION

- (1) The $A_5B_4O_{15}$ (A=Ba, Sr, Mg, Ca, Zn; B=Nb, Ta) ceramics are prepared through the conventional solid-state ceramic route. The $Ba_5Ta_4O_{15}$, $Ba_5Nb_4O_{15}$, $Sr_5Nb_4O_{15}$, $Sr_5Ta_4O_{15}$ have hexagonal structure. The $Mg_5Nb_4O_{15}$ and $Mg_5Ta_4O_{15}$ are orthorhombic in structure. The analogous compounds $Zn_5Nb_4O_{15}$, $Ca_5Nb_4O_{15}$ and $Ca_5Ta_4O_{15}$ do not form. Instead $5ZnO-2Nb_2O_5$ is a mixture of $ZnNb_2O_6$ and $Zn_3Nb_2O_8$. The $5CaO-2Nb_2O_5$ and $5CaO-2Ta_2O_5$ also show multiphase nature, where individual phases are not characterised. The ceramics has ϵ_r in the range 11 to 51, $Q \times f$ in the range 2400 to 88000 GHz and τ_f in the range -73 to $+232$ ppm/ $^{\circ}C$. $5ZnO-2Nb_2O_5$ shows $\epsilon_r = 22$, $Q \times f = 88000$ GHz with $\tau_f = -73$ ppm/ $^{\circ}C$.
- (2) Far infrared and submillimeter spectroscopic studies of $A_5B_4O_{15}$ ceramics are performed. The microwave ϵ' of the ceramic samples is determined by the polar phonon contribution and ϵ' is dispersionless below the phonon frequencies. In single phase ceramics dielectric loss ϵ'' extrapolated from submillimeter down to the MW region according to the simple proportionality $\epsilon''(\omega) \propto \omega$ corresponds satisfactorily to the microwave data.
- (3) The $Ba_{5-x}Sr_xTa_4O_{15}$, $Ba_5Nb_xTa_{4-x}O_{15}$, $Sr_5Nb_xTa_{4-x}O_{15}$ are obtained in phase pure form with very high densities under the preparation conditions employed through solid-state ceramic route. All the ceramics crystallise with the hexagonal

structure. $\text{Ba}_5\text{Nb}_4\text{Ta}_{4-x}\text{O}_{15}$ system shows intermediate dielectric properties of the end compounds. $\text{Sr}_5\text{Nb}_x\text{Ta}_{4-x}\text{O}_{15}$ solid solution show lower dielectric constant than the end members and dielectric constant remain nearly the same in the range $0.5 < x < 2.0$.

4) $(1-x)\text{ZnNb}_2\text{O}_6-x\text{Zn}_3\text{Nb}_2\text{O}_8$ mixed phase ceramics are prepared through $\text{ZnO-Nb}_2\text{O}_5$ and $\text{ZnNb}_2\text{O}_6\text{-Zn}_3\text{Nb}_2\text{O}_8$ routes. Dense ceramics are obtained through both the methods. The mixed phase nature of the ceramics is confirmed through XRD. The ceramics shows intermediate dielectric constant and τ_f of the end members. The quality factors of the mixed phase ceramics are higher than the quality factors of the constituent phases when prepared under similar conditions. The samples prepared by mixing ZnO and Nb_2O_5 gave better dielectric properties. The composition $0.4\text{Zn}_3\text{Nb}_2\text{O}_8\text{-}0.6\text{ZnNb}_2\text{O}_6$ gave $\epsilon_r = 23.7$, $Q \times f = 93100$ GHz and $\tau_f = -64$ ppm/ $^\circ\text{C}$.

5) The $x\text{ZnO-(5-x)MgO-}2\text{Nb}_2\text{O}_5$ ceramics are prepared through the solid state ceramic route. The dielectric constant varies from 11 to 21, τ_f between -54 and -73 ppm/ $^\circ\text{C}$ and $Q \times f$ between 18500 and 88900 GHz. The composition with $x=2$ has $\epsilon_r = 17.5$, $\tau_f = -57$ ppm/ $^\circ\text{C}$ and $Q \times f = 88900$ GHz.

REFERENCES

- [1] Francis Galasso and Lewis Katz, *Acta Cryst.*, **14** (1961) 647
- [2] Joseph Shannon and Lewis Katz, *Acta. Cryst.*, **B26** (1970) 102
- [3] J. L. Hutchison and A. J. Jacobson, *Acta. Cryst.*, **B31** (1975)1442
- [4] J. L. Hutchison, *Chem. Scripta*, **14** (1978-79) 181
- [5] L. M. Kovba, L. N. Lykova, M. V. Paromova, L. M. Lopato and A. V. Shevchenko, *Russian J. Inorg. Chem.*, **22** (10) 1997 1544
- [6] C. D. Whiston and A. J. Smith, *Acta. Cryst.*, **23** (1967) 82
- [7] M. Weiden, A. Grauel, J. Norwig, S. Horn, F. Staglich , *J. Alloys and compounds*, **218** (1995) 13
- [8] H. Sreemoolanadhan, M. T. Sebastian and P. Mohanan, *Mater. Res. Bull.*, **30** (1995) 653
- [9] R. Ratheesh, H. Sreemoolanadhan and M. T. Sebastian, *J. Solid state chem.*, **131** (1997) 2
- [10] S. Kamba, J. Petzelt, D. Haubrich, P. Vanek, P. Kuzel, I. N. Jawahar, M. T. Sebastian and P. Mohanan, *J. Appl. Phys.*, **89** (2001) 3900
- [11] N. Tenze, D. Mercurio, G. Troliard and J.C. Champarnaud-Mesjard, *Z. Kristallogr., NICS* **215** (2000) 11
- [12] E. Brook, R. K. Route, R. J. Raymakers and R. S. Feigelson, *J. Crystal Growth*, **128** (1993) 842
- [13] H. Kasper, *Z. Anorg. Allg. Chem.*, **354** (1967) 208 (Ger)
- [14] F. Abbattista, P. Rolondo, G. Boroni Grassi, *Anna. Chim.*, **60** (1970) 426
- [15] S. Pagola, R. E. Carbonio, M. T. Fernandez-Diaz and J. A. Alonso , *J. Solid*

state Chem., **137** (1998) 359

- [16] H. Sreemoolanadhan, J. Isaac, S. Solomon, M. T. Sebastian, K. A. Jose and P. Mohanan, *phys. Stat. Sol.*, (**a**) **143** (1994) K45
- [17] W. H.Jung, J.H. Sohn, Y.Inaguma, M. Itoh, *The Korean J. of Ceramics*, **2** (1996) 111
- [18] C. Veneis, P. K. Davies, T. Negas and S. Bell, *Mater. Res. Bull.*, **31**(1996) 431
- [19] Nestor E. Massa, Silvina Pagola and Raul Carbonio, *Physical Review B*, **53** (1996) 8148
- [20] N.E. Massa, S. Pagola, R. E. Carbonio, J.A. Alonso, I. Rasines, G. Polla, G. Leyva, SPIE International symposium, San Jose, California, U. S. A.
- [21] S.H. Ra and P. P. Phule, *J. Mater. Res.*, **14** (1999) 4259
- [22] J. Krupka, K. Derzakowski, B.Riddle and J. B. Jarvis, *Meas. Sci. Tech.*, **9** (1998) 1751
- [23] R.D. Shannon, *J. Appl. Phys.*, **73** (1993) 348
- [24] R.D. Shannon, *Acta Cryst.*, **A32** (1976) 751
- [25] H. J. Lee, I. T. Kim, and K.S. Hong, *Jpn. J. Appl. Phys.*, **36** (1997) L1318
- [26] D. W. Kim, I. T. Kim, B. Park, K. S. Hong, *J. Mater. Res.* **16** (2001) 1465
- [27] J. Petzelt, S. Kamba, G. V. Kozlov, and A.A. Volkov, *Ferroelectrics* **176** (1996) 145
- [28] S. Kamba, J. Petzelt, R. Freer, V.M. Ferreira, R. Zurnühhlen, and V. Koukal, *Proc. of Int. Conf. on Electronic Ceramics & Applications, Aveiro, Ed. J.L. Baptista, and J.A. Labrincha*, **2** (1996) 63

- [29] D. S. Keiding, M. van Exter, and Ch. Fattinger, *J. Opt. Soc. Am. B*, **7** (1990) 2006
- [30] K. Wakino, D. A. Sagala, and H. Tamura, *Jpn. J. Appl. Phys.*, **24** (1985) 1042
- [31] G. Ruprecht and R.O. Bell, *Phys. Rev.*, **125** (1962) 1915
- [32] J. Petzelt and N. Setter, *Ferroelectrics*, **150** (1993) 89
- [33] F. Gervais, in *Infrared and Millimetre Waves*, vol. 8, Ed. K.J. Button, Ch. 7 “High-Temperature Infrared Reflectivity Spectroscopy by Scanning Interferometry”, Academic Press, New York (1983) p. 279
- [34] J. Petzelt, S. Pačesová, J. Fousek, S. Kamba, V. Železný, V. Koukal, J. Schwarzbach, B.P. Gorshunov, G.V. Kozlov, and A.A. Volkov, *Ferroelectrics*, **93** (1989) 77
- [35] P. Kuzel and J. Petzelt, *Ferroelectrics*, **239** (2000) 79
- [36] V.L. Gurevich and A.K. Tagantsev, *Adv. Phys.*, **40** (1991) 719
- [37] A.A. Volkov, Yu. G. Goncharov, G.V. Kozlov, S.P. Lebedev, and A.M. Prokhorov, *Infrared Phys.*, **25** (1985) 369
- [38] $\text{Ba}_5\text{Nb}_4\text{O}_{15}$, JCPDS Card No. 14-28, International Centre for Diffraction Data, Newton Square, PA
- [39] $\text{Ba}_5\text{Ta}_4\text{O}_{15}$, JCPDS Card No. 18-193, International Centre for Diffraction Data, Newton Square, PA
- [40] R. Ratheesh, M. Wohlecke, B. Berge and T. Wahlbrink, H. Haeuseler, E. Ruhl, R. Blachnik, P. Balan, N. Santha and M. T. Sebastian, *J. Appl. Phys.*, **88** (2000) 2813

Chapter 4

THE MICROWAVE DIELECTRIC PROPERTIES OF MO-La₂O₃-TiO₂ (M= Ca, Sr, Ba) CERAMICS

In the preceding chapter we have seen microwave resonator materials belonging to the A₅B₄O₁₅ type with dielectric constant in the range 11 to 51. In the present chapter we report a new group of microwave dielectric materials in the MO-La₂O₃-TiO₂ [M=Ca, Sr, Ba] system. The dielectric properties of these materials are being studied for the first time.

4.1 INTRODUCTION

The dramatic advancements during the last two decades in the microwave integrated circuit (MIC) technology have brought a revolution in telecommunication systems. Dielectric resonators (DRs) provide compact low cost and highly reliable choice as the resonator element in microwave circuits and increasingly replace the conventional metallic cavity and microstrip resonators. The size of the microwave circuit is inversely proportional to the square root of its

dielectric constant. The constraints due to size, frequency of operation, frequency stability and selectivity allow only those materials having high dielectric constant (20 – 100), high Q factor (>2000) and low temperature coefficient of resonant frequency ($\tau_f < \pm 20 \text{ ppm}^\circ\text{C}$) for DR applications.

Most of the commercial DRs available at present fall into two groups. (i) Ceramics with low dielectric constant ($20 < \epsilon_r < 40$) and high Q factor ($Q_{xf} > 50000\text{GHz}$) such as BMT, BZT, their solid solution modifications, $\text{Ba}_2\text{Ti}_9\text{O}_{20}$, $(\text{Zr}, \text{Sn})\text{TiO}_4$ etc. (ii) Ceramics with high dielectric constant (> 65) and low Q factor ($Q_{xf} < 10000$) such as the tungsten-bronze type materials in the $\text{BaO-RE}_2\text{O}_3\text{-TiO}_2$ system. Though high dielectric constant materials can give better miniaturization, the applications requiring narrow band width and extremely low insertion loss (0.3 dB) makes the use of ceramics having even $\epsilon_r = 38$ [1]. Dielectric materials with $\epsilon_r > 40$ and $Q_{xf} > 45000 \text{ GHz}$ can help for further miniaturization of the devices without much compromise in quality. The materials with ϵ_r in the range 40 to 65 suitable for such applications are a few and the search for such materials is one of the current areas of research in microwave dielectrics. The $\text{Ba}_5\text{Nb}_4\text{O}_{15}$ type cation deficient hexagonal perovskites were characterized with high dielectric constant and high quality factor. The microwave dielectric properties of $\text{Ba}_5\text{Nb}_4\text{O}_{15}$, $\text{Ba}_{5-x}\text{Sr}_x\text{Nb}_4\text{O}_{15}$, and $\text{Ba}_5\text{Ta}_4\text{O}_{15}$ are already described in chapter 3. The ceramics are characterized with high dielectric constants up to 51.0 and Q_{xf} up to 31600 GHz. Veneis et al. [3]. have reported the microwave dielectric properties of $\text{BaLa}_4\text{Ti}_4\text{O}_{15}$ and $\text{Ba}_2\text{La}_4\text{Ti}_5\text{O}_{18}$ and the ceramics show high dielectric constants and quality factors with small temperature coefficients of

resonant frequency. In the present chapter we report the preparation, characterization and microwave dielectric properties of the cation deficient hexagonal phases $(M, La)_nTi_{n-1}O_{3n}$ ($M = Ca, Sr, Ba; n = 5, 6$) and the orthorhombic type $CaLa_4Ti_5O_{17}$, $Ca_2La_4Ti_6O_{20}$ and $CaLa_8Ti_9O_{31}$ ceramics belonging to the $CaO-La_2O_3-TiO_2$ system. The microwave dielectric properties of the Ca and Sr based ceramics are reported for the first time.

The $(M, La)_nTi_{n-1}O_{3n}$ ($M = Ca, Sr, Ba; n = 5, 6$) ceramics i.e. $CaLa_4Ti_4O_{15}$, $SrLa_4Ti_4O_{15}$, $BaLa_4Ti_4O_{15}$ and $Ca_2La_4Ti_5O_{18}$ crystallize with the hexagonal structure [7-12]. The above compounds belong to the cation deficient hexagonal perovskite family $A_nB_{n-1}O_{3n}$ ($n = 5, 6$ or 8) where the M and La ions occupy the A sites and Ti ions occupy the B sites. The crystal lattice of the cation deficient perovskite related phases $A_nB_{n-1}O_{3n}$ ($n=5, 6, 8$) can be derived from the basic perovskite structure by the periodic introduction of intrinsic stacking faults in the cubic close packing of the AO_3 mixed layers with hexagonal structure. Alternately, the structure may be defined to consist of identical perovskite like blocks of n corner sharing octahedra where successive blocks are shifted by $\frac{1}{3}\langle 10\bar{1}0 \rangle$ vector. $(\frac{1}{n})^{th}$ of the octahedral holes are kept vacant in such a way that B cations are omitted from the face sharing octahedral holes to form the cation deficient structure. The A site ions are 12 fold coordinated whereas B site ions are 6 fold coordinated. The lattice parameters and the atom positions of the homologous phases $BaLa_4Ti_4O_{15}$ and $Ba_2La_4Ti_5O_{18}$ were precisely determined by Harre et al. [10,11] based on single crystal x-ray diffraction and later confirmed by neutron diffraction studies [12].

4. 2 PREPARATION AND CHARACTERIZATION

The ceramics are prepared through the solid-state ceramic route. High purity CaCO_3 (99+ %), BaCO_3 (99+ %) and SrCO_3 (99.9 %) and TiO_2 (99.9%) supplied by Aldrich Chemicals, USA are used as the starting oxide powders. La_2O_3 (99.99%, Indian Rare Earths, Kerala, India) is heated at 1000°C for 3 hours before weighing to remove any hydroxides. The powders are weighed according to the stoichiometry and ball milled in distilled water medium for 24 hours in a plastic bottle using zirconia balls. The wet mixed powder is dried and calcined at 1200°C for 4 h, ground and again calcined at $1400\text{-}1450^\circ\text{C}$ for 4 hours. The calcined mixture is ground well, 3 wt% PVA is added as the binder, mixed, dried and again ground. The resultant fine powder is uni-axially pressed in a tungsten carbide die under a pressure of 150 MPa such that the pressed disks have 6-8 mm height and 14 mm diameter. Stearic acid is used as a lubricant. The green pellets are sintered at different temperatures in the range $1500\text{-}1675^\circ\text{C}$ for 4 hours. The sintering temperatures are optimized to get maximum density. The sintered samples are usually annealed at $1400\text{-}1450^\circ\text{C}$ for 12 h to minimize the reduction of titanium ions. The sintered pellets are polished well. The bulk densities are measured using Archimedes method. The phase purity of the sintered samples is studied by the X-ray diffraction technique using a Rigaku (Japan) X-ray diffractometer. The surface morphology of the samples is studied using Scanning Electron Micrograph (SEM). The sintered samples are thermally etched at

temperatures 50°C less than their respective sintering temperature for 30 minutes and are used for recording SEM. The microwave dielectric properties of the samples are measured using an HP 8510C Network Analyzer. The microwave dielectric constant is measured by dielectric post resonator method suggested by Hakki and Coleman and modified by Courtney [13, 14] and are described in chapter 2. The resonator is placed between two gold-coated copper metallic plates and microwave energy is coupled through E- field probes to excite various resonant modes. Among the various resonant modes the TE₀₁₁ mode is selected for the measurement. The quality factors of the samples are measured at the TE_{01δ} mode resonant frequency using a transmission mode cavity [15]. The temperature coefficient of resonant frequency (τ_f) is measured from the slope of the graph plotted between resonant frequency and temperature. The measurement is usually done in the range 20 to 80°C.

4. 3 RESULTS AND DISCUSSION

The ceramics are sintered into dense bodies. The percentage densities of the sintered samples are given in Table-1. The MaLa₄Ti₄O₁₅ (M= Ca, Sr, Ba) ceramics show densities in the range 95-98 % of their theoretical densities where as Ca₂La₄Ti₅O₁₈ shows only 93.6 % of its theoretical density. The CaLa₄Ti₅O₁₇ and CaLa₈Ti₉O₃₁ are densified to 98.2 and 92.1% of their respective theoretical densities. The BaLa₄Ti₄O₁₅ ceramics is sintered well at 1550°C for 4 hours where

Table 4. 1
The microwave dielectric properties of
MO-La₂O₃-TiO₂ ceramics (M= Ca, Sr, Ba)

Material	% density	ϵ_r	ϵ_r corr	τ_f ppm/ $^{\circ}$ C	Q_0	f (GHz)	$Q_0 \times f$ (GHz)
CaLa ₄ Ti ₄ O ₁₅	95.2	41.6	44.7	-25	8100	4.31	34911
SrLa ₄ Ti ₄ O ₁₅	98.0	43.8	45.1	-14	12100	4.15	50215
BaLa ₄ Ti ₄ O ₁₅	96.2	46.3	49.1	-13	3150	5.15	16222
Ca ₂ La ₄ Ti ₅ O ₁₈	93.6	44.7	49.3	+6	4800	4.19	20112
CaLa ₄ Ti ₅ O ₁₇	98.2	53.7	55.2	-20	4730	3.67	17359
CaLa ₈ Ti ₉ O ₃₁	92.1	48.6	54.9	-6	5300	3.65	19345

as its strontium counterpart is sintered well at 1625 $^{\circ}$ C for 2 hours. The calcium-based compounds are sintered into dense bodies in the temperature range 1650-1670 $^{\circ}$ C for 4 hours.

4.3.1 X-ray Diffraction and SEM analysis

The X-ray diffraction pattern recorded for the ceramics were compared with the standard data available from the JCPDS [File Nos. 39-831, 36-1278, 36-1279, 27-1057, 27-1058, 27-1059]. The X-ray diffraction patterns of the MLa₄Ti₄O₁₅ (M= Ca, Sr, Ba) and Ca₂La₄Ti₅O₁₈ ceramics are shown in Figure 4. 1 and those of the orthorhombic CaLa₄Ti₅O₁₇ and CaLa₈Ti₉O₃₁ are shown in Figure 4. 2. The obtained compounds are phase pure. The CaLa₄Ti₄O₁₅, BaLa₄Ti₄O₁₅ and SrLa₄Ti₄O₁₅ ceramics crystallize with the hexagonal structure and the close

similarity of their X-ray diffraction patterns is well evident from Figure 4. 1. The lattice parameters calculated are found to agree closely with the reported values.

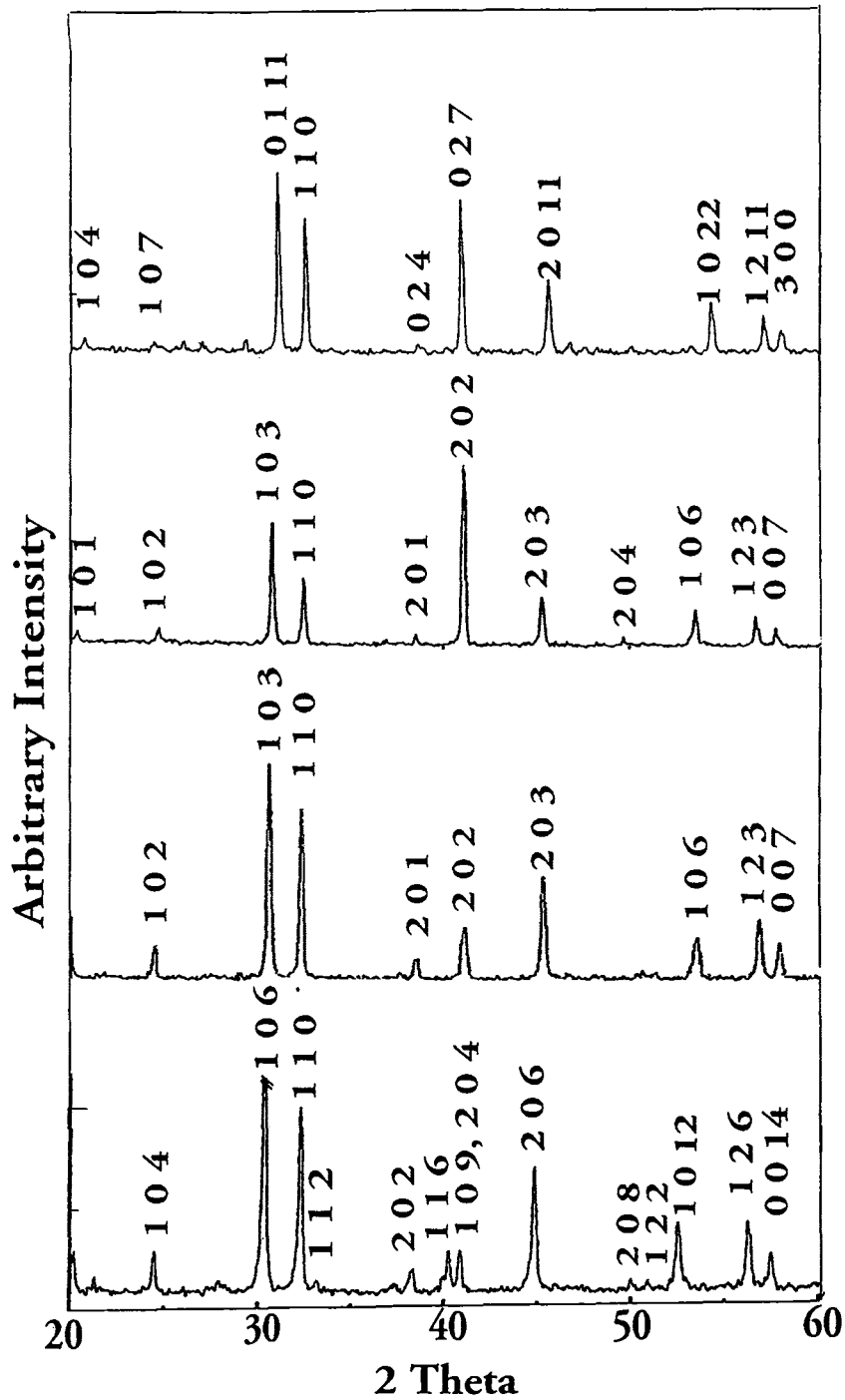


Figure 4. 1 The X-ray diffraction patterns of (a) $\text{BaLa}_4\text{Ti}_4\text{O}_{15}$ (b) $\text{SrLa}_4\text{Ti}_4\text{O}_{15}$ (c) $\text{CaLa}_4\text{Ti}_4\text{O}_{15}$ and (d) $\text{Ca}_2\text{La}_4\text{Ti}_5\text{O}_{18}$

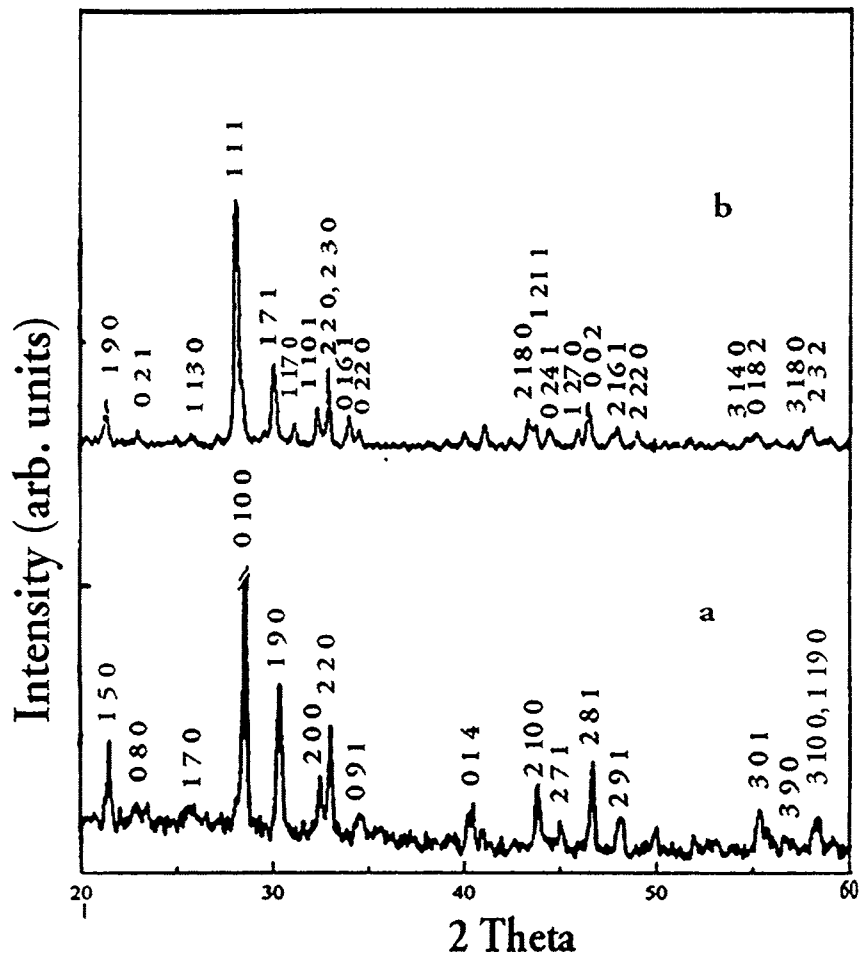
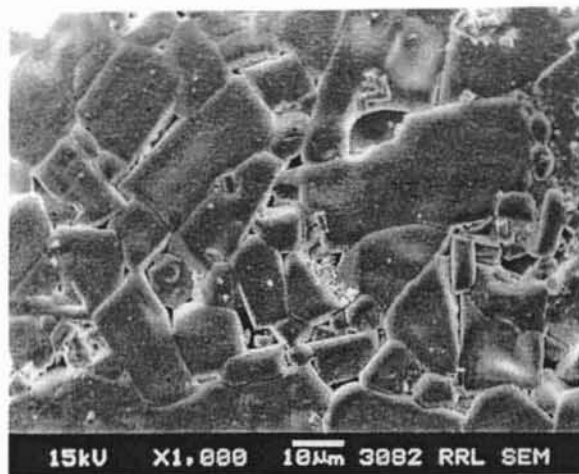


Figure 4, 2 The X-ray diffraction patterns of (a) $\text{CaLa}_4\text{Ti}_5\text{O}_{17}$ and (b) $\text{CaLa}_8\text{Ti}_9\text{O}_{31}$

The pattern recorded for $\text{BaLa}_4\text{Ti}_4\text{O}_{15}$ is indexed by doubling the unit cell along the c axis in order to account for some very weak maxima in the pattern so that the unit cell contains 10 perovskite layers [7,10,12]. The $\text{SrLa}_4\text{Ti}_4\text{O}_{15}$ crystallizes in the hexagonal structure with hhcc stacking [8]. The $\text{CaLa}_4\text{Ti}_4\text{O}_{15}$ belongs to $\text{A}_5\text{B}_4\text{O}_{15}$ with hcch stacking ($p\bar{3}m$) and $\text{Ca}_2\text{La}_4\text{Ti}_5\text{O}_{18}$ belong to the $\text{A}_6\text{B}_5\text{O}_{18}$



a



b

**Figure 4. 3 SEM pictures recorded for
 $\text{BaLa}_4\text{Ti}_4\text{O}_{15}$ and $\text{CaLa}_4\text{Ti}_5\text{O}_{17}$**

with hcccchcccchcccchh stacking [$R\bar{3}m$] and crystallize within the trigonal system with $Z = 3$ [9]. The $A_nB_{n-1}O_{3n}$ compounds usually show a severe distortion of TiO_6 octahedra and the presence of short Ti-O bonds. The decrease in difference between charges of the cations reduces the effect of ordering on the stability of the structure and a hence a distorted distribution of the Ca and La cations is found in $Ca_2La_4Ti_5O_{18}$ [9]. Especially in those cases where hexagonal polytypes of the perovskites are also possible for ABO_3 , the stability of phases with an ordered distribution of vacancies decreases as the Goldsmidht criterion [16] increases and above $1450^\circ C$ the hexagonal $A_6B_5O_{18}$ phases decompose slowly in the solid state [9]. Figure 4. 3 shows typical SEM pictures recorded for $BaLa_4Ti_4O_{15}$ and $CaLa_4Ti_5O_{17}$. The $BaLa_4Ti_4O_{15}$ grains are elongated and are up to about $10 \mu m$ in length. The $CaLa_4Ti_5O_{17}$ grains are large and are up to $15 \mu m$ in size. Other samples also showed similar microstructures. The SEM pictures confirm the single-phase nature of the compounds. The near to melting appearance of the ceramics (Figure 4. 3(b)) may be due to higher sintering temperatures. These DR samples are optimized to have the best Q at these temperatures.

4.3.2 Microwave Dielectric Properties

The ceramics show excellent microwave dielectric properties. The TE_{018} modes of the samples are obtained in the range 4 - 6 GHz. The microwave dielectric properties of the ceramics are given in Table 4. 1. The variation of $(\Delta f/f)$ with temperature for the compounds is given in Figure 4. 4

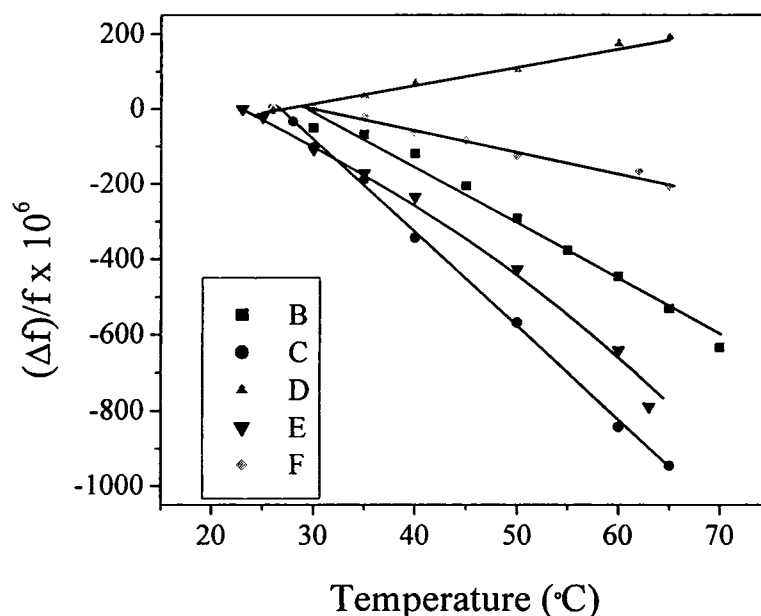


Figure 4. 4 The plot of $\Delta f/f$ against Temperature
(B) $SrLa_4Ti_4O_{15}$ (C) $CaLa_4Ti_4O_{15}$ (D) $Ca_2La_4Ti_5O_{18}$
(E) $Ca_2La_4Ti_5O_{17}$ and (F) $CaLa_8Ti_9O_{31}$

The $BaLa_4Ti_4O_{15}$ shows $\epsilon_r = 46.3$ and $\tau_f = -13 \text{ ppm}/^\circ\text{C}$ with quality factor of 3150 (at 5.15 GHz) for 96.2 % dense sample. It has been reported by Veneis et al. [3] that $BaLa_4Ti_4O_{15}$ has ϵ_r of 43, and Q of 1430 (at 8.10 GHz) with τ_f of $-17 \text{ ppm}/^\circ\text{C}$ for 93.7 % dense ceramics. The higher densification of the present ceramic may

be the reason for the increase in dielectric constant and quality factor of the ceramics. The SrLa₄Ti₄O₁₅ ceramics has ϵ_r of 43.8 with very high Q factor of 12100 (at 4.149 GHz) and a low τ_f of -14 ppm/ $^{\circ}$ C. The Ca₂La₄Ti₅O₁₈ shows a quality factor (4800 at 4.19 GHz) whereas it is 8100 at 4.31 GHz for CaLa₄Ti₄O₁₅. German and Kovba [9] have reported that Ca₂La₄Ti₅O₁₈ has a more diffuse IR and Raman spectra than CaLa₄Ti₄O₁₅. They have suggested a distorted distribution of the Ca and La cation among the equivalent positions to interpret the spectra. This statistical distribution and the resultant disorder of the Ca and La ions may be a cause of lower quality factors of the Ca₂La₄Ti₅O₁₈ as compared to CaLa₄Ti₄O₁₅ apart from the higher porosity. Usually the broadening of the Raman spectra indicates disorder in crystals [17]. The orthorhombic CaLa₄Ti₅O₁₇ and CaLa₈Ti₉O₃₁ are also characterized with very good microwave dielectric properties with ϵ_r of 53.7 and 48.6, quality factors of 4730 (at 3.67 GHz) and 5300 (at 3.65 GHz) and low τ_f of -20 and -6 ppm/ $^{\circ}$ C respectively. The Ca₂La₄Ti₆O₂₀ shows poor resonance due to very high dielectric loss and are not useful for DR applications.

The values of the microwave dielectric constant obtained for the ceramics are corrected for porosity [see Table-2] using the following equation [18]

$$\epsilon' = \epsilon_m \left(1 - \frac{3P(\epsilon_m - 1)}{2\epsilon_m + 1} \right)$$

where ϵ_m is the dielectric constant corrected for porosity, ϵ' is the experimental dielectric constant and P is the fractional porosity. The dielectric constant is calculated using the Claussius – Mossotti equation

$$\epsilon_r = \frac{3V_m + 8\pi\alpha_D}{3V_m - 4\pi\alpha_D}$$

where V_m is the molar volume and α_D is the sum of ionic polarisabilities of individual ions. The calculated dielectric constants usually agree well with the experimental values for well-behaved ceramics [19, 20]. But an inconsistency is found when the equation applied to the La containing $\text{BaLa}_4\text{Ti}_4\text{O}_{15}$ and $\text{Ba}_2\text{La}_4\text{Ti}_5\text{O}_{18}$ ceramics [3]. It has been suggested [3] that if the ionic polarisability of La ion is modified to 4.82 instead of 6.12 given by Shannon this inconsistency can be avoided. We have calculated the dielectric constants of the investigated materials using $\alpha_{\text{La}} = 4.82$. The calculated and experimental dielectric constants (after applying porosity correction) for the ceramics are given in Table 4.2.

Table 4. 2
Comparison of values of experimental and
calculated dielectric constants

Material	α_D ($\alpha_{\text{La}} = 4.82$)	V_m (\AA^3)	Space group	$\epsilon_r(\text{corr})$	calc. ϵ_r	Deviation %
$\text{CaLa}_4\text{Ti}_4\text{O}_{15}$	64.31	291.98	$\bar{P}3m$	44.7	36.74	17.4
$\text{SrLa}_4\text{Ti}_4\text{O}_{15}$	65.39	295.22	$\bar{P}3m$	45.1	39.53	12.4
$\text{BaLa}_4\text{Ti}_4\text{O}_{15}$	67.55	302.48	$\bar{P}3m$	49.1	44.45	9.5
$\text{Ca}_2\text{La}_4\text{Ti}_5\text{O}_{18}$	76.43	349.5	$\bar{R}3m$	49.3	33.71	31.6
$\text{CaLa}_4\text{Ti}_5\text{O}_{17}$	72.34	336.43	---	55.2	28.2	48.9
$\text{CaLa}_8\text{Ti}_9\text{O}_{31}$	131.48	613.47	---	54.9	27.34	50.0

The deviations of the calculated values from the experimental values are also given in Table-2. There is reasonable agreement between the calculated and experimental values. The small difference between calculated and experimental values are due to deviations from the cubic symmetry and also due to the fact that the sample is a ceramic and not single crystal. The calculated values show significant difference from the experimental values for $\text{Ca}_2\text{La}_4\text{Ti}_5\text{O}_{18}$, $\text{CaLa}_4\text{Ti}_5\text{O}_{17}$ and $\text{CaLa}_8\text{Ti}_9\text{O}_{31}$. It may be noted that the equation used for the calculation of dielectric constant is highly sensitive to the value of denominator and even a small error in determining the cell volume can significantly affect the calculated value of dielectric constant. Figure 4.5 shows the variation of the porosity corrected dielectric constant and temperature coefficient of resonant frequency with average ionic radius of the A site ions for the $\text{MLa}_4\text{Ti}_4\text{O}_{15}$ (M= Ca, Sr, Ba) system. The dielectric constant and τ_f of the materials in the system increases with the average ionic radii of the A site ions.

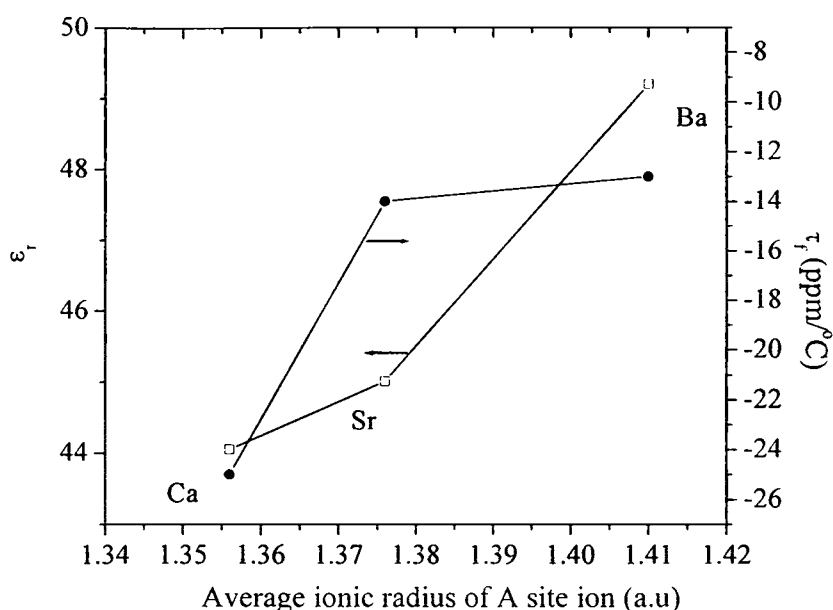


Figure 4. 5 The variation of ϵ_r and τ_f with average ionic radius of A site ion for $MLa_4Ti_4O_{15}$

We have investigated the phase formation within the compositions $SrO-2RE_2O_3-4TiO_2$ ($RE= Sm, Nd, Pr$ and Gd). The mixed oxide powders are calcined in the range $1350-1500^\circ C$ for 4 to 8 hours and sintered at $1625-1650^\circ C$ for 4 hours. No cation deficient hexagonal phases analogous to $SrLa_4Ti_4O_{15}$ compounds are found to exist. The compositions show a multiphase appearance and mostly contain the $RE_2Ti_2O_7$ pyrochlores. The ceramics show good microwave dielectric properties except $SrO - 2Gd_2O_3-TiO_2$ ceramics that has poor resonance due to high dielectric loss. The phase formation within the investigated compositions is found to be sensitive to the preparation conditions and different batches of the ceramics show variation in microwave dielectric properties.

Among the investigated cation deficient hexagonal perovskite, only $\text{Ca}_2\text{La}_4\text{Ti}_5\text{O}_{18}$ shows a positive value of τ_f (+6 ppm/ $^\circ\text{C}$). The investigated ceramics show dielectric constant in the range 42 to 54 and high Qxf in the range 16222 to 50215 GHz with low temperature coefficient of resonant frequency in the range +6 to -25 ppm/ $^\circ\text{C}$. The investigated ceramics are potential candidates for practical applications. These high dielectric constant materials with high Qxf up to 50215 GHz are suitable for applications where narrow bandwidth and extremely low insertion loss is necessary especially at frequencies around 1.9 GHz.

4.4 CONCLUSION

The cation deficient hexagonal perovskites $\text{CaLa}_4\text{Ti}_4\text{O}_{15}$, $\text{SrLa}_4\text{Ti}_4\text{O}_{15}$, $\text{BaLa}_4\text{Ti}_4\text{O}_{15}$ and $\text{Ca}_2\text{La}_4\text{Ti}_5\text{O}_{18}$ and the orthorhombic phases $\text{CaLa}_4\text{Ti}_5\text{O}_{17}$, $\text{CaLa}_8\text{Ti}_9\text{O}_{31}$ are prepared through the solid-state ceramic route. The phases and structure of the ceramics are analyzed through X-ray diffraction and SEM techniques. The microwave dielectric properties of the ceramics are studied. The ceramics show high ϵ_r in the range 42 to 54, high quality factors with Qxf in the range 16222 to 50215 GHz and low τ_f in the range -25 and + 6 ppm/ $^\circ\text{C}$. Their high dielectric constants and high quality factors of Qxf up to 50215 GHz with low temperature coefficients of resonant frequency make them suitable for applications where narrow band width and extremely low insertion loss are necessary especially at frequencies around 1.9 GHz.

REFERENCES

- [1] W. Wersing, *Current Opinion in Solid State & Material Science* **1** (1996) 715
- [2] H. Sreemoolanadhan, M. T. Sebastian and P. Mohanan, *Mater. Res Bull.*, **30** (1995) 653
- [3] C. Veneis, P K. Davies, T. Negas and S. Bell, *Mater. Res. Bull.*, **31** (1996) 431
- [4] S. Kamba, J. Petzelt, E. Buixaderas, D. Haubrich, P. Vanek, P. Kuzel, I. N. Jawahar, M. T. Sebastian and P. Mohanan, *J. Appl. Phys.*, **89** (2001) 3900
- [5] R. Ratheesh, H. Sreemoolanadhan and M. T. Sebastian, *J. Solid. State. Chem.*, **131** (1997) 2
- [6] R. Ratheesh, M. T. Sebastian, P. Mohanan, J. Harnett, R. E. Woode and D. G. Blair, *Mater. Lett.*, **54** (2000) 279
- [7] V. A. Saltikova, O. V. Melnikova, N. V. Leonova and N. F. Fedorov, *Russ. J. Inorg. Chem.*, **30** (1985) 105
- [8] V. A. Saltikova, O. V. Melnikova, N. F. Fedodov, *Russ. J. Inorg. Chem.*, **34** (1989) 758
- [9] M. German and L. M. Kovba, *Russ. J. Inorg. Chem.*, **30** (1985) 176
- [10] N. Harre, D. Mercurio, G. Trolliard and B. Frit, *Mater. Res. Bull.*, **33** (1998) 1537
- [11] N. Harre, D. Mercurio, G. Trolliard, B. Frit, *Eur. J. Solid state Inorg. Chem.*, **35** (1998) 77

- [12] N. Teneze, D. Mercurio, G. Trolliard, B. Frit, *Mater. Res. Bull.*, **35**
(2000) 1603
- [13] B. W. Hakki and P. D. Coleman, *IRE Trans. on Microwave Theory Tech.*,
MTT **8** (1960) 402
- [14] W. E. Courtney, *IEEE Trans. on Microwave Theory Tech.*, *MTT* **18**,
(1970) 476
- [15] J. Krupka, K. Derzakowsky, B. Riddle and J. B. Jarviz, *Meas. Sci. Tech.*,
9 (1998) 1751
- [16] R. S. Roth, *Journal of Research of the National Bureau of Standards*, **58**
(1957) 75
- [17] E. Brük, R. K. Route, R. J. Raymakers and R. S. Feigelson, *J. Crystal
Growth*, **128** (1993) 842
- [18] S. J. Penn, N. M. Alford, A. Templeton, X. Wang, M. Xu, M. Reece and K.
Schrapel, *J. Am. Ceram. Soc.*, **80** (1997) 1885
- [19] R. D. Shannon, *J. Appl. Phys.*, **73** (1993) 348
- [20] R. D. Shannon, *Acta Cryst.*, **A 32** (1976) 751

Chapter 5

A NOVEL METHOD OF TEMPERATURE COMPENSATION BY STACKING POSITIVE AND NEGATIVE τ_f RESONATORS

In the preceding chapter we have seen several new dielectric compositions with excellent quality factor and dielectric constant but with large temperature variation of resonant frequency (τ_f). This large variation in τ_f precludes their use in practical applications. In the present chapter we report a method of improving the τ_f by stacking positive and negative τ_f resonators one above the other. The τ_f can be tuned depending on the volume fraction of the two resonator samples with opposite τ_f sign.

5.1 INTRODUCTION

The application of several high dielectric constant and low loss materials as dielectric resonators is limited mainly by their high temperature variation of the resonant frequency (τ_f). Usually the dielectric properties are tuned by chemical methods like doping

or formation of solid solution of ceramics with opposite τ_f [15-20]. The compatibility of ionic radius, ionic charge and structure are the conditions required for the formation of solid solutions without much degradation of required properties. Several other methods of tuning the τ_f of resonators are also been reported in the literature [3 - 6].

Tsironis and Panker [1] in 1983 first outlined the possibility of obtaining temperature compensation by stacking two cylindrical resonators made of two different materials with τ_f of opposite sign. Santiago et al. [3,9] developed a mechanical compensation technique where a resonator is constructed using two closely spaced identical cylindrical sapphire disks. The thermal expansion of the copper post causes a widening of the gap between the disks which modulates the mode frequency with opposite temperature dependence to the permittivity. However, this type of compensation is inherently sensitive to vibrations.

Tobar et al. [4,7,11] showed that it is possible to annul the frequency temperature dependence of single crystal sapphire dielectric resonators using a dielectric of the opposite permittivity temperature dependence such as rutile or SrTiO_3 . Tobar et al. [4,7,11] developed a composite resonator structure for temperature compensation for Whispering Gallery (WG) modes in certain temperature ranges. In this two very thin slices of rutile single crystal are clamped tight against the upper and lower surfaces of a cylinder of sapphire [4,11]. The rutile has a permittivity temperature coefficient two orders of magnitude higher than that of sapphire and is of opposite sign. Thus temperature compensation is achieved. The temperatures of compensation for the WG quasi TM modes were measured to be below 90K with Q factors of the order of a few million depending on the mode. Using a piece of SrTiO_3 stacking over sapphire the authors could succeed [7] in annulling the temperature dependence of resonant frequency in hybrid WG modes.

Luiten et al. [5,10] used paramagnetic effects of impurity ions in the range 5-13K to compensate the permittivity-temperature dependence to within one part in 10^{15} . But this technique is not applicable at liquid nitrogen and room temperature due to the finite energy gap of a paramagnetic resonance. Hartnett et al. [2, 12] proposed a new method of compensating the frequency temperature dependence of high Q monolithic sapphire dielectric resonators near liquid nitrogen temperature by doping single crystal sapphire with Ti^{3+} ions.

Lim et al. [13] reported a method to design a co-axial ceramic resonator, whose resonant frequency is unchanged with temperature using positive τ_f and negative τ_f materials. High temperature stability of the resonant frequency is realized by obtaining the lengths to be filled with respective materials. More recently Breeze et al. [14] reported a new method of achieving temperature compensation by coating a film of TiO_2 over the surface of alumina disc. Then the composite was fired at $1400^\circ C$. The composite resonators showed temperature compensation depending on the volume fraction of TiO_2 .

So far no systematic study of the variation of dielectric properties of stacked resonators is carried out. The present work consists of a careful study on the variation of dielectric properties for carefully designed samples having opposite τ_f values. The method is illustrated by taking representative materials with varying dielectric properties. These materials are $Ba_5Nb_4O_{15}$, $5ZnO-2Nb_2O_5$ and $Sr(Y_{1/2}Nb_{1/2})O_5$. The properties of $Ba_5Nb_4O_{15}$ and $5ZnO-2Nb_2O_5$ materials are described in chapter 3. The $Ba_5Nb_4O_{15}$ has $\epsilon_r=39$, $Q \times f = 25,000$ and $\tau_f = +78 \text{ ppm}/^\circ C$; $5ZnO-2Nb_2O_5$ has $\epsilon_r = 22$, high $Q \times f$ up to 88,000 and $\tau_f = -73 \text{ ppm}/^\circ C$; The $Sr(Y_{1/2}Nb_{1/2})O_3$ has $\epsilon_r = 28$, $Q \times f = 40,000$ and $\tau_f = -58 \text{ ppm}/^\circ C$. In one set of experiments the effect of stacking of $Ba_5Nb_4O_{15}$ ceramic having positive τ_f with

5ZnO-2Nb₂O₅ having negative τ_f is studied. In the second set of experiments the Ba₅Nb₄O₁₅ ceramic is stacked with Sr(Y_{1/2}Nb_{1/2})O₃ having negative τ_f is investigated.

5. 2 EXPERIMENTAL

The formation of solid solution phases between Ba₅Nb₄O₁₅, 5ZnO-2Nb₂O₅ and Sr(Y_{1/2}Nb_{1/2})O₃ microwave dielectric properties is not possible due to large difference in the ionic radii of A and B site ions and also due to the difference in crystal structures. Attempts to prepare a solid solution between the above ceramics resulted in a multiphase ceramics with very large dielectric loss with no resonance. The preparation of Ba₅Nb₄O₁₅ and 5ZnO-2Nb₂O₅ are described in chapter 4. The Sr(Y_{1/2}Nb_{1/2})O₃ ceramic pellets were prepared through the solid state ceramic route. The Sr(Y_{1/2}Nb_{1/2})O₃ is formed from a stoichiometric mixture of high purity SrCO₃, Y₂O₃ and Nb₂O₅ at 1350°C for 4 hour and sintered at 1625°C for 4 hour through the solid state route. The preparation conditions are well controlled and suitable dies are used such that diameters of the final sintered pellets are nearly the same. The diameter of the pellets are 9.65 ± 0.02 mm for the Ba₅Nb₄O₁₅ stack with 5ZnO-2Nb₂O₅ and 11.96 ± 0.01 mm for the Ba₅Nb₄O₁₅ with Sr(Y_{1/2}Nb_{1/2})O₃. The sintered pellets were polished well. The microwave dielectric constants and Q factors of the pellets were measured accurately using the Hakki & Coleman and cavity methods. The pellets of one type, say 5ZnO-2Nb₂O₅, are placed on the top of the other (Ba₅Nb₄O₁₅) and kept together in between two gold-coated copper metallic plate (Hakki-Coleman setup) and

dielectric constant is measured. The pellets can be glued together using low-loss ceramic glues like cyanoacrylic.

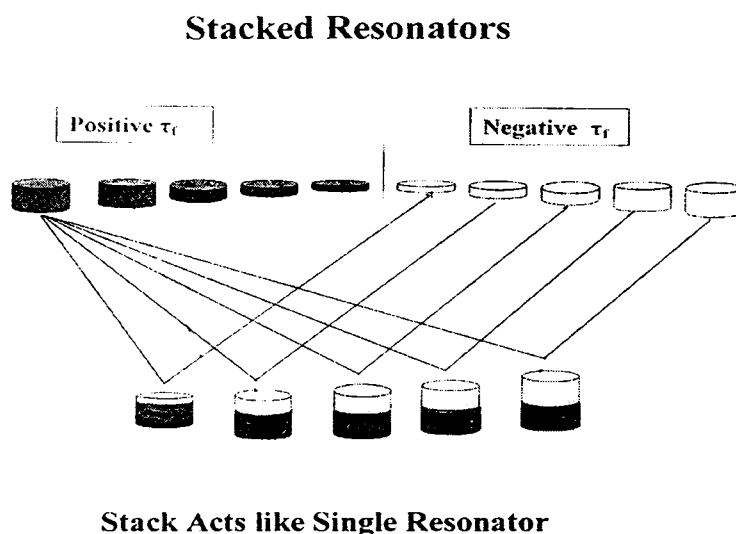


Fig. 1 Stacking of DRs with opposite τ_f

The stacked resonant structure acts like a single dielectric resonator. The pellet of one kind is placed over the other with axial symmetry. The equivalent dielectric resonator can be assumed to have a dielectric constant ϵ_{eff} , length and diameter are obtained respectively from the sum of lengths and average of the diameters of the individual pellets. The TE_{011} mode resonant frequency of the resonant system is noted. The pellets are reversed (top and bottom) and the measurements are made again. The effective dielectric constant (ϵ_{eff}) is determined using the formulae suggested by Hakki and Coleman and described in chapter 2. The experiment is repeated for different possible combinations of the pellets.

The effective dielectric constant is determined by assuming that the stack behaves like a single resonator resonating with a particular frequency with the sum of the lengths of the pellets is the effective length and average of their diameters is their effective diameter.

The quality factors were measured using a cavity method described in chapter 2. The Q factor and resonant frequency vary with the reversal of the pellets. The experiments for determining dielectric constant, τ_f and Q are repeated with different possible combination of pellets with varying lengths. Fig. 5.1 shows a schematic sketch how the combination of stacks made with varying lengths of DR samples with opposite sign τ_f . The DR samples are carefully prepared and polished in order to minimize the air gap between the two types of DRs stacked together.

5. 3 RESULTS AND DISCUSSION

The stacked resonators are showing good resonance without much degradation of the quality factor Q. The dielectric constant and τ_f varies with volume fraction of the positive and negative τ_f materials.

5. 3. 1 $Ba_5Nb_4O_{15}$: $5ZnO-2Nb_2O_5$ stacked resonators

The dielectric constant, Q and τ_f of $Ba_5Nb_4O_{15}$ (BN) and $5ZnO-2Nb_2O_5$ (ZN) dielectric resonators used for stacking one above the other are given in Table 5. 1. The resonators of positive τ_f ($Ba_5Nb_4O_{15}$) and negative τ_f ($5ZnO-2Nb_2O_5$) have varying lengths. The $Ba_5Nb_4O_{15}$ resonators have a diameter of 9.64 mm. The $5ZnO-2Nb_2O_5$ resonators have a diameter of 9.67mm. The slight difference in the diameter is due to the difference in shrinkage during sintering. The average diameter of the stack is 9.655 mm.

Table 5. 1

The microwave characteristics of Ba₅Nb₄O₁₅ and 5ZnO-2Nb₂O₅ samples

Material	Pellet Code	L (mm)	D (mm)	f (GHz)	Q	ϵ_r	τ_f (ppm/°C)
Ba ₅ Nb ₄ O ₁₅	B1	7.960	9.64	4.678	4400	39.0	78
	B2	6.820	9.64	4.7664	4300	39.0	78
	B3	5.690	9.64	4.9275	4500	39.0	78
	B4	4.490	9.64	5.1804	4800	39.0	78
	B5	3.370	9.64	5.5936	4300	39.0	78
	B6	2.230	9.64	---	---	---	--
	B7	1.140	9.64	---	---	---	--
5ZnO-2Nb ₂ O ₅	Z1	7.590	9.670	6.184	12100	22.0	-73
	Z2	6.670	9.670	6.296	12600	22.0	-73
	Z3	5.710	9.670	6.475	12000	22.0	-73
	Z4	4.770	9.670	6.738	11800	22.0	-73
	Z5	3.830	9.670	7.096	11800	22.0	-73
	Z6	2.860	9.670	---	---	---	--
	Z7	1.910	9.670	---	---	---	--

* Could not be measured due to the undersize of sample

The different Ba₅Nb₄O₁₅ DRs with varying heights have $\epsilon_r=39$, $\tau_f = 78$ ppm/°C with slightly varying quality factors (Q=4000-4900). The length and diameter of the resonators are also given in the same Table. The 5ZnO-2Nb₂O₅ resonators with varying heights have dielectric constant 22, $\tau_f = -73$ ppm/°C and Q varying in the range 10900-12600. The DR samples B6, B7, Z6 and Z7 are very small and their individual dielectric properties could not be measured. Table 5.2 gives dielectric constant and τ_f of Ba₅Nb₄O₁₅ stacked with 5ZnO-2Nb₂O₅ resonators of varying heights. The effective heights and diameter of the DRs and the volume fraction (V_f) of 5ZnO-2Nb₂O₅ are also given in Table 5. 2.

Table 5. 2

The ϵ_r and τ_f of the stacked resonators between $Ba_5Nb_4O_{15}$ and $5ZnO-2Nb_2O_5$

Pellets used for stacking	Effective Length (L) mm	Effective Diameter r (D) mm	V_f of $5ZnO-2Nb_2O_5$	$Ba_5Nb_4O_{15}$ (bottom) & $5ZnO-2Nb_2O_5$ (top)			$Ba_5Nb_4O_{15}$ (top) & $5ZnO-2Nb_2O_5$ (bottom)			
				f (GHz)	ϵ_r	τ_f ppm/ $^{\circ}C$	f (GHz)	ϵ_r	τ_f ppm/ $^{\circ}C$	
B1	Z7	9.870	9.655	0.1939	5.0237	38.7	54	--	--	--
	Z6	10.820	9.655	0.2652	4.9295	37.8	50	--	--	--
	Z5	11.790	9.655	0.3255	4.8792	36.7	49	4.8630	36.0	45
	Z4	12.730	9.655	0.3752	4.8211	36.0	44	4.8364	35.8	41
	Z3	13.670	9.655	0.4186	4.8042	35.1	40	4.8021	35.2	39
B2	Z7	8.730	9.655	0.2192	5.2671	38.3	54	5.2676	38.3	52
	Z6	9.680	9.655	0.2964	5.1527	37.2	53	5.1534	37.2	47
	Z5	10.650	9.655	0.3603	5.0700	35.8	50	5.0563	36.2	44
	Z4	11.590	9.655	0.4121	5.0169	35.0	46	5.0151	35.0	39
	Z3	12.530	9.655	0.4556	4.9634	34.3	43	4.9658	34.2	36
B3	Z7	7.600	9.655	0.2518	5.5950	38.0	55	5.5803	38.2	47
	Z6	8.550	9.655	0.3358	5.4308	36.7	47	5.4390	36.6	43
	Z5	9.520	9.655	0.4031	5.3266	35.2	44	5.3368	35.0	42
	Z4	10.460	9.655	0.4566	5.2587	33.6	40	5.2664	33.5	34
	Z3	11.400	9.655	0.5018	5.2011	32.9	37	5.1996	32.9	30
	Z2	12.360	9.655	0.5401	5.1630	31.9	34	5.1720	31.8	25
	Z1	13.280	9.655	0.5720	5.1378	31.1	31	5.1327	31.1	25
B4	Z6	7.350	9.655	0.3900	5.8711	35.5	43	5.8746	35.4	44
	Z5	8.320	9.655	0.4608	5.7344	33.6	40	5.7221	33.6	39
	Z4	9.260	9.655	0.5154	5.6380	31.8	36	5.6326	31.9	30
	Z3	10.200	9.655	0.5604	5.5507	30.9	26	5.5493	31.0	22
	Z2	11.160	9.655	0.5979	5.4956	29.7	20	5.4930	29.8	16
	Z1	12.080	9.655	0.6286	5.4607	28.7	16	5.4590	28.7	13
B5	Z4	8.140	9.655	0.5862	6.1736	29.6	21	6.1642	29.6	13
	Z3	9.080	9.655	0.6293	6.0500	28.3	10	6.0453	28.3	6
	Z2	10.040	9.655	0.6644	5.9471	27.2	7	5.9505	27.2	-1
	Z1	10.960	9.655	0.6926	5.8724	26.4	-3	5.8789	26.3	-9
B6	Z3	7.940	9.655	0.7195	6.7447	25.1	-21	6.7494	25.1	-24
	Z2	8.900	9.655	0.7495	6.5507	24.5	-23	6.5492	24.5	-32
	Z1	9.820	9.655	0.7730	6.3943	23.8	-36	6.3886	23.8	-39
B7	Z2	7.810	9.655	0.8545	7.1497	22.4	-46	7.1552	22.4	-63
	Z1	8.730	9.655	0.8695	6.8612	22.4	-55	6.8627	22.4	-65

The measured dielectric constant is nearly the same on keeping $Ba_5Nb_4O_{15}$ at the bottom and at the top of the stack. The resonant frequency dielectric constant and quality factor of the stacked resonators do not show any significant variation by the reversal of the pellets (top and bottom). But the τ_f shows a significant shift towards that of the bottom pellet in the stack.

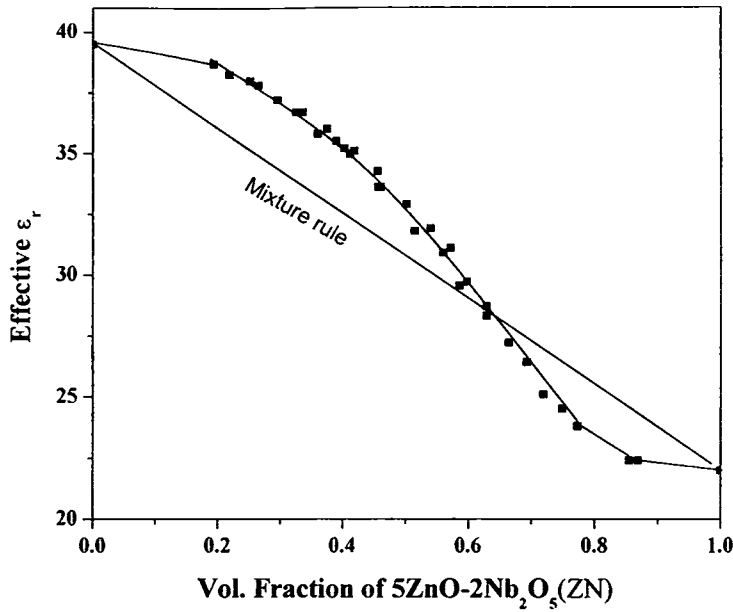


Fig 5. 2 The effective dielectric constant versus volume fraction of ZN

Fig 5. 2 shows the variation of the effective dielectric constant of the stack with the volume fraction of 5ZnO-2Nb₂O₅ (V_f) is $V_f = \frac{V_{5ZnO-2Nb_2O_5}}{V_{5ZnO-2Nb_2O_5} + V_{Ba_5Nb_4O_{15}}}$. The straight line represents the theoretical dielectric constant for a mixture of the above dielectrics. It is found that the effective dielectric constant is greater than that for the mixture up to $V_f = 0.6$. Beyond $V_f = 0.6$ the dielectric constant is lower than that by the mixture rule (theoretical). The QXf increases with increase in volume fraction of ZN (see Fig. 5. 3 and Table 5.3). The quality factor of all combinations of BN with ZN could not be measured because of the very large effective heights inside the measurement cavity. The effective τ_f versus V_f (Fig. 5.4) also shows a similar behaviour. The dots show the variation of effective τ_f when Ba₅Nb₄O₁₅ pellets are mounted at the bottom where as the circles show the effective τ_f when they are

mounted on top. The shifting of τ_f towards that of the bottom pellet is quite evident in Fig.

5. 3. This indicates that the bottom pellet has greater effect on the τ_f .

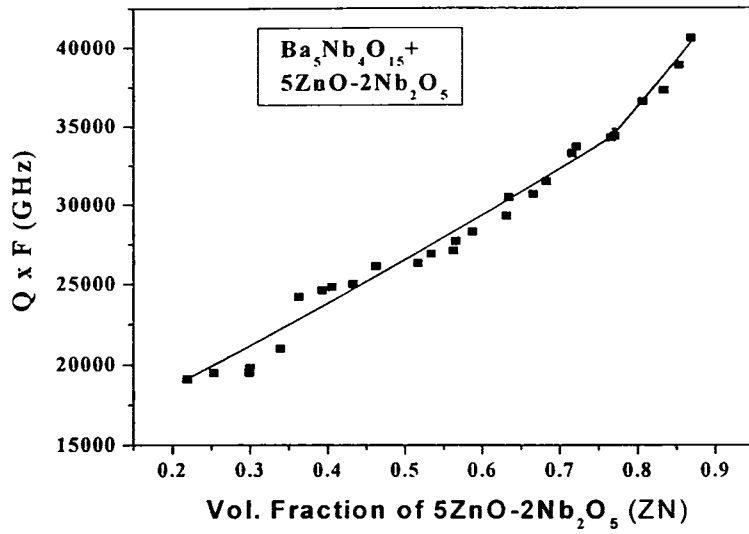


Fig 5. 3. The effective QxF GHz of BN stacked with ZN as a function of volume fraction of ZN

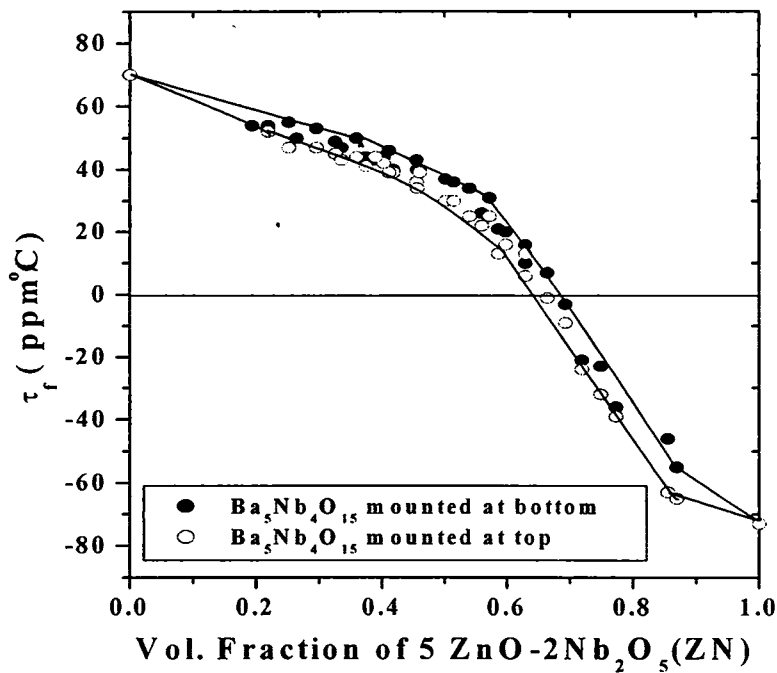


Fig. 5. 4 The effective τ_f versus volume fraction of ZN

The τ_f becomes zero when the V_f is about 0.7 in the case of $Ba_5Nb_4O_{15}$ stacked with $5ZnO-2Nb_2O_5$.

Table 5. 3
The resonant frequency and Q factor of the stacked
Resonators (Q Measured using cavity method)

$Ba_5Nb_4O_{15}$(top) & $5ZnO-Nb_2O_5$(bottom)			
Vol. fraction of ZN	f (GHz)	Q	Q x f GHz
0.2192	4.764	4100	19100
0.2533	4.836	4100	19500
0.2989	4.860	4000	19500
0.2998	4.885	4200	19800
0.3387	4.980	4200	21000
0.3627	5.041	4900	24200
0.3925	5.035	4900	24600
0.4053	5.073	4900	24800
0.4325	5.171	4900	25000
0.4621	5.369	4900	26100
0.4623	5.334	4900	26100
0.5124	5.286	5000	26300
0.5324	5.281	5100	26900
0.5623	5.318	5100	27100
0.5650	5.420	5200	27700
0.5867	5.635	5200	28300
0.6307	5.813	5100	30500
0.6335	5.741	5300	30500
0.6648	5.649	5500	30700
0.6822	5.617	5700	31500
0.7150	5.633	6000	33300
0.7208	5.720	5900	33700
0.7652	6.429	5400	34300
0.7695	6.244	5600	34400
0.8057	6.107	6000	36600
0.8330	6.022	6200	37300
0.8527	5.985	6500	38900
0.8682	5.997	6800	40600

Table 5. 3 gives the variation of resonant frequency and quality factor of $Ba_5Nb_4O_{15}$ with $5ZnO-2Nb_2O_5$ stacked at the bottom and at the top. The quality factor increases with increasing volume fraction of $5ZnO-2Nb_2O_5$ (See Fig. 5. 3). The quality factor for all the combinations of Ba with Zn could not be measured since the effective height became very large inside the measurement cavity. In Table 5. 2 the resonant frequency is measured by the end shorted condition (not inside a cavity) whereas in Table 5. 3 it is measured inside a cavity in order to measure the Q. Hence the difference in the resonant frequencies of the same sample (Table 5. 2 & 5. 3).

5. 3. 2 $Ba_5Nb_4O_{15}-Sr(Y_{1/2}Nb_{1/2})O_3$ (BN-SYN) stacked resonators

The $Sr(Y_{1/2}Nb_{1/2})O_3$ (SYN) has a dielectric constant of 28, $\tau_f = -58$ ppm/C with high quality factor up to 40000. The SYN dielectric resonators have a diameter of 11.98 ± 0.01 mm and $Ba_5Nb_4O_{15}$ (BN) 11.97 ± 0.01 mm. The individual microwave dielectric properties of the SYN and BN are given in Table 5. 4 and 5. 5 respectively.

Table 5. 4
Microwave dielectric properties of $Sr(Y_{1/2}Nb_{1/2})O_3$
[SYN] resonators

	Length mm	Diameter mm	Vs (cm ³)	ϵ_r	Q x f (GHz)	τ_f ppm/°C
S1	1.41	12.96	0.1608			
S2	2.04	11.96	0.2292			
S3	3.06	11.96	0.3449	28	6900x5.89	
S4	4.175	11.96	0.4737	28	7600x5.35	
S5	5.42	11.96	0.6150	28	8150x4.99	-58
S6	6.755	11.96	0.7614	28	8200x4.78	-58

Table 5. 5
Microwave dielectric properties of Ba₅Nb₄O₁₅ [BN]

	Length mm	Diameter mm	V _s (cm ³)	ε _r	Q x f (GHz)	τ _f ppm/°C
B1	1.22	11.97	0.1368			
B2	2.16	11.97	0.2439			
B3	4.03	11.97	0.4535	39	4749x4.65	
B4	5.295	11.97	0.5958	39	4861x4.31	78
B5	6.85	11.97	0.7580	39	5360x4.10	78

The volume fraction of SYN, Q, resonant frequency, dielectric constant and τ_f of stack of SYN with BN is given in Table 5.6.

Table 5. 6
Dielectric constant, Q, τ_f of BN stacked with SYN resonators

Volume Fraction of Sr(Y _{1/2} Nb _{1/2})O ₃ V _f	Effective Dielectric constant ε _r	Quality factor Q	Resonant Frequency F (GHz)	Q x f (GHz)	τ _f (ppm/°C) BN- bottom, SYN-top	τ _f (ppm/°C) BN- top, SYN- bottom
1	28	7600	5.3520	40700	-58	-58
0.8477	29	7400	5.1445	38000	-42	-49
0.8180	29	7200	4.8790	35000	-39	-46
0.7537	29	6800	4.6746	31800	-36	-44
0.6601	30	6300	4.5437	28600	-25	-30
0.6267	32	5900	4.9027	28900	-3	-12
0.5858	32	5714	4.7250	27000	8	-2
0.5610	33	5900	4.5570	26900	12	4
0.5109	33	5500	4.4336	24400	20	14
0.5079	34	5600	4.3245	24200	23	11
0.5011	34	5600	4.4095	24700	22	16
0.4472	35	5500	4.3388	23900	25	23
0.4432	35	5500	4.2601	23400	29	24
0.4429	35	5400	4.1916	22700	31	25
0.3846	36	5500	4.0996	22500	40	31
0.3666	36	5200	4.0645	21100	42	39
0.3357	37	5500	4.1648	22900	45	42
0.3127	37	5600	4.1188	23000	46	43
0.2778	38	5100	4.0705	20800	52	44
0.2322	38	5400	3.9993	21600	53	50
0.2125	38	5000	3.9530	19800	56	52
0.1750	38	5400	4.0085	21600	59	59
0.0	39	5300	4.1000	21700	78	78

The dielectric constant decreases and quality factor increases with increase in volume fraction of SYN (see Table 5. 6 and Fig. 5. 5).

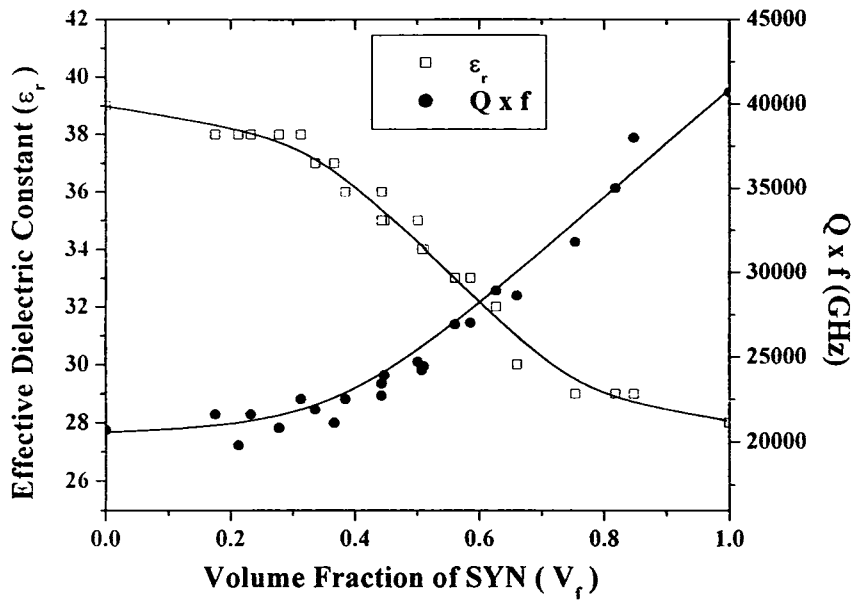


Fig. 5. 5 The variation of effective dielectric constant and $Q \times f$ with Volume fraction of $\text{Sr}(\text{Y}_{1/2}\text{Nb}_{1/2})\text{O}_3$.

This is expected since SYN has a lower dielectric constant and higher Q than BN. The τ_f decreases and becomes negative with increase in volume fraction of SYN as expected. Fig. 5.6 shows the variation of τ_f with V_f of SYN. The bottom pellet of the stack has greater influence on the τ_f of the stack. The τ_f of the stack is on the higher positive side when the bottom pellet of the stack is BN (see Table 5. 6 and Fig.5. 6). The τ_f becomes zero when the volume fraction of SYN is about 0.6

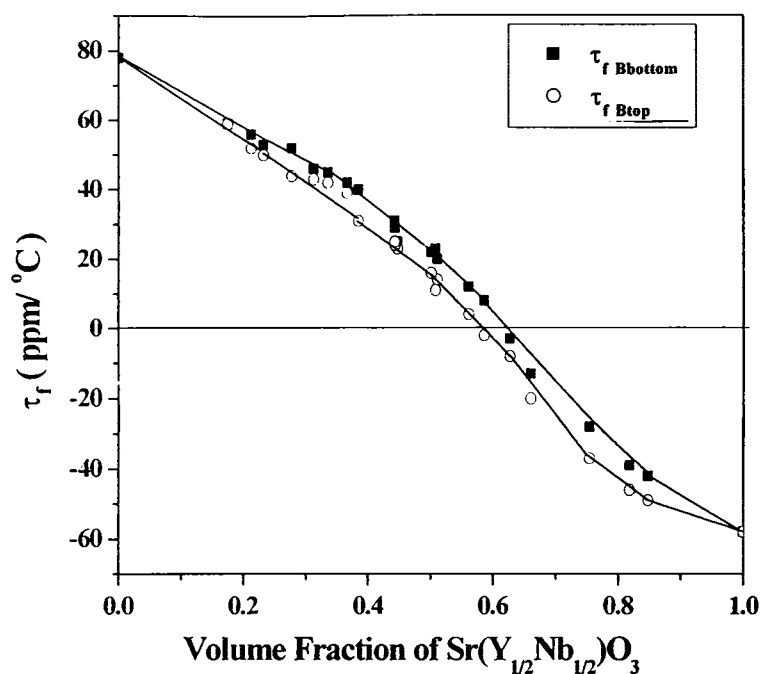


Fig. 5. 6 The variation of effective τ_f with volume fraction of $\text{Sr}(\text{Y}_{1/2}\text{Nb}_{1/2})\text{O}_3$.

5.4 CONCLUSION .

The high τ_f of dielectric resonators can be tuned by stacking positive τ_f DR with a negative τ_f DR. The τ_f can be tuned to zero or to a desired value by adjusting the volume fraction of positive and negative τ_f DRs. The dielectric constant and quality factor also varies with the volume fraction of each type of DR. Reversing the top and bottom DR samples has no influence on the dielectric constant and quality factor (within experimental

error limits) but affects the τ_f . The bottom sample of the stack has greater influence on the resultant τ_f .

REFERENCES

- [1] C. Tsironis and V. Panker, IEEE Microwave Theory Tech., **MTT-3** (1983) 312
- [2] J.G. Hartnett, M. E. Tobar, A.G. Mann, J. Krupka and E.N. Ivanov, Electron. Lett.,
34 (1998) 195
- [3] S.G. Santiago, R.T. Wang, G.J. Dick, Proc. IEEE Intl. Freq. Contl. Symp., (1995) 397
- [4] M.E. Tobar, J. Krupka, J.G. Hartnett, E.N. Ivanov, R. A. Woode, Proc. IEEE Intl. Freq.
Contl Symp. (1997)
- [5] A.N. Luiten, A. G. Mann, D.G. Blair, J. Phys. D. Appl. Phys., **29** (1996) 2082
- [6] J. Krupka, D. Cross, A. N. Luiten, M.E. Tobar, Electron. Lett., **32** (1996) 670
- [7] M.E. Tobar, J. Krupka, E.N. Ivanov, R.A. Woode. J. Phys. D. Appl. Phys., **30** (1997)
2770
- [8] V.I. Panov, P.R. Stankov, Radiotekh Electron., **1** (1986) 213
- [9] G.J. Dick, D.G. Santiago, R.T. Wang. Proc. IEEE Intl. Freq. Contl. Symp., (1994) 421
- [10] A.N. Luiten, A.G. Mann, N.J. Mc Donald, D.G. Blair. Proc. Intl. Freq. Contl. Symp.,
(1995) 433
- [11] M.E. Tobar, J. Krupka, J.G. Hartnett, E.N. Ivanov and R.A. Woode, IEEE Trans.
Ultrasonics, Ferroelectric & Freq. Contl., **45** (1998) 836
- [12] J.G. Hartnett, M.E. Tobar, A.G. Mann, E.N. Ivanov, J. Krupka and R. Geyer, IEEE
Trans. Ultrasonics, Ferroelectrics & Frq. Contl., **46** (1999) 993
- [13] S-K. Lim, H-Y. Lee, J-C. Kim, C. An. IEEE Microwave and Guided wave Letters,
9 (1999) 143
- [14] J. Breeze, S.J. Penn, M. Poole, N. McN. Alford, Electron. Lett., **36** (2000)
- [15] H. Sreemoolanathan, J. Isaac, M.T. Sebastian, K.A. Jose, P. Mohanan. Ceram. Inter.,

21 (1995) 385

[16] N. Santha, I. N. Jawahar, P. Mohanan and M.T. Sebastian. *Mater. Lett.*, **54** (2002) 318

[17] S. Solomon, N. Santha, I.N. Jawahar, H. Sreemoolanathan, M. T. Sebastian and P.

Mohanan, *J. Mater. Sci: Mater. Electron.*, **11** (2000) 595

[18] M. Mizate, K. Uenoyama, H. Ohsato, B. Nishigaki and T. Okuda, *Jpn. J. Appl. Phys.*,

35 (1996) 5065

[19] H. Ohsato, A. Komura, Y. Takagi, S. Nishigaki and T. Okuda *Jpn. J. Appl. Phys.*,

37 (1998) 5357

[20] C.L. Huang, H.L. Chen and C-C. Wu, *Mater. Res. Bull.*, **36** (2001) 1645

Chapter 6

SUMMARY AND CONCLUSION

The thesis reports preparation, characterisation and properties of the cation deficient hexagonal perovskites of the general formula $A_nB_{n-1}O_{3n}$ ($n = 5, 6, 8$) type perovskite compounds. The explored ceramics show dielectric constant between 11 and 54, quality factor in the range 2400 to 88900 GHz and τ_f in the range -73 to $+231$ ppm/ $^{\circ}\text{C}$. Most of the investigated cation deficient hexagonal perovskites show intermediate dielectric constant with high quality factors.

The microwave dielectric properties of the $A_5B_4O_{15}$ ($A = \text{Ba, Sr, Mg, Ca, Zn}$; $B = \text{Nb, Ta}$) ceramics are investigated in chapter 3. The $\text{Ba}_5\text{Nb}_4\text{O}_{15}$, $\text{Ba}_5\text{Ta}_4\text{O}_{15}$, $\text{Sr}_5\text{Nb}_4\text{O}_{15}$, $\text{Sr}_5\text{Ta}_4\text{O}_{15}$ and the $\text{Ba}_{5-x}\text{Sr}_x\text{Nb}_4\text{O}_{15}$ ($x=1, 2, 3, 4$) solid solutions crystallise with hexagonal structure and falls in the cation deficient group. The $\text{Ba}_5\text{Nb}_4\text{O}_{15}$ shows higher dielectric constant than that of $\text{Ba}_5\text{Ta}_4\text{O}_{15}$, which is contrary to the expectations. Both the compounds crystallise in the $D^3_{3d}-P3m1$ space group. This is attributed to the possible local variations of structure of $\text{Ba}_5\text{Nb}_4\text{O}_{15}$. $\text{Mg}_5\text{Nb}_4\text{O}_{15}$ and $\text{Mg}_5\text{Ta}_4\text{O}_{15}$ crystallise with orthorhombic structure. The analogous compounds $\text{Zn}_5\text{Nb}_4\text{O}_{15}$ and $\text{Ca}_5\text{Nb}_4\text{O}_{15}$ and $\text{Ca}_5\text{Ta}_4\text{O}_{15}$ do not form. Attempts to prepare $\text{Zn}_5\text{Nb}_4\text{O}_{15}$ gave a mixture of ZnNb_2O_6 and $\text{Zn}_3\text{Nb}_2\text{O}_8$

(5ZnO-2Nb₂O₅). Far infrared reflection, transmission and TDTTS measurements of the compounds were done. The microwave ϵ' of the ceramic samples is determined by the polar phonon contribution and ϵ' is dispersionless below the phonon frequencies. In single phase ceramics dielectric loss extrapolated from the submillimeter down to the microwave region according to the simple proportionality $\epsilon''(\omega) \propto \omega$ corresponds satisfactorily to the microwave data. The substitution of Sr at the Ba site and Nb at the Ta site are attempted in order to tune the microwave dielectric properties. The Ba_{5-x}Sr_xTa₄O₁₅, Ba₅Nb_xTa_{4-x}O₁₅ and Sr₅Nb_xTa_{4-x}O₁₅ solid solutions were prepared. The Sr containing solid solutions shows a high dielectric loss at the Sr rich end. At this range the compounds may be undergoing some phase transition. In an attempt to compare the microwave dielectric properties of the mixture phases (1-x)ZnNb₂O₆ - xZn₃Nb₂O₈ ceramics are prepared. The samples prepared by mixing Nb₂O₅ and ZnO gave higher density, higher dielectric constant and better τ_f as compared to those prepared by mixing ZnNb₂O₆ and Zn₃Nb₂O₈. The Q of the mixture phases prepared through both the methods shows higher values than the Q factor of the constituent phases.

In chapter 4, the MO-La₂O₃-TiO₂ (M = Ba, Sr, Ca) system is investigated. Cation deficient hexagonal perovskites CaLa₄Ti₄O₁₅, SrLa₄Ti₄O₁₅, BaLa₄Ti₄O₁₅ and Ca₂La₄Ti₅O₁₈ and orthorhombic phases CaLa₄Ti₅O₁₇, CaLa₈Ti₉O₃₁ are prepared through the solid-state ceramic route. The ceramics show high ϵ_r in the range 42 to 54, high quality factor with Q x f in the range 16222 to 50215 GHz and low τ_f in the range -25 to +6 ppm/^oC. Their high dielectric constants with high quality factors of Q x f upto 50215 GHz and low τ_f make them suitable for

applications where narrow bandwidth and extremely low insertion loss are necessary especially at frequencies around 1.9 GHz. The dielectric properties of the ceramic can be tuned (1) by adding suitable dopants such as TiO_2 (2) by replacing Ti by Zr or (3) by replacing Ba site by Sr or Ca. The calculations using Claussius-Massotti equation for ϵ_r shows reasonable agreement with the experimental values for the titanium based hexagonal ceramics.

Chapter 5 describes a novel method of achieving temperature compensation by stacking positive and negative τ_f resonators. The stack acts as a single resonator. The τ_f of the resultant stack depends on the volume fraction of the positive τ_f and negative τ_f DR materials. The τ_f can be tuned to zero or to a desired value by adjusting the volume fraction of the positive and negative τ_f materials. The dielectric constant and quality factor also change depending on the volume fraction of the two different DR materials. The experiment is performed with varying volume fraction of $\text{Ba}_5\text{Nb}_4\text{O}_{15}$ as the positive τ_f DR and $\text{Sr}(\text{Y}_{1/2}\text{Nb}_{1/2})\text{O}_3$ and $5\text{ZnO}-2\text{Nb}_2\text{O}_5$ as the negative τ_f DR materials. The DR material in the bottom of the stack has greater influence on the τ_f of the resultant stacked resonator.

It may be noted that the materials discussed in the thesis can be used as substrates in microwave integrated circuits. Compared to the use of alumina substrates the ceramics reported in this thesis can decrease the size to about more than half, not only for stripline resonators and filters, but also for all microwave circuits.

The materials reported in this dissertation have ϵ_r ranging from 11 to 54, $Q \times f$ 2400 to 88900 GHz and τ_f from -73 to $+232$ ppm/ $^{\circ}$ C with many of them useful for practical applications. Since these materials have very good dielectric properties despite being made by general solid-state preparation route, they are expected to have better characteristics with special preparation routes such as wet methods. The ceramics investigated in the present study are prepared by the conventional solid state ceramic route. It is possible to improve dielectric properties, especially the Q factor, by using chemical methods such as sol-gel process. The τ_f of some of the ceramics are positive and some are negative. Hence it is possible to tune their dielectric properties.

The dielectric Q factor ($1/\tan\delta$) at microwave frequencies is adversely affected by the microstructural factors like grain boundaries, pores, secondary phases etc., and structural factors like point defects, crystal imperfections etc. The loss is governed by the anharmonicity of lattice vibrations. The intrinsic properties of crystals can be understood using phonon scattering theory. It requires that for high Q factors, single crystals are needed. Although several ceramics are developed for DR purposes, very little attention has been paid to grow the single crystals. It might be due to the fact that the difficulties and time involved in the growth of single crystals, big enough to function as microwave resonators make them expensive. However single crystals of these materials may have very high Q values. It is also possible that a better understanding of the dielectric properties in relation to the structure can be arrived using single

crystals. Hence one of the future directions of dielectric resonator research should be to grow good quality single crystals of the above materials.

List of Publications

Patents filed

1. A novel microwave dielectric ceramic composition $5AO-2B_2O_5$ ($A = Ba, Sr, Ca, Mg, Zn$; $B = Nb, Ta$) and achieving temperature compensation by stacking the resonators with positive and negative temperature coefficients of resonant frequency, **Isuhak Naseemabeevi Jawahar**, Mailadil Thomas Sebastian PCT/IN 01/00077
2. A set of novel microwave dielectric ceramic compositions $xMO-yLa_2O_3-zTiO_2$ ($M = Sr, Ca$; $x:y:z = 1:2:4, 2:2:5, 1:2:5$ or $1:4:9$) and devices comprising the same, Mailadil Thomas Sebastian, Narayana Iyer Santha and **Isuhak Naseemabeevi Jawahar** NF 482/01

Papers

1. The $A_5B_4O_{15}$ [$A=Ba, Sr, Ca, Mg, Zn$; $B=Nb, Ta$] Microwave Ceramic Dielectric Resonators, **I. N. Jawahar**, M. T. Sebastian, Jacob George, P. Mohanan, H. Sreemoolanadhan, R. Ratheesh, Bulletin of Electrochemistry 14 (1998) 364-365.
2. Tailoring the Microwave Dielectric Properties of $BaRE_2Ti_4O_{12}$ and $BaRE_2Ti_5O_{14}$ ceramics by compositional variations, S. Solomon, N. Santha, **I. N. Jawahar**, H. Sreemoolanadhan, M. T. Sebastian and P. Mohanan, Journal of Materials Science: Materials in Electronics, 11 (2000) 595 - 602.
3. High frequency dielectric properties of $A_5B_4O_{15}$ microwave ceramics, S. Kamba, J. Petzelt, E. Buixaderas, D. Haubrich, P. Vanek, P. Kuzel, **I. N. Jawahar**, M. T. Sebastian and P. Mohanan, J. Appl. Phys. 89 (7) (2001), 3900 - 3906.
4. The microwave Dielectric Properties of $(1-x)CaTiO_3-xSm(Mg_{1/2}Ti_{1/2})O_3$ [$0.1 < x < 1$], N. Santha, **I. N. Jawahar**, P. Mohanan, M. T. Sebastian, Materials Letters 54(2002)318 - 322.
5. Ceramic Dielectric Resonators for Microwave Telecommunication Systems, M.T. Sebastian, Manoj Raama Varma, N. Santha, **I. N. Jawahar**, K. P. Surendran and P. V. Bijumon, Metals, Materials and Processes 13(2-4) (2001) 327 - 338.
6. Synthesis, characterization and microwave dielectric properties of $A_5Nb_xTa_{4-x}O_{15}$ ($A= Ba, Sr, Mg$) ceramics, **I. N. Jawahar**, M. T. Sebastian and P. Mohanan, Transactions of Indian Ceramic Society, 60(4) (2001) 161-162.

7. The Microwave Dielectric Properties of MO-La₂O₃-TiO₂ (M= Ca, Sr, Ba) ceramics, **I. N. Jawahar**, N. Santha, M. T. Sebastian and P. Mohanan, (Accepted in Journal of Materials Research)
8. A novel method of temperature compensation by stacking positive and negative τ_f resonators, M. T. Sebastian, **I. N. Jawahar**, P. Mohanan, (Communicated to J. Eur. Ceram. Soc.)
9. The microwave dielectric properties of Ba_{5-x}Sr_xTa₄O₁₅, Ba₅Nb_xTa_{4-x}O₁₅ and Sr₅Nb_xTa_{4-x}O₁₅ solid solution phases, **I. N. Jawahar**, M. T. Sebastian and P. Mohanan (to be communicated)
10. The microwave dielectric properties of (1-x)ZnNb₂O₆-xZn₃Nb₂O₈ mixtures, **I. N. Jawahar**, M. T. Sebastian, P. Mohanan (to be communicated)
11. The microwave dielectric properties of xZnO-(5-x)MgO-2Nb₂O₅ ceramics, **I. N. Jawahar**, M. T. Sebastian and P. Mohanan (to be communicated)

Conference Papers

12. Microwave dielectric properties of Mg₅Ta₄O₁₅ and Zn₅Nb₄O₁₅ ceramic dielectric resonators. **I.N. Jawahar**, M.T. Sebastian, Jacob George and P. Mohanan. Proc. Antennas and Propagation, (1998) 298-301. CUSAT, Kochi
13. Novel method for tuning the microwave Dielectric Properties by stacked dielectric resonators, **I. N. Jawahar**, M. T. Sebastian, G. S. Binoy and P. Mohanan, Proc. Antennas and Propagation, 2000, pp 173-175, CUSAT, Kochi